AD NUMBER

AD847276

LIMITATION CHANGES

TO:

Approved for public release; distribution is unlimited.

FROM:

Distribution authorized to U.S. Gov't. agencies and their contractors; Critical Technology; APR 1968. Other requests shall be referred to Army Engineering Topographic Laboratory, Fort Belvoir, VA 22060. This document contains export-controlled technical data.

AUTHORITY

usaetl ltr, 1 oct 1970

INTERIM TECHNICAL PROGRESS REPORT
FIRST SEMI ANNUAL TECHNICAL REPORT, SEPT. 1967 – APRIL 1968
PROJECT THEMIS: A CENTER FOR REMOTE SENSING

COMPILED BY
R. D. ELLERMEIER, ASSOCIATE PROGRAM MANAGER
APPROVED: R. K. MOORE, PROGRAM MANAGER

APRIL 1968

SPONSORED BY
ARPA–DOD, WORK ORDER 1079

MONITORED BY
U.S. ARMY ENGINEERING TOPOGRAPHIC LABORATORIES
GEOGRAPHIC INFORMATION SYSTEMS BRANCH
GEOGRAPHIC SYSTEM DIVISION
FT. BELVOIR, VIRGINIA

CONTRACT NO. **DAAK**02–68–**C**–0089

CRES
THE UNIVERSITY OF KANSAS • CENTER FOR RESEARCH INC
ENGINEERING SCIENCE DIVISION • LAWRENCE, KANSAS

AD _____

INTERIM TECHNICAL PROGRESS REPORT
FIRST SEMI ANNUAL TECHNICAL REPORT, SEPT. 1967 - APRIL 1968
PROJECT THEMIS: A CENTER FOR REMOTE SENSING

compiled by

R. D. Ellermeier, Associate Program Manager

Approved: R. K. Moore, Program Manager

April 1968

Sponsored by: ARPA-DOD, Work Order 1079

Monitored by: U.S. Army Engineering Topographic Laboratories
Geographic Information Systems Branch
Geographic System Division
Ft. Belvoir, Virginia 22060
attn: ETL-GS
Contract No. DAAK02-68-C-0089

With: Center for Research, Inc.
The University of Kansas
Lawrence, Kansas 66044

BLANK PAGE

SUMMARY

Project Themis, A Center for Remote Sensing at the University of Kansas was initiated in September, 1967 as a broad interdisciplinary effort for the improvement of user utility of remotely sensed data. A balanced program involving theoretical work, sensor development, processing and display, and data analysis for specific user application was established. During this report period the program has been implemented by work on broad-spectrum radar-target interactions, on multi-image processing and display systems (expansion of the IDECS)*, and on interpretation of radar images for geographic and geologic purposes. The design of a 4-8GHz continuously swept radar to be mounted on a "cherry picker" truck is almost complete and many components are now on hand. Acoustic simulation of a 5-octave system has started with equipment assembled during the reporting period. Design of interfaces between the existing analog IDECS and digital equipment is well along, with some units already under construction and most equipment ordered. Adaptive multi-image category recognition programs have been tested on multi-polarization radar data from an agricultural area, and the results look quite promising. Preliminary work on use of radar to determine the geomorphology of the Wasatch Range in Utah is complete. A geologic and geomorphologic study of Darien Province, Panama, based on radar imagery, is in the field checking stage.

Project Themis at the University of Kansas is funded under ARPA-DOD Work Order 1079 and is monitored as Contract DAAK02-68-C-0089 by the U.S. Army Engineering Topographic Laboratories, the Geographic Systems Division, Bernard B. Scheps, Project Engineer. The project is supported at the University of Kansas by the following personnel, some of whom are not directly funded under Themis, but whose work is contributory to the effort.

* Acronym for Image Discrimination, Enhancement and Combination system, an electronic scanning device which permits simultaneous viewing and combination of multiple images, with provision for signal processing for optimal presentation of selected terrain phenomena.

A. Faculty Members

Electrical Engineering	5
Geography	1
Geology	2

B. Ph.D. Candidates

Electrical Engineering	14
Geography	5
Geology	1

C. Masters Candidates

Electrical Engineering	7
Geography	0
Geology	3

In addition to the personnel listed, a number of undergraduate students are employed as technicians under the three principal disciplines. A working arrangement is being developed with faculty members of the departments of Psychology and Sociology in the field of pattern recognition and false-color perception and will undoubtedly be formalized in the near future as areas of common interest become more clearly defined.

Since its inception in 1964, the Remote Sensing Laboratory at the University of Kansas has been actively engaged in a number of studies which relate directly to the work being done under Project Themis. Themis is of particular importance to the University of Kansas since, because of its broad objectives, it provides a focus for the work being done under the other studies. As a result, considerable cross-fertilization between projects is occuring almost automatically and the total effort of the Remote Sensing Laboratory is emerging as a conesive entity.

The studies currently underway at the Remote Sensing Laboratory in addition to Project Themis are:

TABLE OF CONTENTS

CRES Project Number	Sponsoring Agency	Contract Number	Title of Investigation
0370-821	NASA	NsG 477	Study of Earth Radar Returns Received from Alouette Satellite and Lower Altitudes; and Lunar Radar Returns.
0870-823	NsF	GK-875	Research Initiation-Waves Backscattered from Layered Rough Surfaces.
1008-821	NASA	NsG 298	Studies on the Geoscience Value of Radar Imagery.
1050-823	NsF	GK-1153	Theoretical and Experimental Study of the Nature of Rough-Surface Scattering.
1120-826	USNOO	NG2306-67-C-0044	Study the Feasibility of Relating Radar Scatterometry and Altimetry as Applied to Oceanographic Problems.
1170-834	US Geological Survey	14-08-0001-10848	Study of the Utility of Radar and Other Remote Sensor Imagery in Thematic Land Use Mapping for Geographic Research.
1180-820	NASA/MSC	NAS 9-7175	Radar Studies Related to the Earth Resources Survey Program.
1210-826	Arctic Institute of North America	ONR-394	Preliminary Study of Radar Signals from Ice.
1220-824	U.S. Army Corps of Engineers	DAAK02-67-C-0435	Multi-Image Correlation Systems Study for Military Geographic Intelligence.
1370-826	USNOO	NG2306-67-C-0044	Arctic Ice Thickness Measurement by Radar (Task V).

PROJECT THEMIS: A CENTER FOR REMOTE SENSING
SEMI ANNUAL TECHNICAL REPORT (U)

I. INTRODUCTION

This report summarizes the technical work which has been accomplished during the first six-month period of contract no. DAAK02-68-C-0089. Technical reports and memoranda which describe the work to date are referenced in the text and are appended. The appended documents, for the most part, are working documents which will be up-dated as the investigations continue. When sufficient progress has been made that significant conclusions may be drawn, these working memoranda will be revised into a form suitable for scientific publication.

The technical work is discussed under the task headings used and defined in the contract purchase description and further defined in the Study Plan which was issued as a report by the University of Kansas in January, 1968. This Study Plan deviates somewhat from the purchase description in subtask definition. The reorientation of some of the tasks was necessary in order to most efficiently utilize the capabilities and interests of the faculty members and graduate students who are performing the investigations. Another factor which was considered in task reorientation was the low level of the manpower budget relative to the level anticipated when the original proposal for contract was written. Although both the Study Plan and a subsequent proposal for renewal indicate some reorientation, the overall purpose and goals of Project Themis at the University of Kansas remain unchanged.

II. TECHNICAL REPORT

TASK 4.1* TARGET-SENSOR INTERACTION STUDIES

The emphasis in this task is on theoretical, modeling and experimental studies of broad-spectrum radar systems. These studies encompass both scattering measurement and imaging systems.

---

* Task numbers are those of the USAETL Purchase Description dated 16 September 1967.

SUBTASK 4.1.1 THEORETICAL STUDIES

At this time theoretical scattering studies are being performed at the University of Kansas under National Science Foundation grants.* Work done in these studies which is applicable to broad spectrum scattering will be reported both to the granting agency and to USAETL. The work reported to USAETL will be in the form of substantiation of empirical modeling studies which are being conducted under task 4.1.2.

SUBTASK 4.1.2 ULTRASONIC MODEL STUDIES

The equipment for ultrasonic modeling of broad-band radar systems is assembled and calibrated, and data are being collected from a variety of targets. The system description is appended to this report as Appendix A (CRES Technical Memorandum 133-2). This memorandum is one chapter of an extensive report on the system design, data acquisition and data processing and analysis. The report, in the form of a Ph.D. dissertation by Mr. John Rouse, will be issued during the summer, 1968.

The principal difficulty in data acquisition at this time arises from the broad frequency spectrum (0.1 MHz to 3.0 MHz) that is being investigated. A single transducer cannot be used across this spectrum due to bandwidth limitations, so it is necessary to use a number of transducers whose spectra overlap. Thus, a continuum of spectrum is not possible in the experimental setup and it is necessary to sweep over a portion of the spectrum, change the transducer and sweep the next portion. The individual transducer characteristics must be well known in order that data may be corrected to produce a continuum of data across the desired band.

SUBTASKS 4.1.3, 4.1.4, 4.1.5, 4.1.6 ELECTROMAGNETIC INSTRUMENTATION AND MEASUREMENT

These subtasks are combined into a single task description because of the close interrelation of subtasks which prevents convenient separation.

---

* NSF Grants GK-875 and GK-1153

A simple octave-bandwidth radar system is being constructed at the University of Kansas which will operate either as fixed or mobile equipment and in either a scattering-measurement or imaging mode. All components have been specified and ordered, and construction will begin in the near future with fixed site operation planned for early summer, 1968. This activity is presently somewhat behind schedule as projected in the study plan.

A GFE boom truck has been received, which, while in poor mechanical condition, can be repaired to be functional for the early phases of ground mobile operation. Expert mechanic's opinion advises that the truck not be driven too far from a repair shop. Effort is being directed in parallel with radar system construction toward fixing antenna mounts atop the movable boom for the mobile ground measurements. The truck should be operational and the antenna mounts in place as scheduled, although some time slippage may occur if repairs must be made to the boom hydraulic operating system.

CRES Technical Memorandum 133-1-1, again the first portion of a major report, is appended as Appendix B. This memorandum outlines system parameters in terms of desired performance and of components which are readily available from commercial sources.

TASK 4.2 SENSOR AND PREPROCESSOR DEVELOPMENT

This task includes parameter and design considerations and development of prototype sensors and sensor systems including associated preprocessing of sensor data. Due to fund limitations, subtasks 4.2.2 (Cartographic radar systems), 4.2.3 (imaging radars for small satellites) and 4.2.5 (semi-focussed imaging systems) are not being pursued under this contract, although preliminary studies of radars for small satellites are being conducted under another contract.* Subtask 4.2.1 (evaluation of broad-spectrum imaging systems) will be commenced when data from the system under development are available.

---

* NASA Contract NAS9-7175

Subtask 4.2.4, a study of radar scatterometer systems is presently being implemented jointly under the auspices of the Naval Ordinance Laboratories (contract #N 62306-67-C-0044) and Project THEMIS. Parameter studies are being conducted for sea-ice measurements and include considerations of roughness, frequency, resolution area, polarization and antenna patterns. The studies are sufficiently general in nature that they can be extrapolated to terrain phenomena. A working memorandum on these studies will be issued in June, 1968. Included will be preliminary results of a comparison study between pulsed, cw and FM systems.

TASK 4.3 DATA PROCESSING AND DISPLAY

The purpose of this task is to improve existing techniques for data display, such as those employed in the IDECS system, and to originate new techniques for processing and display of remote sensor data for improved interpretibility. At this time, the working subtasks under 4.3 fall into two categories, 1) improvement of the IDECS system (Subtasks 4.3.1 and 4.3.3) and 2) implementation of adaptive and Bayes decision techniques (Subtasks 4.3.4 and 4.3.5). As work progresses in these categories, subtasks 4.3.2 (evaluation of color combinations of multiple images) and 4.3.6 (new display techniques) will be implemented. Ultimately, the adaptive and Bayes decision techniques will be instrumented and interfaced with the IDECS system in such a way that the IDECS operator will have maximum flexibility in enhancing data by direct combinations of images along with computer processed data.

Representative of the work accomplished to date under task 4.3 are three memoranda which are appended as Appendices C, D and E. The first of these deals with the mechanization of the IDECS system improvement and is essentially the outline of a working technical report which will be issued when the work underway nears completion. The second and third memoranda describe applications of adaptive and Bayes decision techniques to actual radar data obtained from an agricultural test site.

TASK 4.4 DATA ANALYSIS AND APPLICATION

Although this task specified analyst interaction with tasks 4.1 and 4.3, to date the only interaction which has occured is with task 4.3, data processing and display, since no data are yet available from the broad-spectrum radar systems of task 4.1. A review of the subtasks as outlined in the study plan follows:

SUBTASK 4.4.1 EVALUATE GEOGRAPHIC AND GEOLOGIC INFORMATION AVAILABLE FROM SINGLE RADAR IMAGES

A preliminary study of the geomorphology of the Wasatch Range, Utah, using single radar images is appended as Appendix F. Originally the study plan included single image evaluation not only of general sites but also of a specific vegetation site and the geology between Topeka and Olathe, Kansas as part of Subtask 4.4.1. By agreement with Mr. B. Scheps, Project Engineer, this portion of the study plan has been redirected to field work in and the interpretation of radar imagery of Darien Province, Panama.

This work has come at a most propitious time since the University of Kansas was able to assign to it two graduate students who have had previous experience in interpreting imagery from Darien Province and thus were able to take into the field some a priori knowledge of the area. Because the work was performed in conjunction with a "one-time" data acquisition effort by the Engineering Topographic Laboratories, it was imperative that support be given by the University of Kansas at this particular time. The particular qualifications of the involved University of Kansas personnel should assist significantly in the understanding of the geoscience aspects of this important area. A preliminary report of this investigation will be issued during the summer, 1968.

Subtasks 4.4.2 (relation of image data to wavelength, polarization, depression angle, resolution and bandwidth) and 4.4.3 (information increase with the use of multiple radar images) are not to be implemented until broad-spectrum image data are available and the IDECS system is fully operational, respectively. It is expected that the image data will be available during the second year and that the IDECS system will be operational to the extent described in task 4.3, Appendix C, during the summer, 1968.

It should be noted that the two memoranda listed under task 4.3 (Appendices D and E) required initial geoscience evaluation of both single and multiple image data and thus should properly be included as reports under task 4.4.

III. CONCLUSIONS AND RECOMMENDATIONS

Progress has been made in all phases of Project Themis, with Study Plan target dates, in general, being met. Some delay has been encountered in task 4.1, Target-Sensor Interaction Studies, in the construction of the broad-spectrum radar system. At the conclusion of the next report period, it is anticipated that this portion of task 4.1 will be approximately 60 days behind schedule. The delay is the result of difficulties encountered in obtaining components. Because of the heavy demands being made on manufacturers and suppliers to support the present military effort, stock items are in short supply and numerous delays and back orders have been encountered. Nearly all components have been obtained at this time, however, and construction has been commenced.

Since work is progressing approximately at the rate anticipated by the Study Plan, it must be concluded that the plan is a feasible one and that it is within the constraints of both funding and manpower. It is recommended that work be continued at the present level with no foreseeable redirection during the next report period.

BLANK PAGE

Appendix A

BROAD SPECTRUM BACKSCATTER ACOUSTIC SYSTEM

J. W. Rouse, Jr.

Technical Memorandum 133-2
March 1968

BROAD SPECTRUM BACKSCATTER ACOUSTIC SYSTEM

J. W. Rouse, Jr.

INTRODUCTION

Many researchers have for some time recognized that the monochromatic nature of radar hampered its performance of several specific tasks and restricted the expansion of radar techniques into new fields of remote sensing. Consequently the development of panchromatic radar systems is underway. The panchromatic or broad-spectrum radar system design poses many problems. A major difficulty arises from the fact that the frequency dependence of backscatter is for the most part undefined. Such questions as the appropriate center frequency and spectrum width for any specific application can only be answered intuitively based on a compilation of data from multiple-discrete frequency measurements, which, for the most part, is an educated guess.

Obtaining answers as to necessary system parameters for specific applications is a major concern to broad-spectrum radar designers. Even aside from the issue of system design, the lack of definition of the frequency dependence of backscatter is an issue of concern. The great bulk of theoretical descriptions of scattering from randomly rough surfaces have depended upon experimental results to justify certain simplifying assumptions. In addition, of course, the validity of the individual works is determined by its conformity to experimental results. In the case of angular dependence, considerable data is available and consequently many theories lead to excellent correlation with experiment. Unfortunately no such store of controlled experimental results exists for frequency dependence. The limited number of measurements available are either too widely spaced or the terrain (target) is too inadequately defined to be of much value.

The primary objectives of this work are to obtain an experimental description and an analytical expression for the frequency dependence of

backscatter from randomly rough surfaces. The secondary objectives include providing experimental verification of theories predicting the frequency dependence of backscatter, and examining the broad-wpectrum technique applied to traditional radar problems such as scintillation, glint and the resonance phenomenon.

The entire experiment program is conducted using acoustic waves in water. It is important that the reader appreciate the analogy between acoustic waves and electromagnetic waves, and understands that the results obtained by this research are applicable to broad-spectrum radar systems. Specific cases where the electromagnetic wave and acoustic wave analogy is imperfect are pointed out in the text, however in general one can assume that the results obtained by measurements of acoustic wave returns from, for example, a sand coated target in a water tank may just as well have been obtained by flying a radar over a particular terrain region having the same statistical properties. Polarization effects cannot be determined since the incident acoustic waves are scalar in nature.

Acoustic simulation of electromagnetic problems is well developed and documented. Even so its value as an analog computer is either not understood or not appreciated by many radar engineers. An acoustic simulator makes it possible to perform many of the experiments normally reserved for flight testing in the laboratory, and to adjust parameters of the radar system in a highly controlled and repeatable manner. The simulator is advantageous because both distance and time are scaled by a factor containing the ratio of acoustic propagation in water to the electromagnetic propagation in air; a factor of 2×10^5. Therefore the radar problem is compressed to a size easily accommodated in a water tank, and the electronic system is video rather than rf. The flexibility is further enhanced by the option to scale distance in a non-linear manner. The essence is that model experiments can be performed rapidly, repeatably, and at much smaller cost than full scale experiments, and can provide results completely analogous to a large number of electromagnetic problems.

This research program is subdivided into four action areas: 1) development of instrumentation to implement the broad-spectrum technique,

2) measurement of backscatter from randomly rough targets of known statistics, 3) determination of the frequency dependence predicted by several scattering theories, and 4) correlation of experimental and theoretical results. In addition, emphasis is placed on the effects associated with implementing the broad-spectrum technique in the microwave region. For example, images of a variety of targets illuminated with a broad-spectrum signal will be presented and discussed in a later report.

The design and construction of a system providing broad-spectrum illumination occupied much of the effort of this program. Of particular concern is the behavior of the ultrasonic transducers used as the transmitter and receiver antennas. These devices are piezoelectric crystals constructed for resonance operation at particular discrete frequencies. Operation of these devices off-resonance, as is necessary in the broad-spectrum mode, poses special problems because of the sharp skirts of the transducer responce and spurious resonances due to the transducer casement and mount. Evading these problems and defining the transducer effects on the data are significant achievements of the system effort. A thorough investigation of the transmission and reception methods, data processing, and calibration is necessary to facilitate interpretation of the experimental results and to establish their validity.

The measurements program deals primarily with randomly rough surfaces having known statistics. Measurements of backscatter power are recorded for a variety of target surfaces at various incidence angles across a frequency range of 30:1 (λ = 15 mm to 0.5 mm). The targets are designed to have correlation functions which Fourier transform to functions almost entirely contained within the illuminating frequency spectrum. The text will classify targets by their roughness density spectrum which is the Fourier transform of the correlation function.

Several approaches to describing scattering of electromagnetic and acoustic waves have been developed in recent years.* Each such approach has

---

* Fung, A. K., CRES Report 48-3, Scattering Theories and Radar Return, 1965

a frequency dependence whether intentionally or incidently introduced. To accomplish the comparison of experimental results with theoretical predictions, a detailed review of the pertinent theories is necessary. In each case careful attention must be given to the necessary surface condition imposed by the development.

The strength of this overall study rests in the use of broad-spectrum illumination to determine the frequency dependence of backscatter. The technique provides information for a broad, continuous range of frequencies, thus eliminating extrapolation errors and unknowns. It is an extremely flexible experimental approach. In essence it is a new concept in radar systems and the overall study includes an evaluation of this concept.

SYSTEM INSTRUMENTATION

The system used for this measurements program was designed and built by the Center for Research, Inc., Engineering Science Division. Funding was shared by the Department of Defense under contract DAAK02-68-C-0089, the National Aeronautical and Space Administration under contract NAS 9-7175, and the Center for Research, Inc. The need for flexibility heavily influenced the selection of subassemblies throughout the instrument, and in many cases the subassembly used has many times the actual capability required.

A. System Function

To produce data necessary for precisely describing the frequency dependence of backscatter, the experiment system ideally must transmit a uniform amplitude, variable-width, broad-spectrum acoustic wave in a frequency independent beam. Such a system cannot be built; however, an approximation to this system is possible.

The system as built operates in what is termed a "slow-sweep" mode.

In this mode the transmitted frequency is swept from minimum to maximum in a fixed time. The transmitter is gated on by a narrow pulse at a repetition rate from 10^2 to 10^3 faster than the sweep rate, hence the transmitter output consists of a pulse train in which each pulse contains a different carrier frequency. This technique is illustrated in figure A.1. The approach is actually a multiple-discrete frequency method where several hundred discrete frequencies are used and the spacing is such that the output spectrum of one overlaps the spectra of neighboring pulses.

The envelope of the average amplitudes of the returns associated with pulses t_o through t_f is the average return power spectrum for the particular target being tested. The handling of the data necessary to obtain this spectrum is complex and is described in detail later.

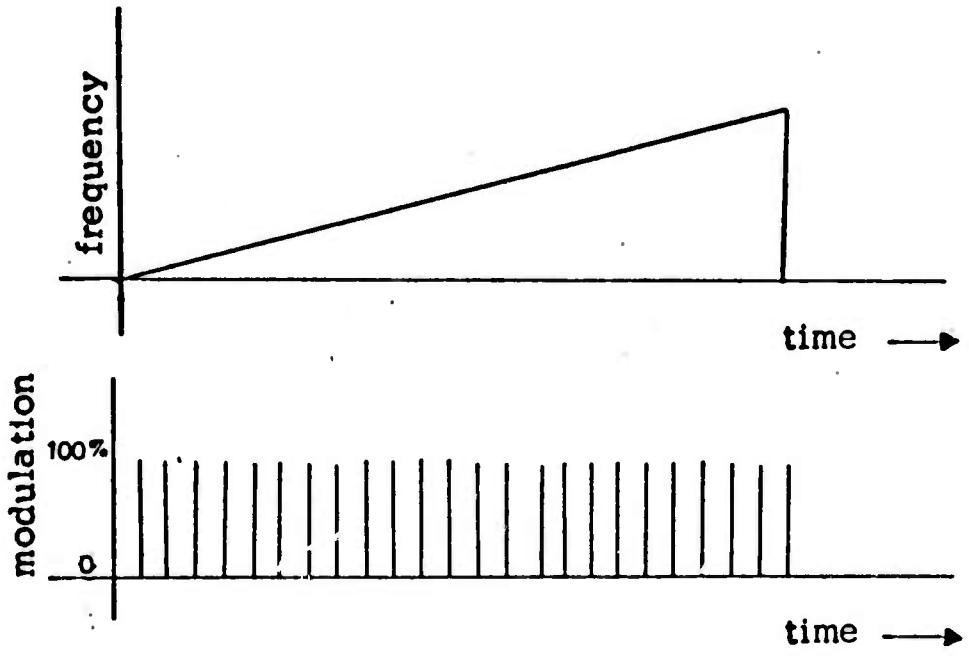

Figure A.1. Slow-sweep mode sampling technique

The principle of operation of the broad-spectrum, slow-sweep mode is simple, however the implementation is difficult. The primary problem is the piezoelectric transducers used as the transmitting and receiving antennas. Their beamwidth and gain are highly frequency sensitive, and careful attention is needed to insure the validity of the experimental results.

B. System Description

The block diagram of the system is shown in figure 1. It consists of three main sections: 1) transmitting, 2) receiving, and 3) data processing.

1. Transmitting Section

This section consists of a function generator, swept frequency oscillator, pulse generator, gate, gated power amplifier, transformer, and a transmitting transducer.

The function generator provides two outputs. One output is a triangle wa...orm on a dc voltage level. This output drives the swept oscillator. The other output is a square wave and is used to gate the pulse generator "on" during the interval of positive slope of the triangle waveform, and "off" during the negative slope interval.

The swept-frequency oscillator provides a leveled output across the frequency range programmed by the function generator. The output is fed through a gate and into a gated power amplifier. Each gate is switched "on" (closed) by the output pulse of the pulse generator. The purpose of the double gate is to increase the "on" - "off" ratio and thus minimize the noise subsequently experienced at the receiver input.

The power amplifier has a gain of approximately 30 over the frequency range 0.1 MHz to 3.0 MHz. The push-pull output stage in the tester drives 25 feet of 23 ohm cable (two 50 Ω cables in parallel) which connects to a 3:1 step-up transformer and a 200 Ω terminating resistor. In addition a small inductor is in

series with the transducer to form a low pass filter arrangement.

2. Receiving Section

This section consists of a receiving transducer, cable driving amplifier, low-noise preamplifier, and final amplifier.

The cable driving amplifier is a unity gain impedance transformer having a 92 Ω output impedance matched to the cable.

The low-noise preamplifier provides 80 db gain over the frequency range of 0.1 MHz to 3.0 MHz with a noise voltage of less than 30μ volts. The unit has a 92 Ω output impedance and is divided into two stages with variable attenuation between stages.

The final amplification is obtained in a Tektronix oscilloscope preamplifier (type CA).

3. Data Processing Section

The fundamental unit in the data processing section is a 256 channel pulse height analyzer. This unit counts the number of pulses of equal amplitude and stores the counts in a storage element corresponding to the pulse amplitude. Each of the 256 storage channels represents a particular pulse amplitude range, and each count in the channel indicates the number of pulses occurring within that amplitude range.

In this system the 256 channels represent frequency ranges rather than amplitude ranges. The data processing section converts the return amplitude at a particular frequency into a number of counts at a set amplitude corresponding to the return signal frequency. This is accomplished by converting the analog return to digital and causing the digital count pulse to vary in amplitude in direct proportion to the swept frequency.

Following figure 2 ., the data processing operation is as follows. The return signal is obtained from the VERT SIG OUT of the Tektronix 545B oscilloscope. The signal is sampled in a high speed solid-state switch controlled by the Tektronix 545B +A GATE. The sample is stretched and compared to a ramp function

in a differential amplifier. The differential amplifier gives a -3v output for an interval equal to the time during which the stretched pulse is greater than the ramp. This interval serves as a gate on a 5 KHz clock (5 KHz is the maximum rate acceptable by the pulse height analyzer). The clock output is compared with the triangle waveform driving the swept frequency oscillator. The comparison is made by an operational amplifier that changes gain proportional to the triangle input. The result is that the pulse height analyzer receives a pulse train of amplitude proportional to frequency and duration proportional to return amplitude.

The results of several sweep intervals are stored and the average spectrum is displayed on a CRT. The CRT is photographed and subsequently analyzed.

C. System Calibration

The calibration program is concerned with four system sections. These are 1) power amplifier, including output transformer section, 2) low-noise amplifier, 3) data processor, including pulse height analyzer, and 4) transducers. Of these, the transducers occupy the prime attention.

1. Low-noise Preamplifier

The low-noise preamplifier consists of two 40 db gain integrated circuit amplifiers (RCA 3022). Each unit has an upper 3 db point at 7.5 MHz with a noise figure of approximately 5 db. The two stages are separated by a 0 - 101 db variable attenuator. The gain of the unit is 55 db $\pm$ 1 db across the frequency range 0.1 - 3.0 MHz.

2. Power Amplifier

The power amplifier consists of two sections. The first is a basic push-pull amplifier with an optional gating feature. The gain of this stage is 10 $\pm$ .1 over the frequency range 0.1 MHz

to 3.0 MHz. The second stage consists of a step-up transformer, termination, and low-pass filter. The transformer ratio is 2.65 ± 0.1 over the frequency range. The assembly is separated from the amplifier by 25 feet of 25 ohm coxial cable. The separation is advantageous to the operation since it isolates the cable capacity from the transducer capacity. The transducer impedance is highly capacitive and the variation of impedance from unit-to-unit is great. This requires special attention in design since the maximum power deliverable is a function of the particular transducer cloud, hence calibration is required individually according to the transducer in use.

3. Data Processor

The data processor calibration consists of determining the input signal voltage required to produce each addition count. The voltage versus count curve is linear and has a slope of 0.066 volts/count with an intercept of 0.15 volts at 8 counts. The reference count is six, i.e. with no signal in, a six count is present.

4. Transducers

Measurements in the acoustic system are made by means of piezoelectric transducers. This program used the simple flat disk, barium titanate transducer for all data. These transducers were designed for use at a single, electrical and mechanical resonance frequency. Attempting to employ them in a broad spectrum system created special problems.

It would be advantageous to use only one pair of transducers to record measurements over the entire frequency range of interest. Unfortunately, no transducer was located that would meet the requirements. The basic difficulty is that the transducer gain pattern is frequency dependent to the extent that reasonable size beam patterns at 3.0 MHz become too large for the limited size

water tank at 0.1 MHz. Additional problems arise with regard to resonance and harmonics.

In most documented acoustic wave experiments, transducer gain is measured by transducer pairs and seldom is the gain of an individual transducer obtained. In this study an attempt was made to determine the absolute gain of a single transducer. To accomplish this two type measurements were necessary.

a) Single Transducer Measurement

The test setup for this measurement is shown in figure 3. A single transducer is used as both the transmitting and receiving antennas. The transducer is oriented so that the acoustic wave propagation is normal to a 0.25 inch thick plate glass target.

The operation for single transducer measurements is as follows. The sweep frequency oscillator is set to a fixed frequency. The output of the oscillator is gated twice to provide a high on-off ratio, and transmitted. On transmission, the switch is in position A. After the transmitted pulse interval, the switch is thrown to position B, and the return signal enters the preamplifier. The measurement is the ration of V_{IN}/V_{OUT}. The transducer gain is calculated from the equation.

$$G = \frac{V_{IN}}{V_{OUT}} \frac{4\pi (2h)}{\lambda K} \qquad \text{C.1.}$$

where 2h is the distance to the target, λ is the wavelength, and K is the reflection coefficient, which is unknown. Equation C.1. is developed from the equation for one-way propagation by assuming the receiving transducer is at the image point of the transmitting

transducer and that K = 1. The correct value of K is determined later.

Plate glass is used as the target to insure a smooth surface to all wavelengths in the range of interest. The calculated reflection coefficient for glass in water is 0.83.

As will be evident in the data, using the plate glass as a target created some unexpected difficulties. The glass target is approximately 0.25 inches thick. This width is equal to one wavelength at about 1 MHz (velocity of propagation of sound in glass is 6 km/sec). Assuming the glass acts as a low-loss transmission line, the terminating impedance on the backside of the plate is reflected to the front side and thus presents a matched impedence termination to the incident energy. The matched condition should appear at about 0.5 MHz, 1.0 MHz, 1.5 MHz, 2.0 MHz, 2.5 MHz, and 3.0 MHz based on the thickness of the glass. The results confirm the condition at these frequencies. Fortunately the nulls are very sharp for frequencies above 1 MHz. The two nulls at 1 MHz and 0.5 MHz are generally broad, and hence the data are suspect in this range.

b) Transducer Pair Measurements

The test set up for this measurement is shown in figure 4. Two transducers are aligned directly facing each other, 1.0 meter apart. The measurement recorded is the ratio of voltage at the receiving transducer to the voltage at the transmitting transducer, V_{OUT}/V_{IN}.

In this arrangement signals are recordable for the entire frequency range of 0.1 MHz to 3.0 MHz for

nearly all transducers. The gain, either receiving or transmitting, is calculated using the equation for one-way propagation.

$$G_t = \left(\frac{V_{OUT}}{V_{IN}}\right)^2 \quad \frac{(4\pi R)^2}{G_r \lambda^2} \qquad \text{C.2.}$$

where: G_t = gain of transmitting (or receiving) transducer

G_r = gain of receiving (or transmitting) transducer measured by single transducer method

R = spacing between transducers

λ = wavelength

Although it was mentioned that the entire frequency range can be covered in the pair measurements, G_t can only be calculated over small segments. This is due to limited number of values of G_r (equation C.2.) available for calculation from the single transducer measurements.

The data plots are very similar in shape to those obtained in the single transducer measurement, especially above 1 MHz. However, there is a difference in magnitude of 14 - 15 db. This difference is due to the fact that the reflection coefficient, K, was assumed to be unity in equation C.1. The actual value of K can be determined using both the single and pairs data.

$$K = \left(\frac{2h}{R}\right)\left(\frac{V_{IN}}{V_{OUT}}\right)\left[\left(\frac{V_{OUT}''}{V_{IN}''}\right)\left(\frac{V_{OUT}'}{V_{IN}'}\right)\right]^{1/2} \qquad \text{C.3.}$$

where h = height above target (single)

R = spacing (pairs)

V_{IN}'' and V_{OUT}'' = input and output of receiving transducer (single)

V_{IN}' and V_{OUT}' = input and output of transmitting transducer (single)

V_{IN} and V_{OUT} = input and output of pairs measurement

The value of K for the 3.0 MHz 12^{o} and 6^{o} pairs is 0.21. This compares with a calculated value for K of 0.83. The difference is most likely due to a combination of effects such as 1) difference in the power delivered to the transducer mount as compared to that actually delivered to the water, 2) difference in actual properties of the glass target and ideal properties of glass; density equal 2400 kb/cu 3 and velocity of propagation equal 6 km/sec, and 3) transmission line impedance transformation effects.

Using a K value of 0.21 the receiving gain is computed for each transducer used in the experiment both as individual units and in pairs.

The disk or piston transducers used in this work have an active surface area measuring several wavelengths across and produce a directive antenna pattern. The far field pattern for a flat disk transducer operating in an infinite baffle is given by

$$F(\Theta) = \frac{2 J_1 (k a \sin \Theta)}{k a \sin \Theta} \qquad C.4.$$

where J_1 = Bessel function of first kind and first order

k = wave number

a = radius of flat disk

Θ = angle from surface normal

D. Summary

The broad spectrum acoustic system provides accurate, high sensitivity measurements over the frequency range 0.1 MHz to 3.0 MHz. The calibration tests confirm that no single transducer will operate satisfactorily over the full range and hence data must be recorded in segments as dictated by the transducers used.

Acknowledgement: This work was supported by Project Themis (USAETL Contract DAAK02-68-C-0089, ARPA order No. 1079) and NASA Contract NAS9-7175.

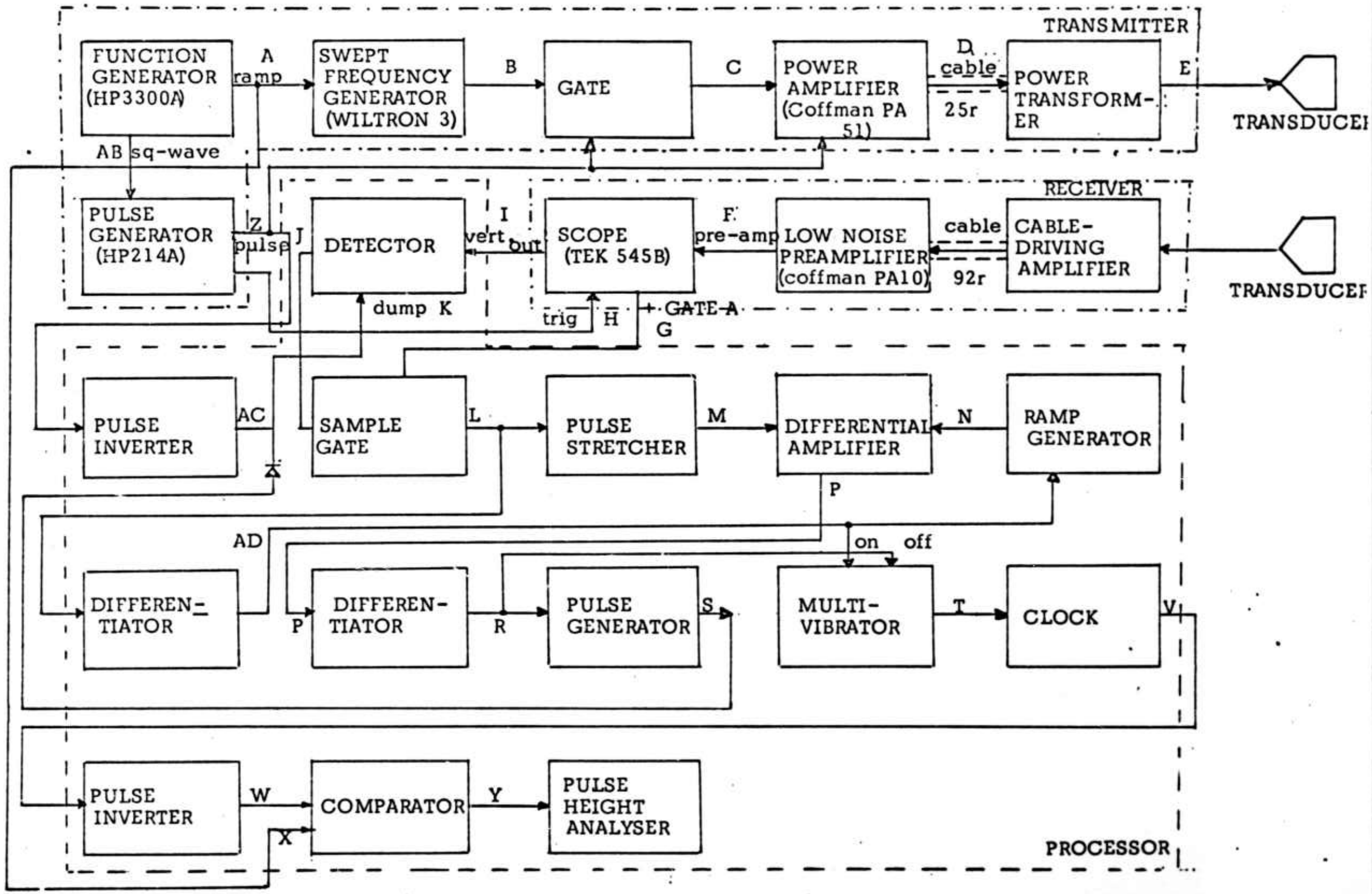

Figure 2. BROAD-SPECTRUM ACOUSTIC GENERATOR AND RECEIVER

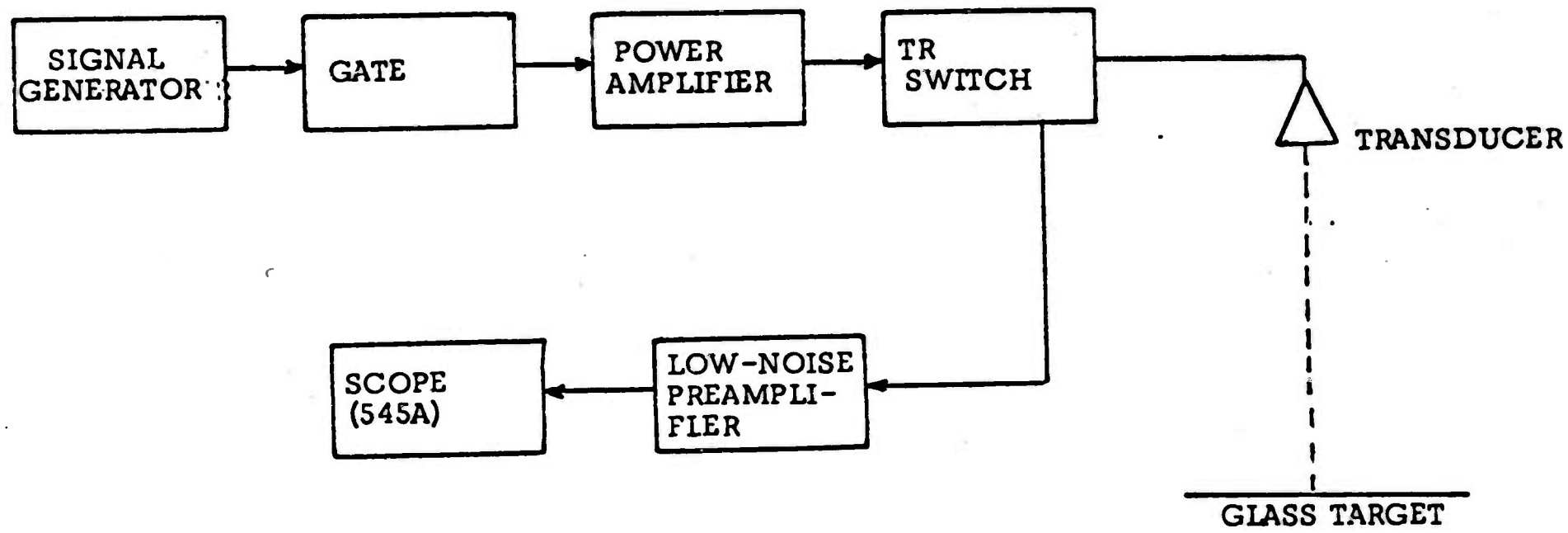

Figure 3. SINGLE TRANSDUCER TEST

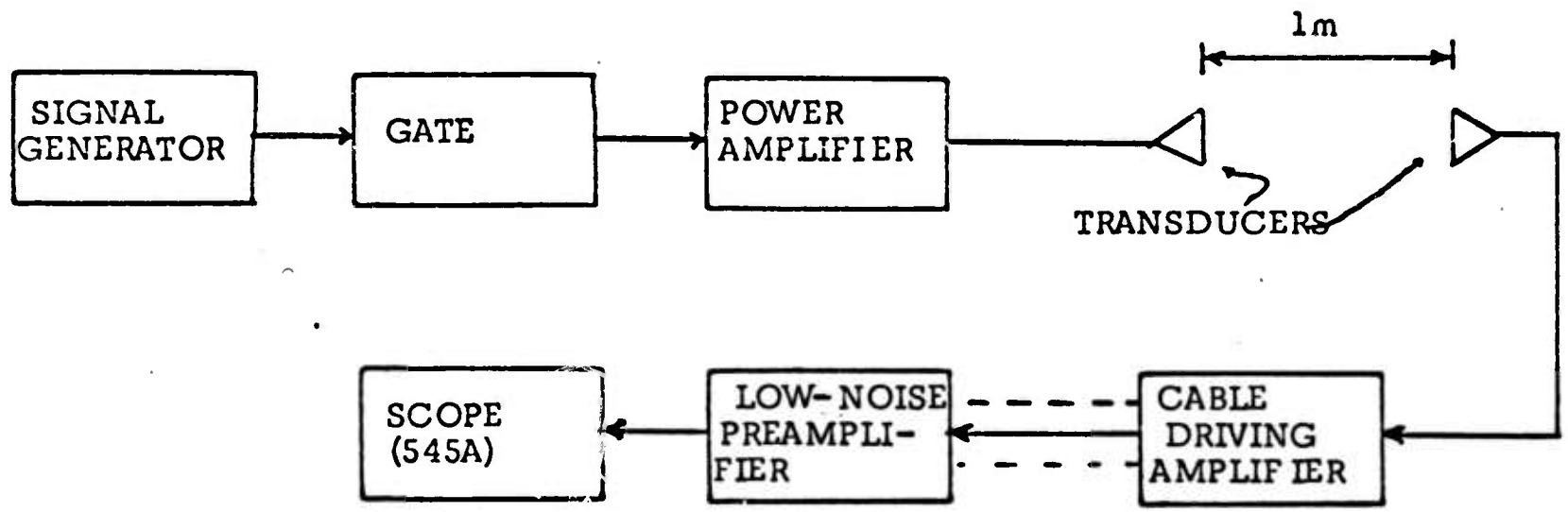

Figure 4. TRANSDUCER PAIR MEASUREMENT

Appendix B

ANTENNA AND OUTPUT POWER CONSIDERATIONS FOR THE POLYPANCHROMATIC RADAR SYSTEM

W. P. Waite

January 1968

TECHNICAL MEMORANDUM
133-1-1

ANTENNA AND OUTPUT POWER CONSIDERATIONS FOR THE POLYPANCHROMATIC RADAR SYSTEM

by

W. P. Waite

1. INTRODUCTION

The polypanchromatic radar is a device for performing broad-spectrum electromagnetic scattering and imaging measurements. The system is designed to operate from a truck-mounted boom and is completely self-contained and easily transportable to various target areas of interest.* The system design is necessarily specialized; however, the individual components of the system are standard commercially available laboratory and test equipment.

This memorandum examines the requirements and performance of the system both from a general standpoint and in view of the components available from industry and within the budget limitations of the THEMIS contract. A specific antenna and transmitter are recommended for purchase and use as a result of this study.

2. GENERAL

The basic design goals of the polypanchromatic radar system are

1. Operation over a bandwidth of at least one octave.
2. Measurement of backscattering cross section as a function of
   a) Frequency
   b) Bandwidth
   c) Incidence Angle (from 0^{o} to as near grazing as possible)
3. Production of panchromatic imagery as a function of
   a) Frequency
   b) Bandwidth

* The measurement program for which this equipment is to be used will be similar to the discrete frequency measurements described in the following reference:

Cosgriff, R. L., W. H. Peake, and R. C. Taylor. "Terrain Scattering Properties for Sensor System Design", Terrain Handbook II, Engineering Experiment Station, Ohio State University, Antenna Lab, Columbus, Ohio, 1959.

4. Maximum usage of commercially available components.

Figure 1 shows a block diagram of the proposed system. This system is the same as that shown in the original THEMIS proposal with the exception that the operating frequency range has been changed from 8.0-12.0 GHz to 4.0-8.0 GHz.

In the following sections the desired resolution and range are examined for their effect upon the antenna configuration and the required output power. These effects are examined in view of the commercial equipment available and specific model numbers are recommended for purchase as a result of this study.

3. ANTENNA CONSIDERATIONS

The truck upon which the system is to be mounted will be furnished as GFE and B. B. Scheps (ETL Project Engineer for this contract) has indicated the boom height above ground of the available vehicle to be 42 feet. This height refers to the vertical distance from the ground to the bottom of the bucket when the boom is fully extended and in the vertical position. For performance of the desired backscattering measurements the return at vertical incidence must be measured. In this mode of operation the minimum range of the system is determined by the antenna height above ground.

Figure 2 illustrates the deployment of the boom when performing backscattering measurements. The angle between the boom and vertical should be at least 30 degrees. This is required not only to position the antenna over the target area, but to prevent the truck itself from significantly contributing to the return through the antenna sidelobes.

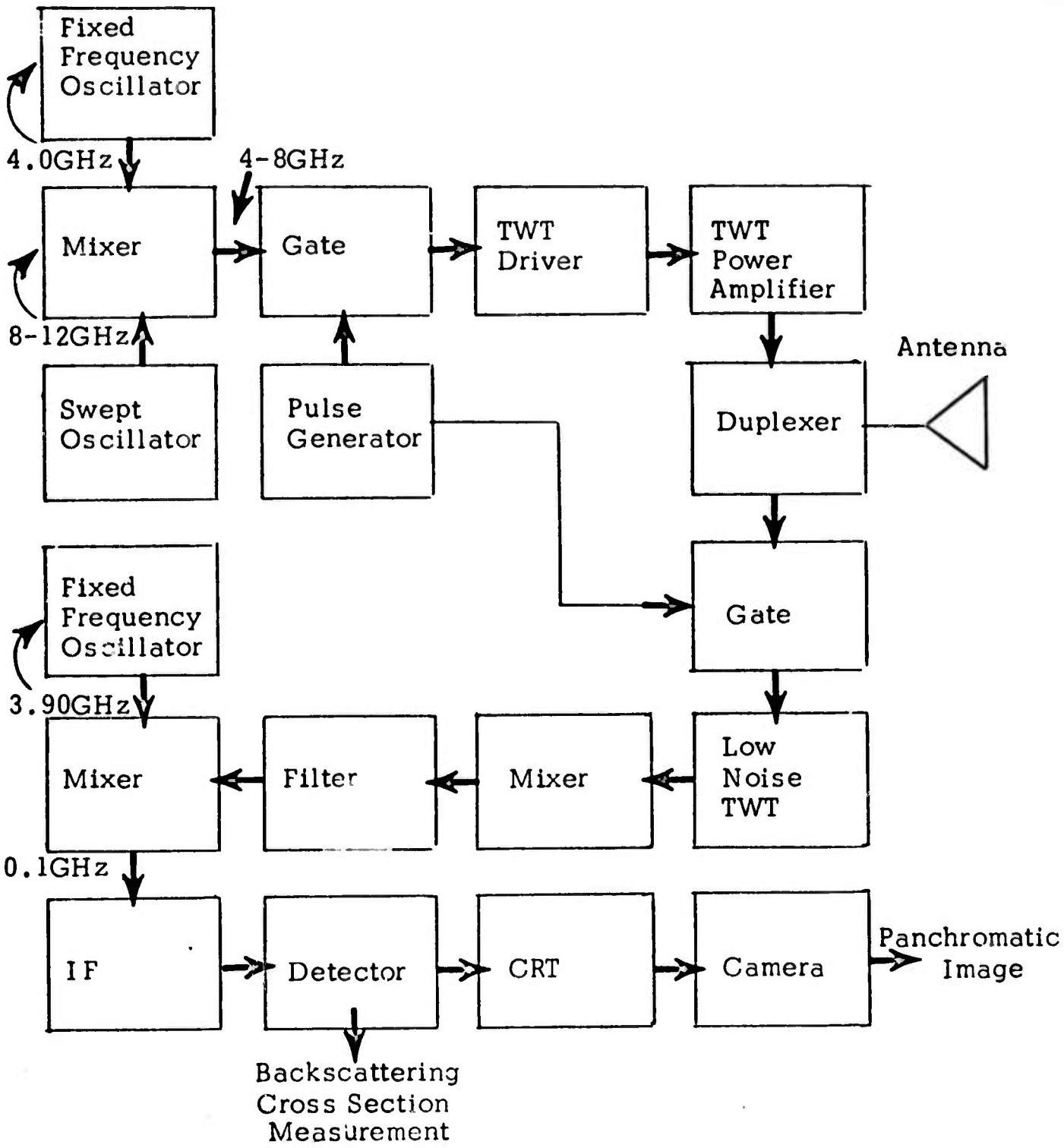

Figure 1 -- Polypanchromatic Radar System

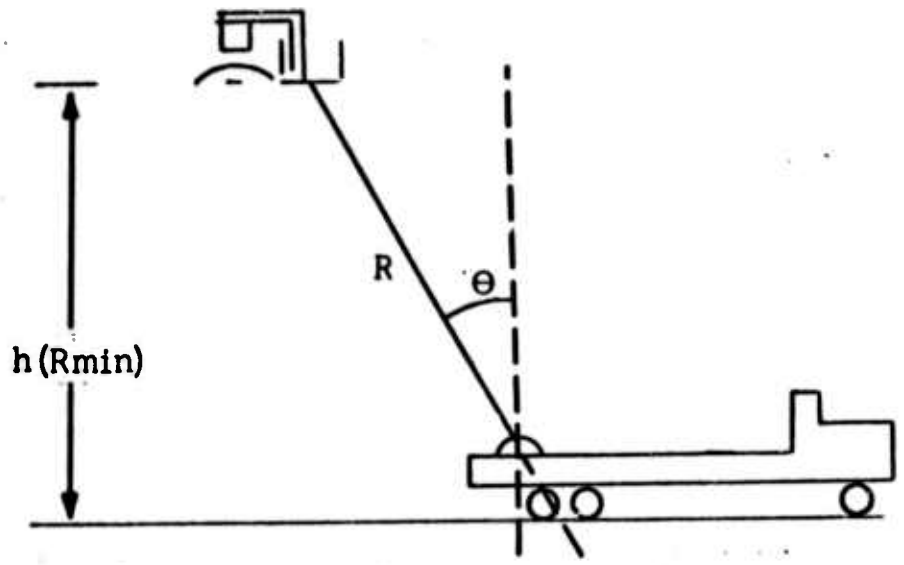

Figure 2 -- Boom Deployment for Backscattering Measurements

If we assume the antenna to be mounted at about the same level as the bottom of the bucket, the antenna height above ground or the minimum required range is given approximately by

$$R_{min} = R \cos \Theta = 42\ (0.866) = 36.4 \text{ feet}$$
$$= 11.1 \text{ meters}$$

This minimum range corresponds to a transmitted pulse length of

$$\tau = \frac{2\ R_{min}}{c} = \frac{2 \times 11.1}{3 \times 10^8} = 74 \text{ nsec}$$

where τ = transmitted pulse length

R_{min} = minimum range

c = velocity of light

To allow sufficient time for receiver recovery after the main bang the maximum pulse length should not exceed 50 nsec and operation with even shorter pulse lengths may well be desirable.

The resolution requirements imposed upon the antenna will be distinctly different, dependent upon the mode of operation of the system (backscattering measurement or imaging). The azimuth resolution of the system must be accomplished by beamwidth limitation of the antenna in

either mode of operation. The range resolution may, however, be provided by either beamwidth limitation of the antenna or by the pulse length limitation of the ground illumination. Figure 3 shows the various types of azimuth and range resolution geometry.

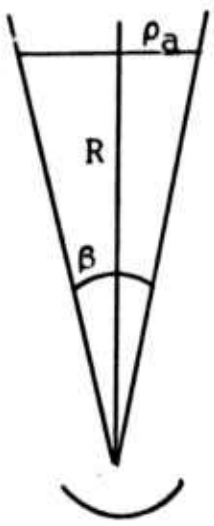

a) Azimuth Resolution Geometry

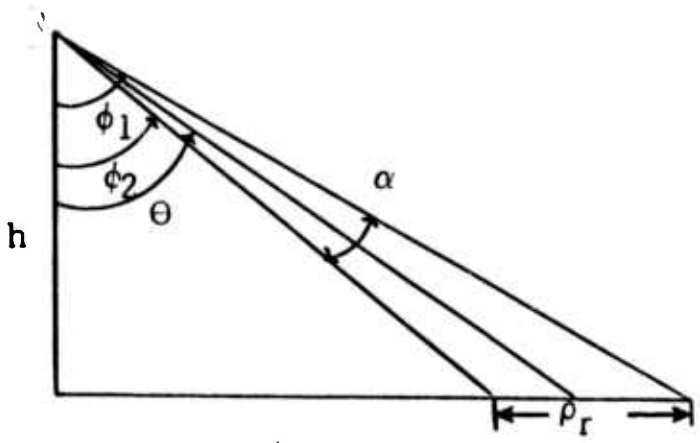

b) Range Resolution Geometry for Antenna Beam Angle Limitation

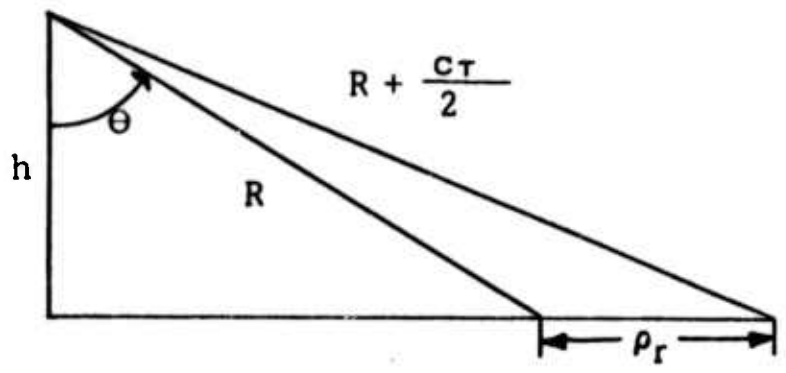

c) Range Resolution Geometry for Pulse Length Limitation

Figure 3a, 3b, 3c -- Resolution Geometry

The azimuth resolution is given approximately by

$$\rho_a = R\beta = R\frac{\lambda}{\ell} = \frac{h\lambda}{\ell \cos \theta} \qquad (1)$$

where ρ_a = azimuth resolution

R = range of resolution cell

β = antenna azimuth beam angle

λ = wavelength

ℓ = length of antenna aperture

h = height of antenna

θ = incidence angle

The resolution cell on the ground when obtained by beam limitation in both azimuth and range will actually approximate an ellipse (except at vertical where it is circular) when the antenna aperture is circular, such as with a parabolic reflector. The above expression for azimuth

resolution is then the minor axis of the elliptical illuminated area. The major axis dimension is determined from Figure 3 (b) and is given by

$$\rho_r = h\,(\tan \phi_2 - \tan \phi_1) \qquad (2)$$

where $\phi_2 = \Theta + \frac{\alpha}{2}$, $\phi_1 = \Theta - \frac{\alpha}{2}$

and ρ_r = range resolution (length of major axis)

h = height of antenna

Θ = pointing angle

α = antenna elevation beam angle

The range resolution when determined by pulse length illumination of the ground is shown in Figure 3 (c) and is given approximately by

$$\rho_r = \frac{c\tau}{2 \sin \Theta} \qquad \Theta > 0^\circ \qquad (3)$$

where ρ_r = range resolution

τ = transmitted pulse length

c = velocity of light

Θ = incidence angle

The above expression for range resolution is accurate only for Θ greater than approximately 10° and for $\frac{c\tau}{2} \ll R$. At vertical incidence the resolution cell provided by pulse length limitation is circular, with a diameter given approximately by

$$D = 2\sqrt{hc\tau} \qquad (4)$$

where D = diameter of illuminated area (at vertical)
h = height of antenna
c = velocity of light
τ = transmitted pulse length

The antenna resolution requirements for each mode of operation (backscattering or imaging) will differ and will consequently first be examined separately.

3.1 Backscattering Mode of Operation

In the backscattering mode, measurements must be made at and near vertical incidence. Examination of Equation (4) shows that pulse length limited operation is not practical in this region of operation, for if we assume

$h = 3.64$ feet $\qquad \tau = 10$ nsec (the minimum practical pulse length)

then

$$D = 2\sqrt{hc\tau} \approx 38 \text{ feet}$$

and the diameter of the illuminated area is far too large.

The operation of the system must be with beamwidth limitation at angles near vertical incidence. The diameter of the circular illuminated area at vertical incidence is then given by Equation (1).

It may also be seen from Equation (1) that the beamwidth is a function of the operating frequency. Correction for the change in illuminated area must be made during the sweep in frequency.

Table 1 lists maximum and minimum resolution cell diameters at vertical incidence for a variety of available parabolic reflector sizes.

TABLE 1 -- Variation of Illuminated Area at Vertical Incidence

$h = 36.4$ $\Theta = 0^{o}$

Reflector Size (feet)	Beam Angle Min (8.0 GHz) (degrees)	Beam Angle Max (4.0 GHz) (degrees)	Diameter of Illuminated Area Min (8.0 GHz) (feet)	Diameter of Illuminated Area Max (4.0 GHz) (feet)
1	7.0	14.1	4.5	9.0
2	3.5	7.0	2.2	4.5
3	2.3	4.7	1.5	3.0
4	1.8	3.5	1.1	2.2
6	1.2	2.3	0.7	1.5
8	0.9	1.8	0.5	1.1

Table 1 illustrates the advantage of a large reflector, which is desirable to constrain the angular variation within the beam. However, at this relatively short range a large reflector reduces the total illuminated area to such a small size that only targets or areas of relatively small scale structure and size may be adequately illuminated. The best compromise between these conflicting requirements seems to be a reflector size of 2 or 3 feet for use near vertical incidence.

Table 2 shows the variation of azimuth and range resolution as a function of incidence angle. Range resolution through pulse length limitation is included for angles away from the vertical. The figures of Table 2 show beam limited operation to work quite satisfactorily out to an incidence angle of approximately 60^{o}. After this point, however, range resolution must be provided by pulse length limitation.

Another interesting aspect illustrated by Table 2 is the variation

Table 2 - Variation of Resolution with Incidence Angle

h = 36.4 feet Aperture Diameter = 2 feet

Incidence Angle (degrees)	Ground Range (feet)	Slant Range (feet)	Azimuth Resolution (feet)	Range Resolution: Beam Limitation 4.0 GHz (feet)	Range Resolution: Beam Limitation 8.0 GHz (feet)	Range Resolution: Pulse Length Limitation 20 nsec (feet)	Range Resolution: Pulse Length Limitation 40 nsec (feet)
0	0	36	4.5	4.5	2.2		
10	6	37	4.5	4.6	2.3		
20	13	39	4.8	5.1	2.5		
30	21	42	5.2	5.9	3.0	19.7	39.4
40	30	47	5.8	7.6	3.8	15.3	30.6
50	43	57	7.0	10.8	5.4	12.8	25.7
60	63	73	9.0	18.0	8.9	11.4	22.7
70	100	106	13.1	39.2	19.1	10.5	20.9
80	206	210	25.7	168	76	10.0	20.0
85	416	418	51.5	1050	334	9.9	19.8

of slant range with incidence angle. Angles up to 85 degrees may be measured at a range of less than 500 feet, even with the boom at maximum elevation. If angles even nearer grazing are desired, it would be a simple matter to decrease the boom height and measure out to approximately 89° with little increase in range.

For instance, with an assumed boom height of 8 feet, the slant range required for an incidence angle of 89 degrees is 458 feet. Thus, the maximum range required of the system in the scattering mode is well under 1000 feet and the maximum range capability will probably be set by the imaging requirement.

3.2 Imaging Mode of Operation

In the imaging mode it is desirable to maximize the total range covered in elevation. In this mode the azimuth resolution must again be provided by the beam limiting of the antenna; however, the range resolution must be provided by pulse-length limitation.

The difficulty here is one of procurement. The only reflector shape compatible with the necessary broadband feeds and available as a standard item is a paraboloid. The azimuth and elevation beam angles are thus approximately equal.

This offers another contradiction in requirements. The reflector size should be large to provide resolution at the maximum range. On the other hand, the reflector size should be small, with the resultant large beam angle in elevation, to provide maximum coverage of the ground from near to far range.

The requirements of the system, then, would best be met by a rectangular aperture giving fan beam illumination of the area. This may possibly be obtained by locating a manufacturer who has produced a rectangular reflector of the required size for some previous project and would supply another of the same design for a reasonable (within the budget) price. Alternatively, it may be possible to procure a standard circular

dish with the desired maximum dimension and then deliberately spoil the elevation beam. This might be done by adding absorbing material as shown in Figure 4.

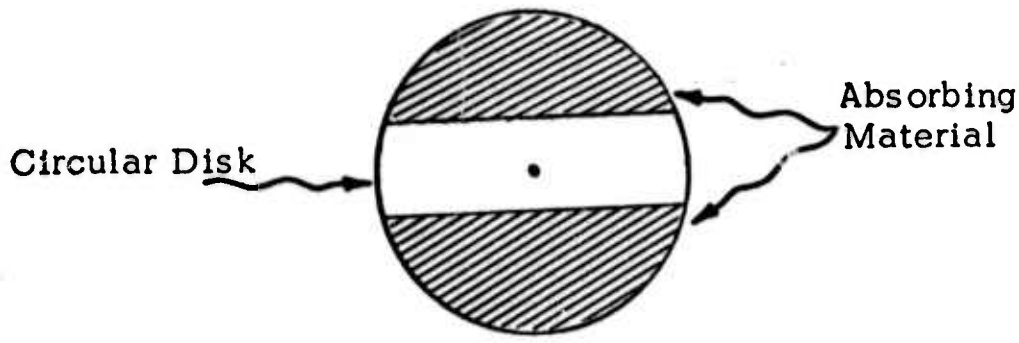

Figure 4 - Possible Means of Elevation Beam Spoiling

Virtually every major manufacturer of broadband antennas has already been contacted and none of them has available as a standard or semi-standard item the rectangular shape desired. The modification of a standard item such as shown in Figure 4 promises to be both time consuming and expensive. It is recommended that the imaging system be designed for operation with the standard parabolic dish sizes while continuing the search for a more desirable aperture that might be added at a later date.

Imaging operation with a parabolic dish will restrict the elevation beam angle such that the angle of incidence must be very near grazing if a reasonable range is to be illuminated. This poses the problem of operating in an undesirable range of incidence angles. This might be at least partially alleviated by selecting operating locations on steep hills or bluffs and thus increasing the effective antenna height above the ground being imaged.

Table 3 shows the variation of slant range with incidence angle for a variety of effective antenna heights.

Table 3 - Slant Range as a Function of Incidence Angle

Incidence Angle (degrees)	Slant Range h = 40 ft. (feet)	h = 100 ft. (feet)	h = 200 ft. (feet)	h = 300 ft. (feet)
90	----	----	------	------
89	2,290	5,730	11,500	17,200
88	1,150	2,860	5,720	8,580
87	765	1,910	3,820	5,730
86	572	1,430	2,860	4,300
85	459	1,150	2,290	3,440
84	382	956	1,910	2,870
83	328	821	1,640	2,460
82	287	718	1,440	2,150
81	256	639	1,280	1,920
80	230	576	1,150	1,730
78	192	481	960	1,440
76	165	413	825	1,240
74	145	363	725	1,090
72	129	324	647	970
70	117	292	585	876
68	107	267	533	800
66	98	246	491	736
64	91	228	456	685
62	85	213	426	640
60	80	200	400	600
55	70	174	349	523
50	62	156	311	466
45	57	141	282	424
40	52	131	261	392

Some estimate of the maximum range of the system must now be made. We will assume that the maximum usable resolution is 100 feet (in either azimuth or range). Table 4 lists the standard reflector sizes and the maximum range corresponding to an azimuth resolution of 100 feet. The frequency used is the lowest operating frequency (4.0 GHz).

Table 4 - Maximum Range for 100 Foot Resolution

Reflector Size	Beam Angle (4.0 GHz)	Maximum Range
8	1.8	3,180
6	2.3	2,490
4	3.5	1,640
3	4.7	1,220
2	7.0	820
1	14.1	410

From a comparison of Tables 3 and 4 several interesting conclusions may be drawn. First, even with an effective antenna height of 300 feet, a range of over approximately 3,500 feet will place operation in the region of 85 to 90 degrees incidence angle. This is undesirable for imaging of real targets, as airborne imagery is sparse in this region. The images obtained in this program should, as nearly as possible, simulate those which might be obtained by an aircraft system. This would require operation below an incidence angle of approximately 80 degrees. For operation in this range of incidence angles, the range is even less for any reasonable assumption of effective antenna height.

Second, if incidence angles below 80 degrees are desirable, the use of a smaller antenna may be advisable to maximize the angular elevation

coverage. It is possible to use even a 2 or 3 foot dish, as the range corresponding to these incidence angles is sufficiently short that the azimuth resolution is still reasonable.

From the above considerations it is apparent that long range capability is not required if the purpose of the imaging mode is to investigate effects in normal airborne imaging systems. Some argument for increased range capability might be offered, however, if the system is to be used to investigate the effects of broad bandwidth on ground-based battlefield surveillance radar. The frequency range of the Phase I system (4 to 8 GHz) is probably higher than would be desired for this application. Some investigation of the foliage penetration and resonance effects in metallic targets would be possible in this area, even at short ranges. The decreased range would merely prevent complete simulation of an operational system, but the parameter of interest in this mode could still be investigated.

There is another problem presented by the short range obtainable at lower incidence angles, even for the simulation of airborne radar imagery. This is that the spatial distribution of composite targets (such as fields, grassland, woods) is greater than the system range at normal incidence angles. Thus, the range of an image would only span one or two such composite targets. This objection may be partially overcome by increasing the effective antenna height through careful site selection. Another possibility, for agricultural investigations, would be to image a small agricultural experiment station where the individual fields are quite small (50 to 100 feet maximum extent) and the variety of crops is great.

To summarize, it appears that even though imagery of several miles effective swath width (depth in range for this system) would be desirable, such imagery cannot be produced at appropriate angles with a ground-based system. Relatively narrow-swath imagery, however, can be produced and will be extremely valuable for investigating the broad bandwidth aspects of radar imagery. The overall system range, then, to produce this type of imagery need only be in the order of 3,000 feet.

From other considerations, namely the mechanical aspects of obtaining and mounting the antenna and azimuth-elevation positioner, a maximum diameter of 6 feet is placed upon the reflector size. An antenna of this size should be procured for use at maximum range. As mentioned previously, another antenna of smaller size and larger elevation beam angle is desirable for short-range imaging at lower incidence angles. The 2 or 3 foot diameter reflector recommended for scattering mode measurements would also be usable for this application.

The foregoing analysis has assumed throughout that the E and H plane radiation patterns are the same. This, of course, is not necessarily the case: however, it is proposed that the feed system be capable of both horizontal and vertical polarization, so that any advantage gained in one case would be lost when operating with the orthogonal polarization.

Before drawing final conclusions based on the above, the required power output will be studied. For the purpose of initial calculations a 2-foot-diameter paraboloid will be assumed for scattering and near-range imaging operation and a 6 foot diameter is assumed for maximum-range imaging operation. A tentative maximum range of 500 feet for the scattering mode and 3,000 feet for imaging operation is assumed.

4. OUTPUT POWER CONSIDERATIONS

Using the tentative conclusions of the preceding sections, the required output power will be calculated for both the scattering and imaging mode of operation.

The required radiated power is given by the radar equation as

$$P_t = \frac{(4\pi)^3 P_r R^4}{G^2 \lambda^2 \sigma} \qquad (5)$$

where P_t = transmitted power

P_r = minimum required received power

R = range

G = antenna gain

λ = wave length

σ = radar cross section

The minimum required received power may be expressed as

$$P_r = K\,T\,B\,F\,S \tag{6}$$

where K = Boltzman's constant

T = temperature ^{o}Kelvin

B = received bandwidth

F = receiver noise figure

S = minimum required output signal-to-noise ratio

The antenna gain may be expressed as

$$G = \frac{4\pi \epsilon A_p}{\lambda^2} \tag{7}$$

where ϵ = antenna efficiency

A_p = aperture area

The radar cross section may be expressed as

$$\sigma = \sigma_o A \tag{8}$$

where σ_o = radar scattering cross section per unit area

A = illuminated area

Using the above relations, the required radiated power may now be expressed as

$$P_t = \frac{4\pi K T B F S \lambda^2 R^4}{\epsilon^2 A_p^2 \sigma_o A} \tag{9}$$

Some additional simplifications may still be made by noting that we are primarily interested in the maximum required power. First we note that

$$A_p = \frac{\pi d^2}{4} \tag{10}$$

where d = diameter of paraboloid

The radar scattering cross section will be a minimum for composite type targets, and may be expressed as

$$\sigma = \sigma_o A \tag{11}$$

where σ_o = scattering cross section per unit area

A = illuminated area

Now, if we approximate the antenna pattern by a square beam, the illuminated area may be expressed as

$$A = \rho_a \rho_r \tag{12}$$

where ρ_a = azimuth resolution

ρ_r = range resolution

The azimuth resolution is provided by beamwidth limitation in all operating modes, thus

$$\rho_a = R \frac{\lambda}{d} \tag{13}$$

For the purpose of calculating the maximum required power we are interested in near-maximum range, which corresponds to high incidence angles. At the higher incidence angles, or near maximum range, the range resolution is provided by pulse-length limitation of the illuminated area in any operating mode. Thus

$$\rho_r = \frac{c\,\tau}{2 \sin \Theta} \tag{14}$$

where c = velocity of light

τ = pulse length

Θ = incidence angle

The required radiated power may now be expressed as

$$P_t = \frac{128}{\pi} \frac{K\,T\,B\,F\,S\,\lambda\,R^3 \sin \Theta}{\epsilon^2\, d^3\, \sigma_o\, c\,\tau} \tag{15}$$

Some additional simplification of the above expression is possible with the following assumptions.

The input noise temperature of the receiver is assumed to be at the standard temperature of 290°K (approximately 62°F). The factor KT is then

$$KT \approx 4 \times 10^{-21} \text{ watts/hertz of bandwidth}$$

The receiver bandwidth is taken as that compatible with the design goa. for minimum pulse length. The design goal for maximum operating pulse length is taken as 20 nsec. The compatible bandwidth is given by

$$B = \frac{1.2}{\tau} = \frac{1.2}{2 \times 10^{8}} = 60 \text{ MHz} \qquad (16)$$

Since we are interested primarily in the maximum required power, the wavelength is taken as the maximum across the operating range

$$\lambda \text{ (f = 4 GHz)} = \frac{c}{f} = 0.075 \text{ meters} \qquad (17)$$

Again, since we are interested primarily in the maximum range condition we assume

$$\sin \Theta \approx 1$$

The antenna efficiency is taken from manufacturers' data. The efficiency figure used is the lowest value given for any feed-reflector combination considered for this application. Assume

$$\epsilon = 0.3$$

Of course c, the velocity of light, is taken as

$c = 3 \times 10^8$ meters/sec

To summarize, the assumptions made regarding the parameters of Equation (15) are

$KT = 4 \times 10^{-21}$ watts/hertz of bandwidth

$\tau_{min} = 20$ nsec

$B = \frac{1.2}{\tau} = 60$ MHz

$\lambda = 0.075$ meters

$\sin \Theta = 1$

$\epsilon = 0.3$

$c = 3 \times 10^8$ meters/sec

Equation (15) may then be expressed

$$P_t = 2.72 \times 10^{-22} \frac{F S R^3}{d^3 \sigma_o \tau} \tag{18}$$

If the minimum pulse length is used, we have

$$P_t = 1.36 \times 10^{-12} \frac{F S R^3}{d^3 \sigma_c} \tag{19}$$

The expression above is for the power required at the antenna port, in terms of the power received at the same port, and does not take into account the internal system losses. To arrive at the figure for the power required from the power amplifier we must make some assumptions regarding these internal losses.

Referring to the block diagram of Figure 1, we shall assume a duplexing loss of 2 db (each way) and a cabling and mismatch loss of 1.5 db for both transmit and receive. The total system internal losses are then

$$L = 2.0 + 2.0 + 1.5 + 1.5 = 7.0 \text{ db}$$

The power required from the power amplifier is then increased by this ratio, and is given by

$$P_a = 6.8 \times 10^{-12} \frac{F S R^3}{d^3 \sigma_o} \qquad (20)$$

4.1 Scattering Mode of Operation

From the discussion of section 3.1 we make the following assumptions for calculating the power required in the scattering mode.

$F = 10$ db

$S = 20$ db

$R_{max} = 500$ feet $= 152$ meters

$d = 2$ feet $= 0.61$ meters

$\sigma_o = -40$ db

With these assumptions, the required amplifier power given by Equation (20) is

$$P_a = 6.8 \times 10^{-12} \frac{F S R^3}{d^3 \sigma_o} = 1050 \text{ watts}$$

The survey of traveling wave tube amplifiers for use in this application has shown the available amplifiers to fall into three general power ranges. There are a wide variety of tubes available in the range of 1 to 20 watts CW power output. The price range for these tubes runs from approximately $2,500 to $5,500 including power supply. The next range is 100 watt CW power output, and the average cost of these tubes is $7,000 less power supply. The highest power available in the desired one-octave frequency range is 1 KW. These tubes are pulse modulated with approximately a 1% duty cycle and a 1 μ sec minimum pulse. The cost of these tubes is in general over $10,000 without power supply.

Comparing these prices with the THEMIS budget, we see that only the low-power CW tubes are within the price range allotted for this component. This makes it extremely desirable to operate in this power range if at all possible. There is yet another consideration making this still more desirable. If a 1 KW tube is used, it cannot be driven directly from the mixer output of the system, as the B. W. O. sweep generator has a leveled output of 10-15 MW and the conversion loss of the mixer is approximately 10 to 13 db. This means an intermediate stage of wide-band amplification must be provided. The lower power tubes (1-20 watts) have enough saturated gain that they may be driven directly without an intermediate stage. It would, then, be extremely desirable to initially operate the system with a lower power tube. If more power is required at a later date for either ground-based or possibly airborne operation, the higher power output could be added with the previous low-power output

amplifier serving as a driver.

Let us again examine the required power output to see if it may be reduced from the 1050 watt level shown previously.

The output signal-to-noise ratio of 20 db may be obtained by postdetection integration of several pulses. The improvement over the predetection signal-to-noise ratio decreases the required power by the same factor. This averaging or integration is not only desirable for power output reduction, but is actually required ir the differential scattering cross section of composite targets is to be measured without significant error due to Rayleigh fading of the return signal.

The radar return signal from an area target is made up of component signals re-radiated from numerous small scatterers and simultaneously observed by the radar. The average power received is the sum of the powers received from the individual scatterers. The differential scattering cross section is then an average and can only be calculated when enough measurements to compute a good average have been made at points where the signals are essentially independent of each other.

The fading nature of the return signal described above is evident whenever there is relative motion between the target and radar. In this ground-based operating mode, there is no constant velocity difference as with airborne systems. When measuring a single discrete target such as a car or truck there will be essentially no effect. However, when measuring a composite target such as a wheatfield, the movement caused by the wind will produce a widely varying return signal. If the effects of this variation are to be overcome, the return signal must be averaged.

If we assume the return to be made up of many components with relatively the same amplitude and random phase, the return will be characterized by a Rayleigh distribution. This distribution is characterized by equal mean and standard deviation: that is, the distribution after square law detection is given by

$$p(V) = \frac{1}{V_o} e^{-\frac{V}{V_o}} \qquad (21)$$

$$\sigma = \mu = V_o$$

where μ is the mean, V is the postdetection voltage, and σ is the standard deviation.

For relatively small numbers of independent samples, the standard deviation for the mean of Rayleigh-distributed variables differs somewhat from that for normally-distributed variables. As the number of samples increases, the central limit theorem applies, and Rayleigh and normal results are very close. The standard variation of the mean is given approximately by

$$\sigma_m = \frac{\sigma}{\sqrt{n}} = \frac{V_o}{\sqrt{n}} \qquad (22)$$

For n larger than 20 or 30, this approximation is quite good. For smaller values of n, it is off, both because of the necessity to apply small-sample theory and because of the difference between the Rayleigh distribution and the Gaussian.

The 5% and 95% range that the mean can take on is given by

$$\text{Range} = 2 \times 1.645\ \sigma_m = \frac{3.29\ \mu}{\sqrt{n}} \qquad (23)$$

when the assumptions of Equation (22) are made. Expressed in decibels, this range is plotted in Figure 5. Clearly, a range of 2 or 3 db is easy to achieve, but a range much better than 1 db requires a very large number of independent samples. The experiment design must take this into account,

and compromise is necessary between the integration time allowed and the desired range for the mean value.

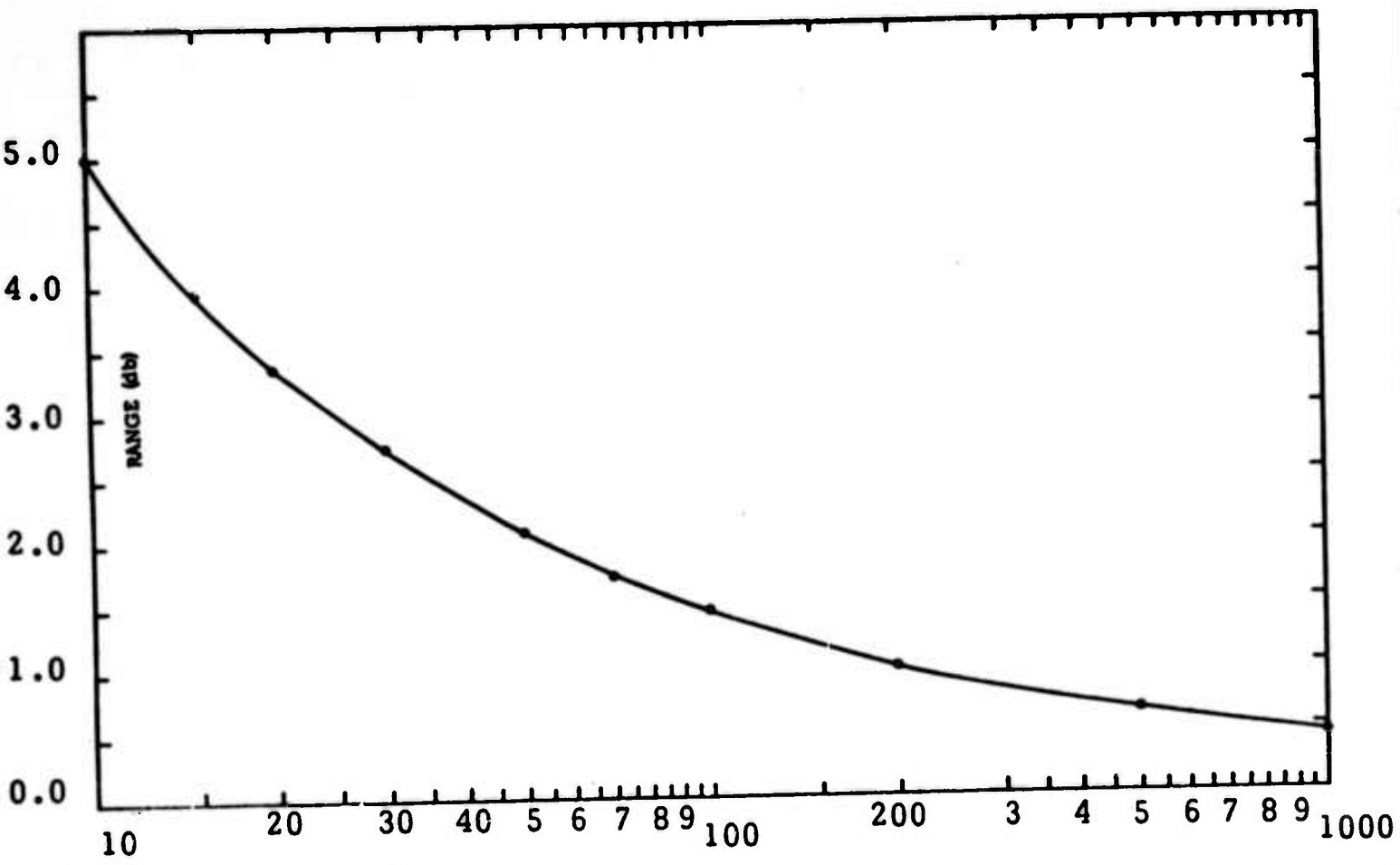

NUMBER OF INDEPENDENT SAMPLES (n)

Figure 5 - Accuracy of Averages

The required independence of the samples to be averaged may arise from variation in either time or frequency. The individual and composite effects of both these types of averaging will be studied in a later Memorandum. We will concern ourselves here only with determining the number of independent samples desired. Examination of Figure 5

shows it to take 200 independent samples to reduce the range of the mean to 1 db. We will assume this to be the desired range.

With this assumption that 200 independent samples will be averaged, we may take advantage of the integration improvement of signal-to-noise ratio. If we assume postdetection integration, the single-pulse signal-to-noise ratio is given by

$$s_1 = \frac{s}{n^x} \tag{24}$$

where s_1 = single pulse signal-to-noise ratio

s = output signal-to-noise ratio

n = number of pulses integrated

x = 0.5 to 0.9, depending on integration efficiency assumed

If we assume $x = 0.75$ and $n = 200$

$$n^x = (200)^{0.75} = 53$$

$$= 17.2 \text{ db}$$

Referring again to Table 2, we note that the pulse length may be increased by a factor of 2 at the higher incidence angles (above 75 degrees) while maintaining a range resolution equal to or less than the azimuth resolution. If we use a 40 nsec pulse at the higher incidence angles, another 3 db improvement over the result obtained from Equation (20) may be realized. Applying this 20.2 db improvement to the 1050 watt figure obtained previously, we find the power required from the final amplifier to be

$$P_a = 1050 \times \frac{1}{105} = 10 \text{ watts}$$

To summarize again, with a 10 watt final amplifier we may measure the differential scattering cross section to an incidence angle of at least 85 degrees and down to a level of -40 db. This may be accomplished with a 2 foot diameter paraboloid and a relatively inefficient broadband feed.

4.2 Imaging Mode of Operation

From the discussion of section 3.2 we make the following assumptions for calculating the power required in the imaging mode.

$$F = 10 \text{ db}$$

$$S = 20 \text{ db}$$

$$R_{max} = 3{,}000 \text{ feet} = 915 \text{ meters}$$

$$d = 6 \text{ feet} = 1.83 \text{ meters}$$

$$\sigma_o = -30 \text{ db}$$

With these assumptions, the required amplifier power given by Equation (20) is

$$P = 6.8 \times 10^{-12} \frac{F S R^3}{d^3 \sigma_o} = 850 \text{ watts}$$

Again,at the more distant ranges we may use a pulse length of at least twice the minimum, which reduces the required power to 425 watts.

Assuming the same postdetection integration efficiency as before, we must integrate the following number of pulses to operate with 10 watts:

$$n^{0.75} = \frac{425}{10} = 42.5$$

$$n = 150$$

This amount of integration may easily be provided by slowing the azimuth sweep rate. Some trade-off between signal-to-noise ratio and the assumed value for differential scattering cross section is also possible and will be studied in a later memorandum.

Summarizing once again, it appears feasible to meet the imaging requirements with a power amplifier output in the range of 10 watts.

5. COMPONENT SPECIFICATIONS

A thorough survey of available broadband antenna and TWT amplifiers has been conducted. The available components are now evaluated in light of the foregoing analysis.

5.1 Antenna

The initial survey of antenna manufacturers has been completed. On the basis of price, delivery and completeness of line, consideration has been reduced to two companies; American Electronics Laboratories and Scientific Atlanta.

Before comparing specific model numbers the antenna requirements will be summarized.

1. Frequency range: 4.0-8.0 MHz minimum
2. Polarization: linear
   The feed system should be capable of either vertical or horizontal polarization.
3. Reflector size: one 6 foot diameter paraboloid
   one 2 or 3 foot diameter paraboloid
   A rectangular aperture would be preferable for imaging operation: however, it appears that none is available at this time.

4. Movement range: -2° to $+90^{\circ}$ elevation
$\pm 90^{\circ}$ azimuth

The azimuth movement must be capable of sector scanning. Elevation movement need merely be remotely adjustable.

Both of the firms under consideration have logarithmic feeds with linear polarization and a frequency range of 1-11 GHz. The polarization of this type feed is variable by adjustment of the feed mounting. Scientific-Atlanta also has a line of dual-polarized feeds. These feeds are ridged waveguide horns and are available with frequency ranges compatible with available sweep equipment.

The choice between the types of feeds is basically one of trading frequency coverage for the ability to measure the depolarized component. The increased range (over just the 4.0-8.0 GHz) is desired, as the system will be expanded in Phase II to cover at least one additional band. With the logarithmic type feed the same antenna could be used. With the horn type feed the antenna would have to be changed along with the other RF equipment when changing operating bands. However, the dual polarization of the feed makes it possible to easily change linear polarization and to measure the depolarized return. With the addition of matched feed lines and a 90° broadband hybrid it is even possible to transmit and receive circular polarization

Shown below are three comparative antenna models.

Table 5 - Comparison of Antenna Models

Manufacturer	Freq. Range	Reflecter Dia.	Type Feed	Price
AEL	1-11 GHz	6 ft.	Logarithmic	$ 995
S-A	4.0-12.4 GHz	6 ft.	Logarithmic	$1,670
S-A	3.95-8.1 GHz	6 ft.	Dual Polarized Horn	$1,825

The AEL unit does not include either mounting hardware or feed lines, as do both Scientific-Atlanta units. The AEL unit may be provided with a remote-control feed mounting adjustment for changing polarization. This is, of course, at additional cost.

Primarily on the basis of ability to measure the depolarized return, and secondarily because of the ease of switching polarization, the Scientific-Atlanta dual-polarized horn type feed system is selected.

Table 6 shows a listing of the antenna equipment recommended for purchase.

Table 6 - Recommended Antenna Components

Manufacturer	Item	Model No.	Quantity	Price
S-A	6 ft. dia. Parabolic Reflector	22-6	1	$1,050
S-A	2 ft. dia. Parabolic Reflector	22-2	1	$ 350
S-A	Dual Polarized Horn Feed	28-3.9/6	1	$ 775
S-A	Dual Polarized Horn Feed	28-3.9/	1	$ 775
S-A	Elevation-over-Azimuth Positioner	5403-1-E	1	$3,190
S-A	Positioner Control Unit	4112	1	$ 495
S-A	Local Positioner Control	4112L	1	$ 250
S-A	Slip Ring Assembly	-16	1	$ 500
S-A	Control Cables (60ft)	5051-12	2	$ 210
S-A	Control Cables (60ft)	5051-8	1	$ 92
S-A	Indicator Unit	4422-12	1	$ 590
S-A	Rotary Joint	10-1	1	$ 300
				$8,577
An additional $700 will be spent for factory alignment of feeds and patterning of each unit at 3 frequencies.				$ 700
				$9,277

5.2 Transmitter

As shown previously, the required power is in the range of 10 watts. The power ranges and approximate price ranges of TWT amplifiers (tube and power supply) are shown in Table 7.

Table 7 - TWT Power Ranges

Power	Operation	Price
1 - 20 watt	CW	$ 2,500 - $ 5,500
100 watt	CW	$10,000 - $15,000
100 watt	pulse	$10,000 - $15,000
1 kilowatt	pulse	$15,000 and up

From the above it is seen that the 10-watt range not only suits the system, but is also the only range that likewise suits the budget. During Phase III the system will become airborne and will then, in all probability, require a 1 kilowatt power amplifier. The proposed 10 or 20 watt amplifier for the ground-based system will serve quite nicely as the driver for a later airborne system. At the upper end of the price range shown, it is possible to obtain a 20-watt amplifier with sufficient gain to be driven directly by the swept oscillator or mixer output. The lower-priced amplifiers are in reality not adequate by themselves, for most have a saturated gain of 30 db or less, which is not sufficient for this application without a low-power driver stage.

The TWT amplifier recommended for purchase is the Alto Scientific Company Model 20C4.0-8.0-Q60. This unit has a maximum output of 20 watts CW with a saturated gain of 50 db. The cost of the unit (TWT and power supply) is $5,055.

Acknowledgement: This work was supported by Project Themis (USAETL Contract DAAK 02-68-C-0089, ARPA Order No. 1079).

BLANK PAGE

Appendix C

IDECS SYSTEM DEVELOPMENT

G. Kelly, G. Dalke

Technical Memorandum 133-3
March 1968

IDECS* SYSTEM DEVELOPMENT

G. Kelly, G. Dalke

Introduction

The IDECS System consists of real-time and near real-time image processing equipment. The individual devices in the IDECS System are designed primarily for versatility of operation and interconnection to allow evaluation of different image processing techniques. The basic capabilities of the IDECS System have been added under various research contracts with the principal contributions as follows:

1. Real-time video processing devices, color matrixing, and initial research were supported primarily under NASA contract # 17-004-003.
2. A six image synchronous flying spot scanner system and general purpose real-time decision logic with color coding capabilities (the spectrance selector) are being supported under USAETL contract # DAAK02-67-C-0435.
3. Improved operator control, digital interface and the capabilities for automatic control card processing are being supported under project Themis.

The final configuration of the IDECS System as it is now envisaged is shown in Figure 1. The subsystems which are being supported by Project Themis are indicated by asterisks and are described individually in the text.

I. ANALOG-TO-DIGITAL CONVERSION SUBSYSTEM

A. Function. The function of this subsystem is to convert analog signals from the scanning densitometer or any of the flying-spot scanners into digital information. Each analog value is converted to a binary number variable between six and twelve binary digits and then stored in one or two 6-bit words on magnetic tape. This subsystem is also to have sufficient flexibility so that several channels can be multiplexed together. This would allow the repetitive sampling of each flying-spot scanner in a sequence.

---

* Acronym for Image Discrimination, Enhancement and Combination System

B. Status. The analog-to-digital converter and the magnetic tape unit are on order and should be received next month. Unfortunately, the orders were delayed for some time because of the involved procedure required to obtain approval for digital equipment. The control logic and circuits have been designed for maximum flexibility and are currently being implemented. The analog-to-digital conversion subsystem is currently scheduled for completion by July 1, 1968, and at that time a detailed report will be written. A block diagram of this subsystem is shown in Figure 2.

II. DIGITAL-TO-ANALOG SUBSYSTEM

A. Function. The function of this subsystem is to convert digital information from a digital magnetic tape, a small computer, or other digital information sources into an analog voltage. Initially this subsystem will be able to convert two binary numbers of ten bits each into two analog voltages suitable for input into a CRT display.

B. Status. The two required digital-to-analog modules have been ordered and received. The necessary control circuits are being designed and implemented. This subsystem is scheduled for completion by August 1, 1968, and at that time a detailed report will be submitted. The block diagram for this subsystem is shown in Figure 3.

III. DISPLAY INTERFACE SUBSYSTEM

A. Function. The function of this subsystem is to enter data at a slow rate into the video memory and then display this information at video rates onto the color display unit or any black-and-white monitor. Also this subsystem will eventually have the capability of sampling the video signal to produce an analog signal in the audio range which can be transmitted directly over telephone lines.

The magnetic disc video recording subsystem will be capable of the following functions.

1. Simultaneous playback of six separate signals
2. Simultaneous "real-time" recording or erasure of three data tracks, this function to be mechanically switchable to a second group of three data tracks.

3. Sequential "slow-scan" recording of any or all of the above data tracks, again by means of mechanical switching.
4. Provision for the use of a suitable electrical input signal to accomplish the functions of selective recording and erasure of data.
5. A TV keying generator with output signal compatible with the requirements of (4) and generating a rectangular pattern (as seen on a TV monitor screen) of variable dimensions and position. The same generator will supply separate, variable delay, vertical and horizontal drive outputs.
6. A video converter which accepts a standard "real-time" television input signal and uses high-speed sampling to produce a "slow-scan" output in the audio frequency range.

A block diagram of this subsystem is shown in Figure 4.

B. Status. An extensive study was made to determine the best method of storing at least two images with reasonable cost. The result was that there is no commercial unit readily available that would satisfy all requirements; however, one equipment manufacturer is willing to modify an existing product to meet most of our requirements. The video memory order has been placed but it will not be received until next fall. Some of the control circuits have been designed, although none as yet have been built. Completion date for this subsystem is tentatively set for January 1, 1969.

IV. SMALL COMPUTER INTERFACE SUBSYSTEM (Optional. To be included if funding for the computer is obtained either through THEMIS or other sources).

A. Function. The purpose of this subsystem is to interface a computer so that data may be processed and various control functions performed in "real time."

B. Status. The analog-to-digital conversion subsystem and the digital-to-analog subsystem are being designed so that only a small additional cost will be incurred if these units are connected directly to a small computer. Also, techniques have been investigated for coding data so that one frame of video information at reduced resolution could be stored in an 8K computer memory by utilizing the redundancy in the data.

V. SCANNING DENSITOMETER

A. Function. To process an image on a digital computer, it is required that the image information be changed to an analog signal. This can be done by using a scanning densitometer which consists of a rotating and translating glass drum with a photomultiplier tube inside. The image is placed around the glass drum. A light source placed above the drum shines through the image into the photomultiplier tube. The output of the photomultiplier is an analog signal proportional to the grey scale of the image. The translation of the image and the spot size are set so that 20 line pairs/mm are produced.

B. Status. The basic unit has been designed and built; however, the control circuits have not been designed.

VI. MASTER VIDEO CONTROL

A. Function. To evaluate the functions and subsystems individually and combinationally, it is necessary that the IDECS system have the capability to connect and disconnect any device. This is the function of the video control. By switching the video control, various combinations of input and processing devices are presented at the output devices. The IDECS block diagram (Figure 1) shows the input, processing, and output devices that are connected to the video control.

B. Status. The video control has been designed and constructed but has not been connected into the system.

VII. POSITION AND SIZE DEVICES

A. Function. In order to combine and process more than one image, it is necessary that the images be geometrically congruenced. This can be accomplished by controlling the raster on the flying spot scanning units. The position and size devices control this raster.

The positioning device will translate and rotate the raster, causing the image on the display to move horizontally, vertically, and angularly. The size device will expand or contract the raster; therefore, the size of

the image on the display is controlled horizontally and vertically. The position and size devices are shown in Figure 5.

B. Status. Both the position and size devices have been implemented for all six flying spot scanning units.

VIII. SYNCHRONIZATION DEVICE

A. Function. For the information on the input and output devices to correspond, it is essential that these devices scan in unison. The synchronization device accomplishes this by sending pulses to the horizontal input of the sweep circuits at a rate of 15,750 Hz and to the vertical input of the sweep circuits at a rate of 60 Hz. The synchronization device is shown in Figure 5.

B. Status. A synchronization generator is in operation to match the flying spot scanning units to the displays.

IX. MONITOR DISPLAY

A. Function. The monitor display will exhibit any input or processing device when connected properly through the master video control. Since it will be mounted in the operator's console, it will be convenient for use in congruencing several images. It will also be used in calibrating the flying spot scanning unit and other circuits.

B. Status. A 10" cathode ray tube capable of 20 MHz has been ordered. A Tektronix oscilloscope is operational as a monitor display at present.

X. COLOR DISPLAY

A. Function. The color display is used to convert video signals proportional to grey scale on photographs or radar images into a color which varies in intensity and hue.

B. Status. The color display is operational.

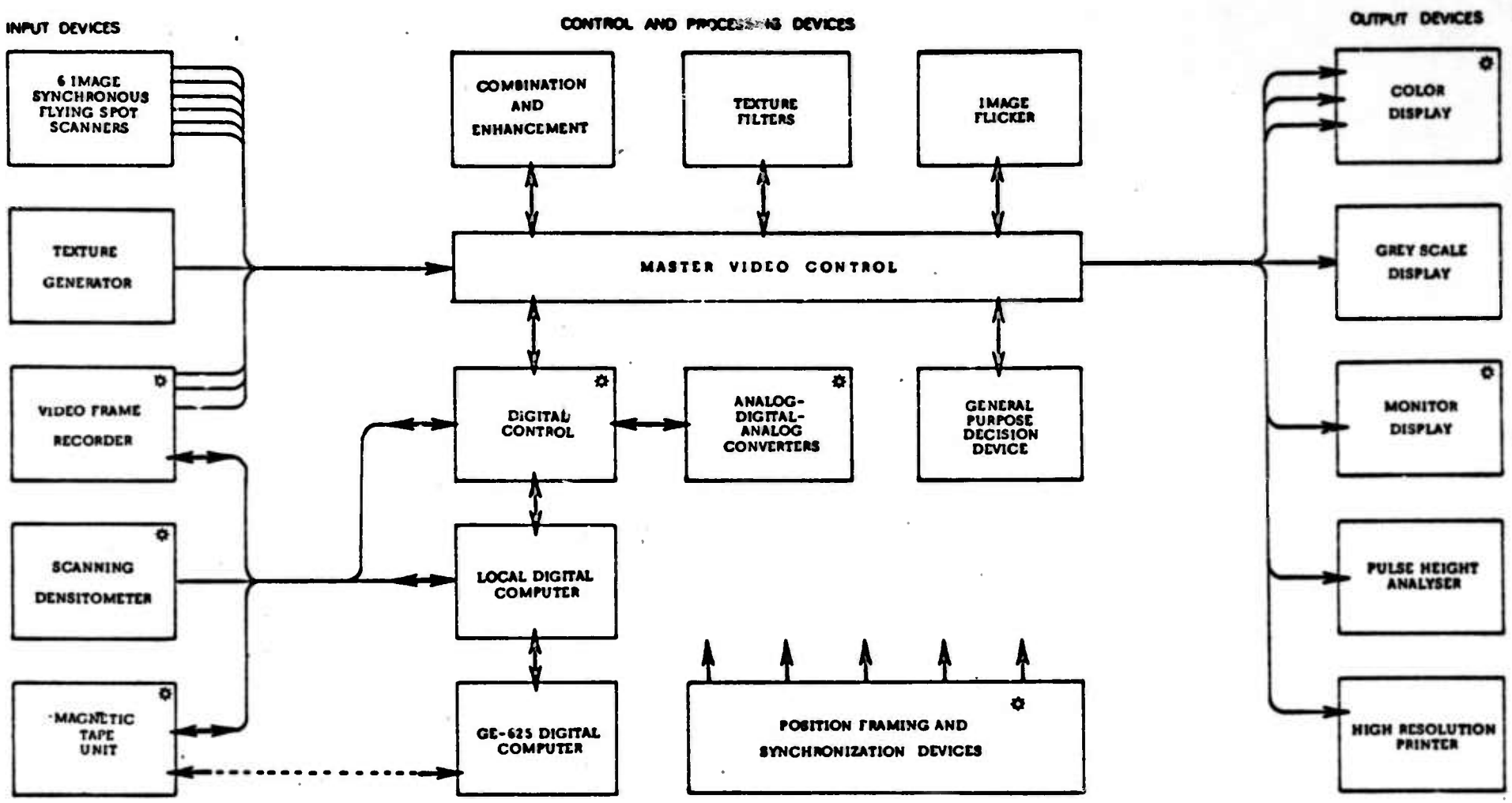

Figure 1. IDECS SYSTEM DIAGRAM

* EQUIPMENT SPONSORED BY PROJECT THEMIS

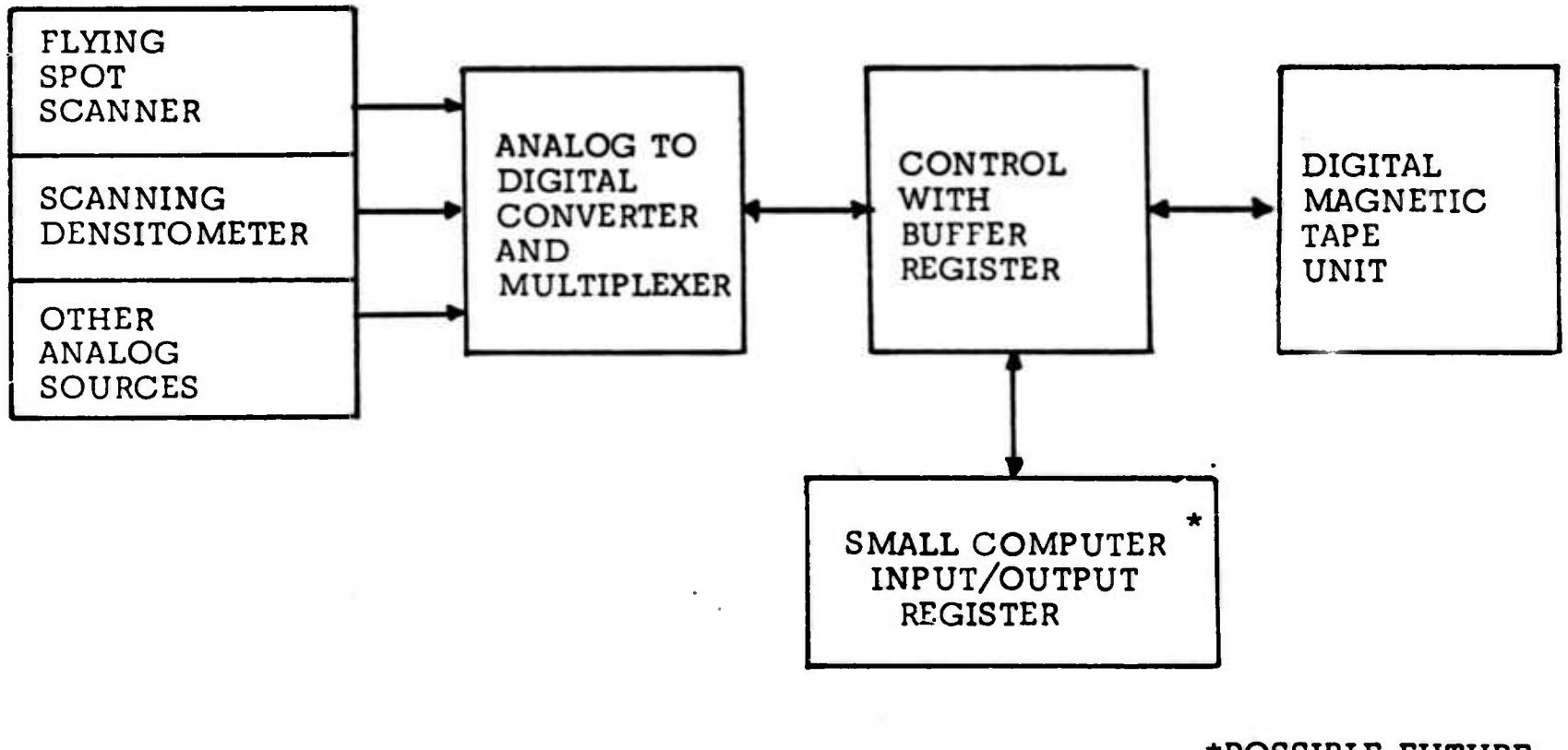

Figure 2. ANALOG TO DIGITAL CONVERSION SUBSYSTEM

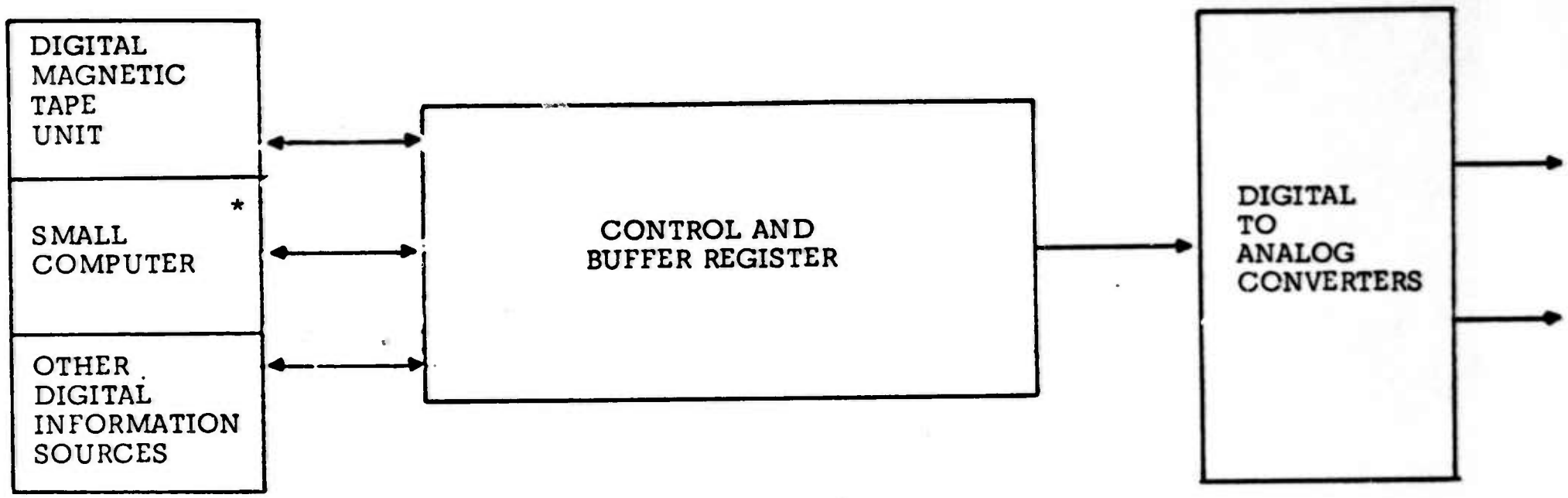

Figure 3. DIGITAL TO ANALOG CONVERSION SUBSYSTEM

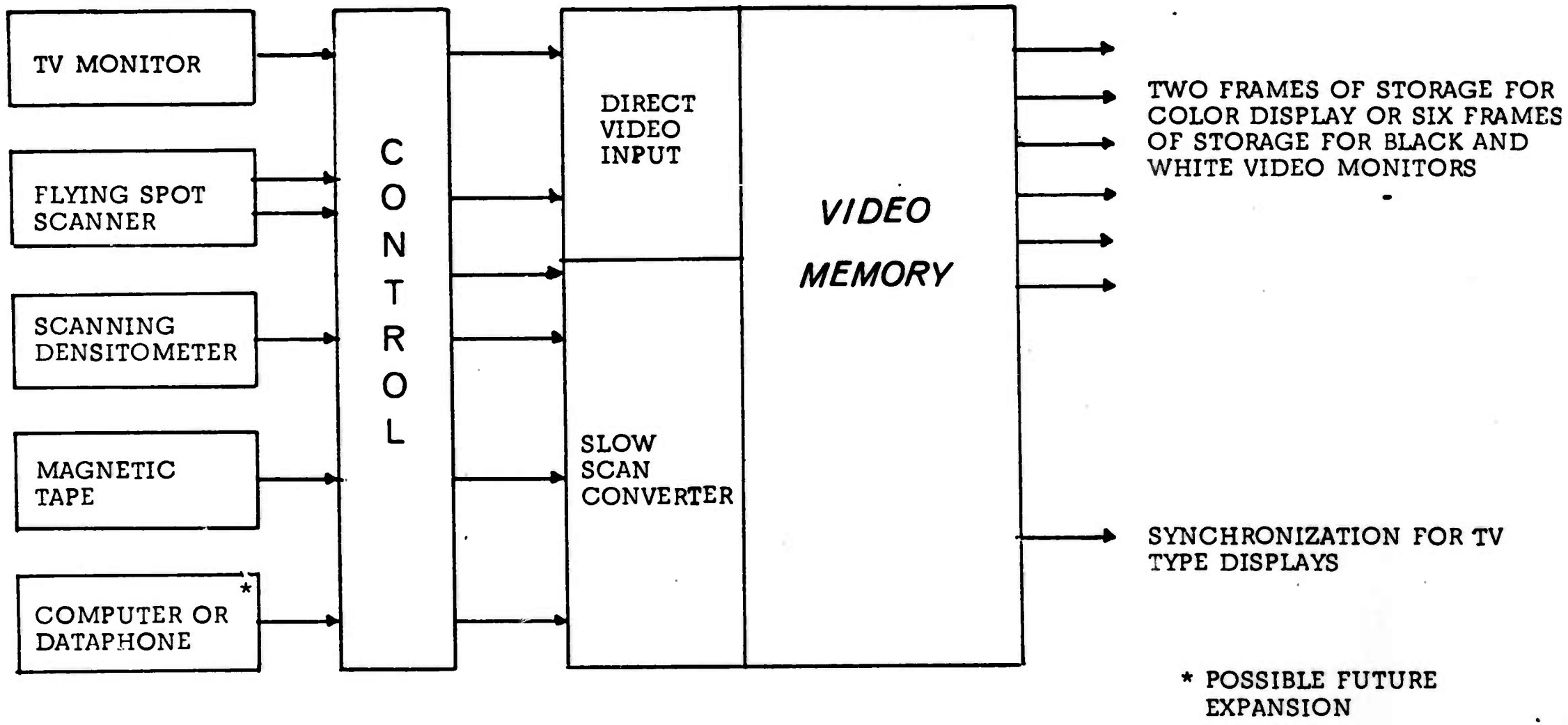

Figure 4. VIDEO STORAGE SUBSYSTEM FOR IDECS

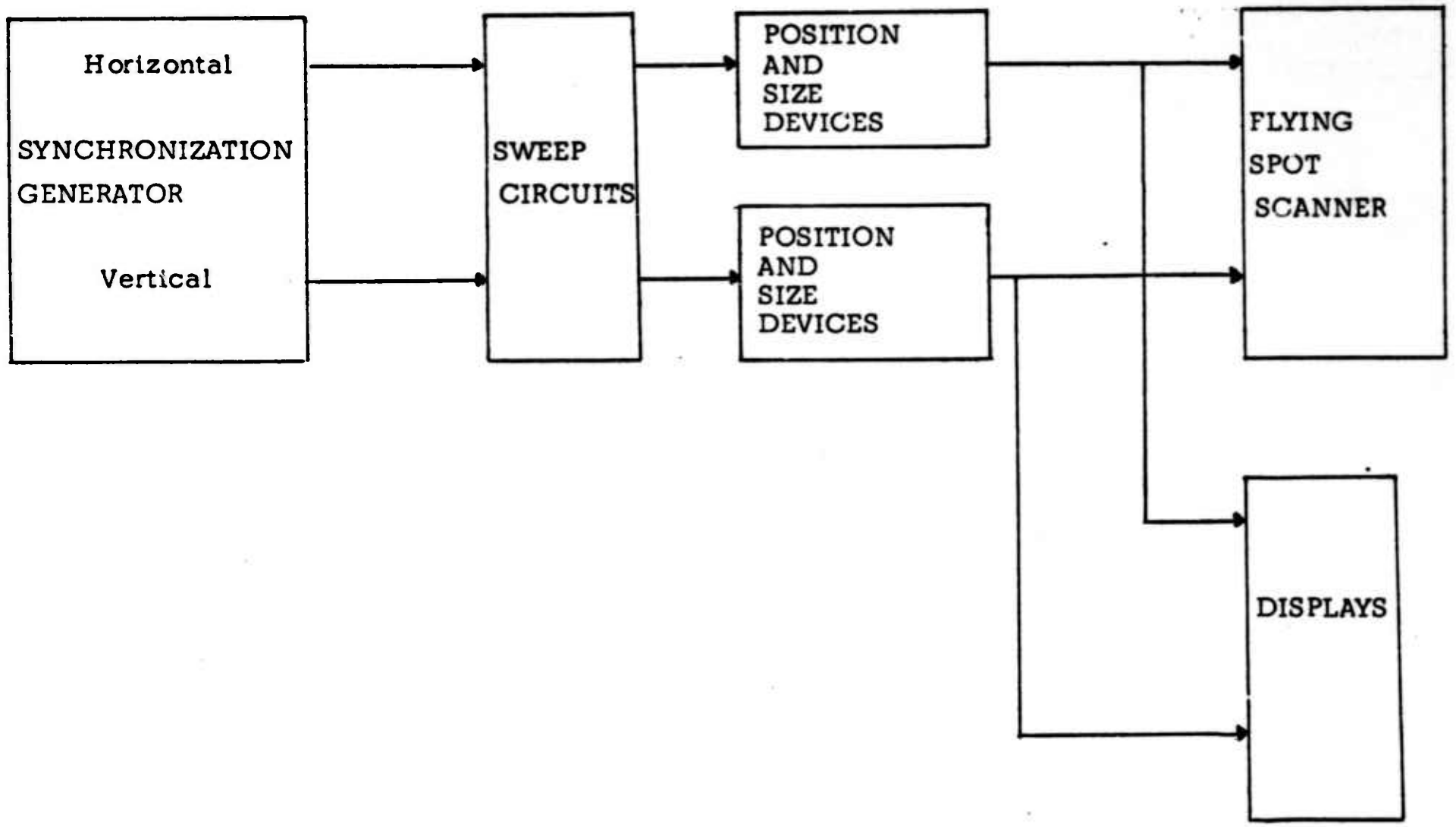

Figure 5. POSITION, SIZE, AND SYNCHRONIZATION DEVICES

Appendix D

ADAPTIVE PATTERN RECOGNITION OF AGRICULTURE IN WESTERN KANSAS BY USING A PREDICTIVE MODEL IN CONSTRUCTION OF SIMILARITY SETS*

R. M. Haralick

* This report was presented at the Remote Sensing of Environment Symposium at the University of Michigan, Ann Arbor, Michigan, April 16-18, 1968.

BLANK PAGE

Technical Report 133-3
March 1968

ADAPTIVE PATTERN RECOGNITION OF AGRICULTURE IN WESTERN KANSAS BY USING A PREDICTIVE MODEL IN CONSTRUCTION OF SIMILARITY SETS

R. M. Haralick

Center for Research Inc., Engineering Science Division
University of Kansas
Lawrence, Kansas

ABSTRACT

Automatic classification of remote sensed data is a necessity since satellite remote sensors currently on the design board are expected to gather more data each hour than could be analyzed by traditional methods in a year. A machine which could determine the structure of the sensed environment by grouping together similar data signals and relabeling these signals with the same label would reduce both storage requirements and transmission times for the remote sensor in addition to doing pattern recognition in space or on the ground.

The paper is introduced by a discussion concerning the adaptive process of how predictive models of an environment can be generated. This discussion leads into a mathematical description of such a model for pattern recognition. The model was programmed for the GE 625 and four possible combinations of transmitted and received like and complementary polarized K-band radar images of agriculture in western Kansas were used as data.

Results confirm that various categories of vegetation such as alfalfa, grain sorghum, wheat stubble and corn cannot be distinguished from one another on the basis of their structure within the radar data. This suggests that for pattern recognition purposes, certain categories may be expanded with little or no information loss and an increase in efficiency of the pattern recognition process. Further it also suggests that if the investigator wants to distinguish between the confused categories such as alfalfa, grain sorghum, wheat stubble and corn, an additional sensor must be used which can make the distinction.

Non-imaging sensor systems such as geiger counters magnetometers, gravity gradiometers, spectrometers, photometers, and particle counters at present are collectively gathering a quarter billion bits of information per day. Some planned high-resolution imaging systems are expected to gather by themselves over three billion bits of information per day. This makes automatic pattern recognition of remote-sensed data a necessity. Over one hundred thousand analog tapes of remote sensed data are stored in ESSA's library and about two hundred additional such tapes are created daily. The only way such a great volume of information can be utilized is by automatically recognizing the pattern of relationships which exist within the data.

A pattern-recognition system is one kind of system which determines the relationship of category or type. We will endeavor to describe an adaptive pattern-recognition system, which needs no teacher, is easily built, and is able to automatically classify data. The system we describe has been simulated and tested with agricultural radar images, and the results of the test will follow the description.

A pattern-recognition system takes patterns for inputs and produces outputs which are either direct symbols for categories or binary M-tuples which form a code for categories. The input

patterns form N-tuple of measurements (or sometimes their binary code) taken of some environment. Each component of the N-tuple could represent the output of one sensor system. Figure 1 illustrates the pattern recognition process.

We begin with a few elementary definitions. A system is a structured device which produces an output related to its past and present inputs according to some deterministic or probabilistic rule. The rule is called the structure of the system. If the output is related only to the present input, the system is memoryless. If the output is related to both the past and present input, the system has memory. If the form of the rule at time t depends on some of the inputs before time t, then the system is changeable; otherwise, the system is fixed.

An example of a memoryless fixed system could be a radio, the electromagnetic field at its antenna being considered the input and the acoustical field generated by its loudspeaker being considered the output. It is memoryless because the output does not depend on previous inputs: only on the present input. Past radio programs do not influence the radio's present operation. An example of a fixed system with memory could be an adding machine, the buttons pushed on the keyboard register being considered the input and the number displayed on the carriage register or paper tape being considered the output. The adding machine has memory of the sum of all the past inputs. Examples of changeable systems can be found in any of the self-learning, self-organizing or adaptive systems.

A pattern-recognition system can either have a memory or be memoryless, and can be fixed or changeable. If the system changes its own structure the change will, if it is to be meaningful, depend on the input-pattern sequence, so that the present state of structure will provide some indication of past input history; hence, a self-changeable system is a system with memory. Fixed pattern-recognition systems have limited use, since the precise transformation from input pattern to category type must be known beforehand. With the present state of the art for imaging sensors, prior knowledge is a strict requirement. Radar images, for instance, can be calibrated at best to only 3 db from the initial transmitted signal to the final developed image. Different pictures taken with the same sensor system of exactly the same environment at two different times can vary by a two-to-one gray scale variation. A fixed pattern-recognition system would have little use here, because the data has an unknown bias. All of its information is relative to the bias levels. Thus, what is needed is some kind of pattern recognition system which can change or adapt according to the biases and stochastic non-linearities of the sensor system and according to the structure of the environment sensed, so that the structure of the pattern-recognition system is optimum for the kind of job it is supposed to do.

The set of all logically possible measurements we will call measurement space. To each point in measurement space a pattern-recognition system assigns one category, so that the set of points which are assigned to each category forms a cell in a partition of measurement space, as illustrated in Figure 2.

The pattern-recognition problem is usally presented as follows: The investigator forms I training sequences S_i, $i = 1,\ldots I$ of measurements such that the measurements in the i^{th} sequence all represent measurements of objects which the investigator knows are in the i^{th} category. The i^{th} sequence actually is a sample from the i^{th} population, which is a population of objects in the i^{th} category. It is possible for the same measurements to occur in several sequences so that it is a problem to decide what category to assign to such measurements. Given the sequence S_i, $i = 1,\ldots I$, the investigator would like to find a decision rule (equivalence relation) which partitions measurement space into I cells so that the i^{th} cell contains the set of measurements which are most representative of the i^{th} category. A pattern-recognition system is a system which has such a decision rule for its structure. Since the structure of the system is determined from the training sample we may say that the system has memory relative to the training sample.

With the problem posed in this way, there is no guarantee that the categories which the investigator makes up are really representative of the structure of the measurement space. Hopefully, the categories and sensors chosen present each category as an isolated cluster in the measurement space. However, this does not always happen: sometimes there are two clusters in the measurement space which the investigator groups together as the same category. In this case, structural information of the measurement space is lost, since once categorization is done there can be no further distinctions made between these two clusters. Sometimes what the investigator calls two categories actually form only one cluster in the measurement space. In the first case the investigator is losing information, and in the second case he is wasting effort.

On the basis of these ideas we will restate the pattern-recognition problem. Given an empirical probability distribution on measurement space, we would like to find a rule (equivalence rela-

tion) which partitions measurement space so that each cell of the partition represents a cluster or similarity set in measurement space. Each point in such a set is similar to every other point in the set because they all belong to the same grouping or cluster.* Pattern recognition, approached from this perspective, becomes a method of handling data in terms of families of aggregates, each aggregate being a cluster of points.

The information which a measurement conveys to the investigator is not contained in the precise values of the components of the N-tuple, for those values, if perturbed just a little, would still usually give a measurement conveying as much information to the investigator as in the unperturbed case. Rather, the information which a measurement conveys to the investigator is contained in the aggregate family to which it belongs.

We illustrate this idea about information: suppose there are five different kinds of objects or occurrences in the environment sensed, Further suppose that to each object or occurrence there corresponds an ideal measurement, the measurement which would be made if the environment were not stochastic and if the sensor system were accurately calibrated, completely linear, and noiseless. However, due to all the conditions mentioned, measurements of the same object or occurrence will deviate a little from the ideal, distributing themselves around the ideal as illustrated in Figure 3. Since these deviations were caused by the random effects of the environment, thermal noise in the sensors, etc., the investigator is not interested in their exact values. In a classification problem the only item of interest is: which object or occurrence caused the measurement we made--i.e., which aggregate family does the measurement come from?

A pattern-recognition system which would handle the data in terms of aggregate families would have large application to the remote sensing field. Without any knowledge or training from the investigator, the system could transmit back the occurrence of an aggregate family instead of the actual measurement made. This would yield a large saving of channel capacity and preserve the information in the structure of the environment sensed.

The problem, then, is how to go about designing such a system. The key to this lies in our understanding of similarity. Similarity of measurements means that the difference between the measurements is statistically unimportant. The reason the difference is unimportant is that two measurements which are similar both belong to the same cluster (to the same aggregate family), and what characterizes the location of the cluster also characterizes the location of the measurements within it. This is the basis of similarity.

Clusters could be located by finding subsets of measurement space whose general location also characterizes the measurements within it. Location implies a given metric, however, the general problem may have a measurement space which can have no metric on it at all. The generalization of location may be easily done with measures of concomitant variation, an example of which follows. Suppose we have in mind a subset which we think is a cluster. Every time a measurement occurs which is in the subset, we will designate it "a." Every time a measurement occurs which is not in the subset, we will designate it "b." Here there is a 100% concomitant variation of the measurements in the cluster designated by the letter "a." If we wanted to remember these associations, we could store all those points designated by the letter "a" in one place in memory and those points designated by the letter "b" in another place in memory. However, if the measurement space has high dimensionality, as in multi-sensor systems, it would have so many points within it that storing all the associations would be almost impossible if not a waste of machinery and money.

Thus we divide each measurement into a number of characteristics, just as we could divide the perception of a chair into a number of characteristics which describe it. For the chair, these might be:

characteristic 1-2	-- number of legs, 3 or 4
characteristic 3	-- back or no back
characteristic 4	-- if back, is it hard or soft
characteristic 5	-- soft or hard seat
characteristic 6	-- arms or armless
characteristic 7-14	-- color of upholstery: red, orange, yellow green, blue, indigo or violet
characteristic 15-18	-- material of upholstery (cotton, leather, or plastic)

*We will use the concepts cluster and similarity set interchangeably. When the emphasis is on geometric compactness we will use the concept cluster. When the emphasis is on the similarity of the points within a cluster, we will use the concept similarity set.

Now we try to find the association between the letter "a" and each one of the characteristics. If "a" is always associated with the occurrence of the i^{th} characteristic, then a measure of concomitant variation between the letter "a" and the i^{th} characteristic would attain its maximum. If it is never associated with the occurrence of the i^{th} characteristic, then a measure of concomitant variation between the letter "a" and the i^{th} characteristic would attain its minimum. To find the total measure of concomitant variation between a measurement and the letter "a," we could appropriately sum the individual measures between each of the characteristics and the letter "a." If we wanted to compare the general characteristics of the subset (associated with the letter "a") with any one of the measurements belonging to it, we could use the measure of concomitant variation backwards. We could ask: given that we have a measurement which has been assigned the letter "a," is each characteristic more likely to be associated with the letter "a" or is it more likely not be associated with the letter "a"? To answer the question, we could look at the measure of concomitant variation between the i^{th} characteristic and the letter "a." If it is larger than its neutral concomitant-variation value, then we could answer by saying that the i^{th} characteristic is indeed associated to some extent with the letter "a"; if it is less than its neutral concomitant-variation value, then we could answer by saying that the i^{th} characteristic is not associated with the letter "a." Using such a measure of concomitant variation, a system could find a cluster by finding a subset of measurement space for which the general characteristics of the subset are sufficiently related to its measurements. This relatedness is a relation of prediction or estimation.

A subset of measurement space can be called a cluster if we are able to predict or estimate the kind of measurements which are representative of it from the characteristics we have chosen. The kind of system we seek, then, is one which produces an output from which it can predict the input measurement or some similar measurement. Such a system is an adaptive system with a predictive criterion.

An adaptive system is one which examines its own output, evaluating it according to some built-in criterion, and then modifies its structure in a way which tends to improve the evaluation of the output. A predictive criterion is one which attaches high value to the ability of the system to predict or estimate the input pattern or some similar pattern, given only the output.

We not proceed to design a system of the type we just described. It is a <u>two-layered</u>* adaptive system with a predictive criterion, First the following definitions are in order: let $L_i = \{l_{ij}\}_{j=1}^{N_i}$, $i = 1,\ldots K$ be the set of possible quantized measurements from the i^{th} sensor in a total of K sensors. Measurement space G is the set of all possible measurements; $G = L_1 \times L_2 \times,\ldots \times L_K$. For any subset A of G, $A \subset G$, define $A_d = \begin{cases} A & \text{when } d = 1 \\ A^c & \text{when } d = -1 \end{cases}$. Construct characteristic or feature sets E_i, $i = 1,\ldots K$ such that the probability of E_i is strictly greater than zero $P(E_i) > 0$, and for every $g \in G$ where $P(g) > 0$, there exists a vector $\delta(g) = \begin{pmatrix} \delta_1 \\ \delta_2 \\ \delta_N \end{pmatrix}$ such that $\{g\} = \bigcap_{i=1}^{N} E_{i\delta_i}$. Let the pattern set Δ be the set of all such possible vectors. A pattern here, is considered to be, not the measurement vector itself, but a binary-coded N-tuple of the measurement vector.

Of course, measurements are not naturally binary but usually analog. At some point in the recognition process, if only during transmission the analog measurement is quantized and converted to binary form. The binary code is determined by using information-theory techniques on channel capacity and noise distribution. However, the binary N-tuples which we have called patterns have little to do with such transmission codes. Rather, the binary codes which form the patterns have to do with feature or characteristic sets. We illustrate this in Figure 5, where the large rectangular area represents measurement space. The fine partition on measurement space represents the quantizing. Each measurement which occurs within a particular cell of the partition will have the same quantized value. The outlined area represents a connected subset of measurement space. Each point within the subset is close to other points within the subset. Such a subset can be called a feature or characteristic set, since it characterizes in this particular case what we can loosely call the upper-left-hand corner of measurement space. If a measurement is made which belongs to the characteristic subset, we can code the i^{th} component of the pattern corresponding to the measurement as a binary 1; otherwise, as a binary 0.

* The term layer is used in accordance with the terminology Rosenblatt developed for his perception devices. In the perception, a layer refers to a grouping of associative units which function together.

This kind of coding is quite different from a regular binary code. Suppose that the measurement vector has two components and that each component is bounded by 0 and 4 inclusive. Measurement space quantized by unit intervals is illustrated in Figure 5. A regular binary code for the quantized measurement can be formed as follows:

(0,0)	00 00	(2,0)	10 00
(0,1)	00 01	(2,1)	10 01
(0,2)	00 10	(2,2)	10 10
(0,3)	00 11	(2,3)	10 11
(1,0)	01 00	(3,0)	11 00
(1,1)	01 01	(3,1)	11 01
(1,2)	10 01	(3,2)	11 10
(1,3)	01 11	(3,3)	11 11

The first two binary bits represent the binary code for the first component while the last two binary bits represent the binary code for the last two components.

Figures 6, 7, 8, and 9 illustrate the characteristic sets which would correspond to the first, second, third and fourth binary bits in the code.

In general such codes do not have corresponding characteristics which actually characterize a connected neighborhood in measurement space. In fact, the 2nd and 4th bit just indicates whether the first and second components are even or odd. Whether a quantized measurement is even or odd does not have the slightest bearing on recognizing categories such as corn or wheat.

For any S-dimensional real vector $V = \begin{pmatrix} v_1 \\ v_2 \\ v_S \end{pmatrix}$ let the function Sgn: $R^S \rightarrow \{-1, 1\}^S$ be defined by Sgn $(V) = \begin{pmatrix} \mu_1 \\ \mu_2 \\ \mu_S \end{pmatrix}$ where $\mu_i = \begin{cases} +1 \text{ if } v_i - \bar{v} > 0 \\ -1 \text{ if } v_i - \bar{v} \leq 0 \end{cases}$, $i = 1, \ldots S$ and $\bar{v} = \frac{1}{S} \sum_{i=1}^{S} v_i$. Let $\eta = \begin{pmatrix} \eta_1 \\ \eta_2 \\ \eta_M \end{pmatrix}$ be the binary $\{-1,1\}$ code for the output categories. The form of the structure for the first layer of the adaptive system is defined by the equation $\eta = \text{Sgn}\ (Q^T S)$ where $Q = (q_{ij})$ is the matrix of concomitant variation coefficients and δ is the input pattern vector. The first layer is illustrated in Figure 10.

Each q_{ij} is a measure of the concomitant variation between the i^{th} pattern characteristic with the j^{th} similarity set characteristic. If it generally happens that when a pattern has the i^{th} characteristic, the similarity set into which it is classified has the j^{th} similarity set characteristic, then q_{ij} will be positive. If it generally happens that when a pattern does not have the i^{th} pattern characteristic, the similarity set into which it is classified does not have the j^{th} similarity set characteristic, then q_{ij} will also be positive. In the other two cases q_{ij} will be negative. Thus $\sum_{i=1}^{N} \delta_i q_{ij}$ is an overall measure of concomitant variation between the input pattern δ and the j^{th} similarity-set characteristic. If this sum is great enough, the system will decide that the similarity set to which it will classify δ will have the j^{th} similarity set characteristic: otherwise it will decide that it does not.

The binary $\{-1,1\}$ vector η is the output of the system. η is a function of the input δ and the present Q matrix, which is conditioned by past inputs. The system tests its output η by forming a prediction or estimation of δ. This is done in the second layer of the system whose structural form is described by the equation $\hat{\delta} = \text{Sgn}\ (Q\eta)$, and is illustrated in Figure 11. The vector $\hat{\delta}$ is the system's prediction or estimation of δ, the input pattern. The output is evaluated by comparing δ and $\hat{\delta}$ component by component. The system then modifies the appropriate elements in the Q matrix in a way which tends to improve the prediction or estimation, $\hat{\delta}$. An adaptation rule of the sort $q_{ij}(t+1) = q_{ij}(t) + \epsilon\, \delta_i\, \eta_j\, |\delta_i - \hat{\delta}_i|$ can produce just such a change. Suppose $\delta_i = \hat{\delta}_i$, then there would be no change since $|\delta_i - \hat{\delta}_i| = 0$. Suppose $\delta_i = 1$ and $\hat{\delta}_i = -1$, an error situation. In order

for this to happen, $\sum_{K=1}^{M} q_{ik}\,\eta_k$ is small; therefore, the system increases each term in the sum by an appropriate change in each q_{ik}, $k = 1,\ldots M$. To increase each term $q_{ik}\,\eta_k$ the system must increase q_{ik} if $\eta_k = 1$ and decrease q_{ik} if $\eta_k = -1$. Suppose $\delta_i = -1$ and $\delta_i = 1$, also an error situation. In order for this to happen, $\sum_{k=1}^{M} q_{ik}\,\eta_k$ is large; therefore, the system decreases each term in the sum by an appropriate change in each q_{ik}, $k = 1,\ldots M$. To decrease each term $q_{ik}\,\eta_k$ the system must decrease q_{ik} if $\eta_k = 1$ and increase q_{ik} if $\eta_k = -1$. We may summarize these changes in the table of figure 12 and compare them with the change $\epsilon\,\delta_i\,\eta_j\,|\delta_i - \hat{\delta}_i|$ produces.

An adaptive pattern-recognition system of the kind just described was simulated with the GE-625 computer, using K-band radar imagery with polarizations HH, HV, VV taken in July 1966 over agricultural areas in western Kansas. Since automatic image digitization equipment was not available, a few line scans across each field were manually taken at random with a micro-densitometer. The average of these scans was used as an estimate for the average radar return for each field. A total of 253 such fields consisting of land-usage categories of bare ground, wheat stubble, wheat stubble-weeds, wheat stubble-mulch, weeds, corn, alfalfa, grain sorghum, pasture, and sugar beets were examined.

Measurement space in this example consisted of all possible three-tuples, the first component being the average return from HH, the second component being the average return from HV, and the third component being the average return from VV. From our data the minimum, M_i, and the range, R_i, (maximum minus the minimum) for the i^{th} component, $i = 1, 2, 3$ was determined. The characteristic sets were defined as:

$$E_{ijkm} = \left\{ X = \begin{pmatrix} x_1 \\ x_2 \\ x_3 \end{pmatrix} \;\middle|\; M_i + \frac{jR_i}{10} \le x_i \le M_i + \frac{(j+4)R_i}{10} \text{ and } M_k + \frac{mR_k}{10} \le x_k \le M_k + \frac{(m+4)R_k}{10} \right\},$$

$i = 1, 2$; $j = 0,\ldots,5$; $k = i+1, 3$; $m = 0,\ldots,5$. The geometric configuration of the characteristic sets are displayed in figure 13.

The adaptive pattern-recognition system worked as follows. For each iteration a measurement from the set of 253 measurements was chosen at random. Given the definition of the characteristic sets, the system determined the δ vector which corresponded to the randomly chosen measurement. Via the first layer of the adaptive system, η, a 3 x 1 binary $\{-1,1\}$ vector, was computed from Sgn $Q'\delta$. Via the second layer of the adaptive system $\hat{\delta}$, the prediction of δ given η, was computed from Sgn $Q\eta$. The system then compared δ and $\hat{\delta}$ and reinforced the elements q_{ij} of Q appropriately and started another iteration.

The reinforcement parameter ϵ was chosen at .002. Values of .009 and .02 were also tried but they made little difference in the final classification. (There was a random shift of at most seven points with the different values of ϵ.) The cycling of iteration after iteration was kept up until the total classification for all the data points, based on the updated Q matrix, did not change for more than 30 cycles. It took 189 cycles to reach this situation.

Figure 14 illustrates a scattergram of the data, and figure 15 illustrates a scattergram of the data coded by their respective land-usage categories as determined from ground truth. The axes of the scattergrams are the first two normalized eigenvectors of the covariance matrix for the data. These axes are usually called the first two principal axes. A frequency chart, as determined after 189 cycles, of similarity sets versus the land-usage categories is shown in figure 16. Similarity sets II and III are closely related, their difference mainly being that III has all the corn while II has most of the wheat stubble-weeds. For illustration and basic interpretation purposes we group together similarity set II and III as in the chart of figure 17. If we now group together those categories which appear to occur in mostly the same similarity sets, we will obtain the chart in figure 18. Scattergram of the similarity sets (clusters) which the adaptive system determined is shown in figure 19.

Bare ground had formed a cluster of low returns; wheat stubble, wheat stubble-weeds, wheat stubble-mulch, and pasture formed a cluster of medium-low returns which meshed with each

other almost completely and overlapped with bare ground; alfalfa, grain sorghum, weeds and corn formed a cluster of medium returns; and sugar beets formed a cluster of high returns. The chart in figure 20 shows the conditional probability of the category group given the similarity set. The purpose of this chart is to arrive at some quick intuitive interpretation of the goodness of the results. Basically the chart indicates that the similarity sets correspond to the category groups with about an 85% probability.

These results show that, without a priori knowledge, categories of vegetation such as:

(1) wheat stubble, wheat stubble-weeds, wheat stubble-mulch, and bare ground
(2) grain sorghum, corn, weeds, and alfalfa

cannot be distinguished from one another solely on the basis of their structure within the K-band radar data taken during the month of July. However, from empirical knowledge, we know the returns from bare ground are probably less than the returns from wheat stubble, wheat stubble-weeds and wheat stubble-mulch; therefore, we may further partition the cluster of low returns into two parts, the first part being bare ground and the second part being the wheat stubble, etc. Also, we know that the returns from alfalfa are probably less than the returns from corn, so that we may partition the cluster of medium returns into two parts, the first part being alfalfa and the second part being corn. It is impossible to separate grain sorghum and weeds from any part within their cluster, so if they must be recognized, an additional sensor must be used which can detect them separately from the returns of other categories.

The confounding of categories within a cluster leads to the conclusion that a pattern-recognition system of the type we have described should preserve to some extent the information contained by the locality of the pattern within the cluster. This leads to a pattern-recognition system which finds clusters and then sets up a principal coordinate axis for each cluster. The output of such a system would consist of two pieces of information, the first being the cluster in which a pattern occurs and the second being the projection of the pattern onto the principal axis of that cluster. Figure 21 illustrates the principal axis idea. It would allow for a natural categorization by the clusters and a finer categorization using the principal axes, where the finer categorization depends on our empirical knowledge of the environment sensed.

The operation of such a system would closely correspond to the way our perception system works. When we see an environment we first see the environment in an appropriate general frame of reference. Then we examine the environment in fine detail from the perspective of this frame of reference. The appropriate general frame of reference is analogous to the determination of cluster (similarity set). The finer examination is analogous to the determination of the location of pattern relative to the cluster (similarity set), i.e. the projection of the pattern on the principal axis for the cluster.

ACKNOWLEDGMENTS

Financial support for this study was provided by Project Themis (DoD), DAAK02-68-C-0089; the financial support and cooperation of the University of Kansas Computation Center is also gratefully acknowledged.

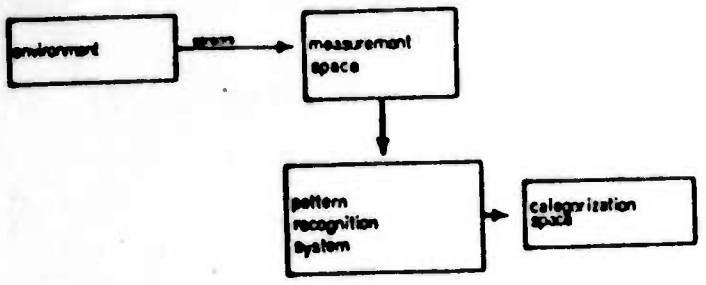

FIGURE 1. PATTERN RECOGNITION PROCESS

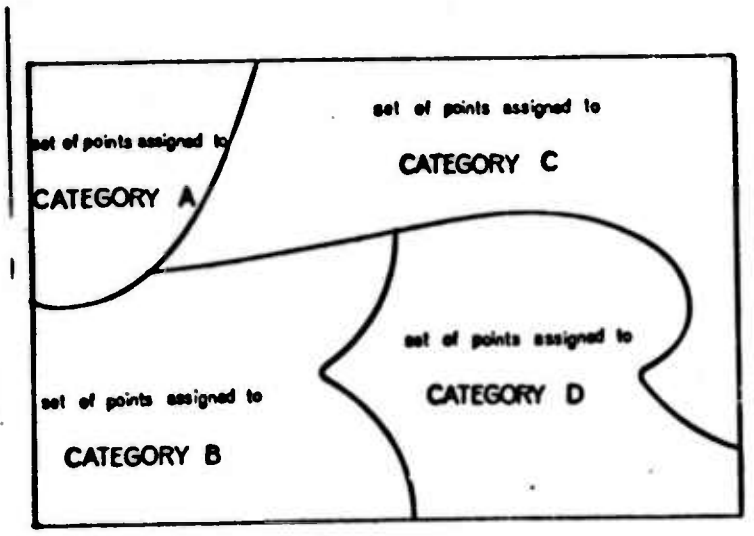

FIGURE 2. MEASUREMENT SPACE AND CATEGORIES

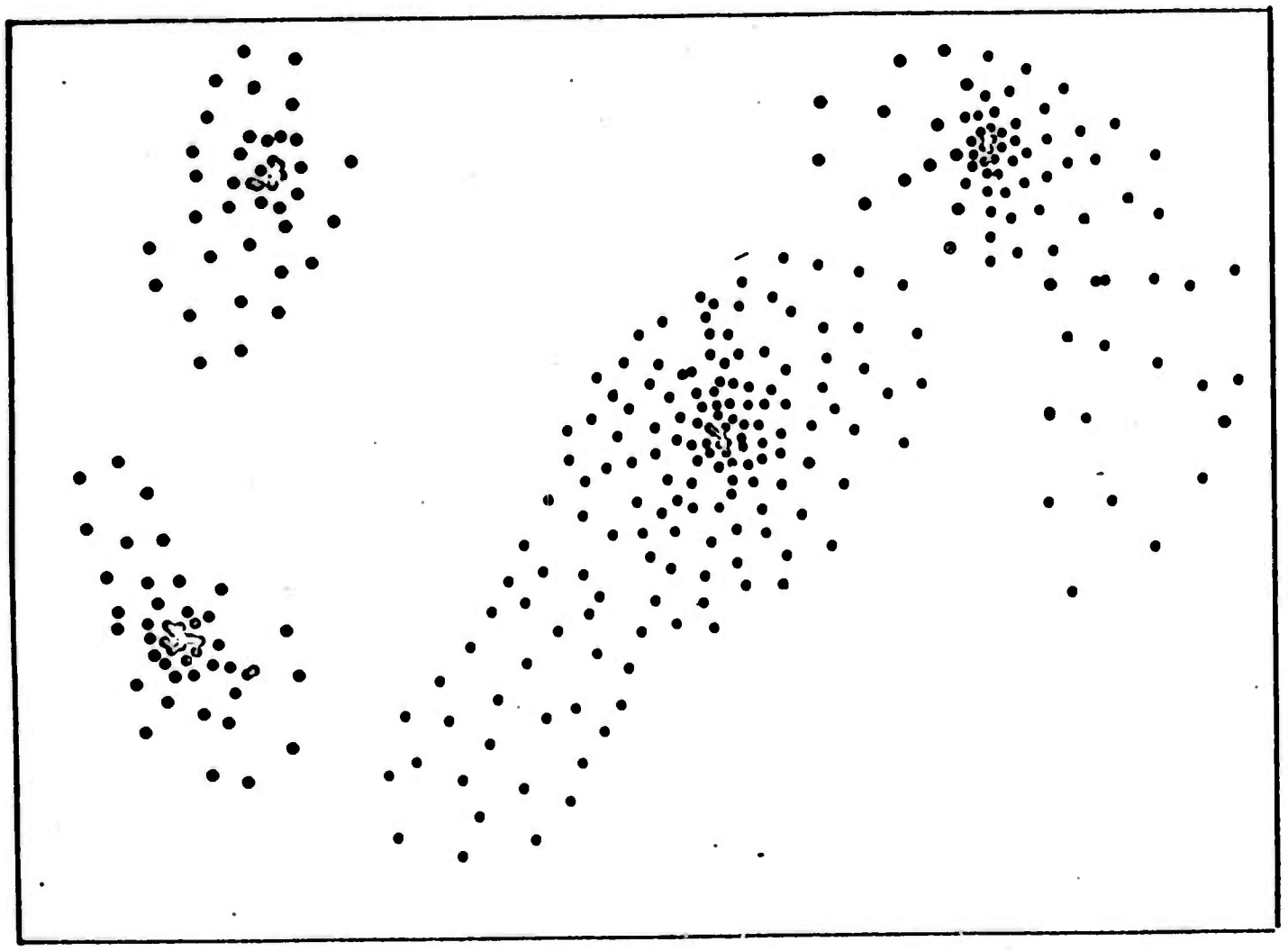

FIGURE 3. SCATTERGRAM OF MEASUREMENTS OF STOCHASTIC ENVIRONMENT WITH FOUR OBJECTS

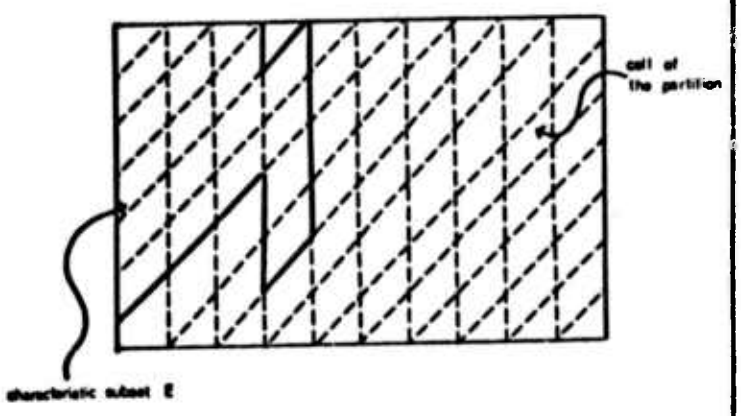

FIGURE 4. MEASUREMENT SPACE QUANTIZED

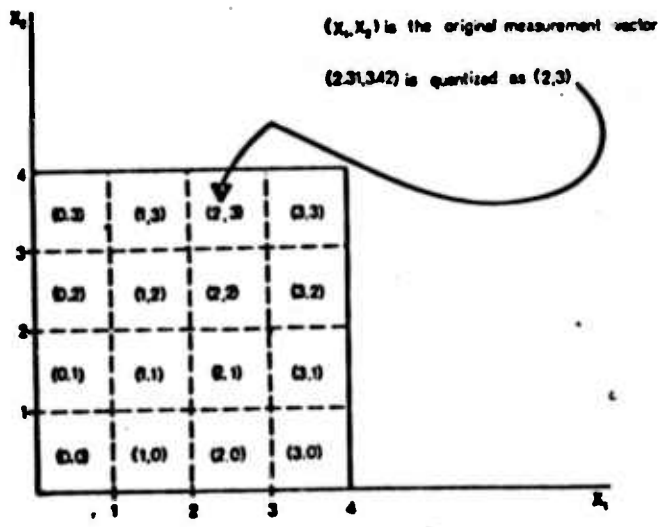

FIGURE 5. MEASUREMENT SPACE QUANTIZED BY UNIT INTERVALS

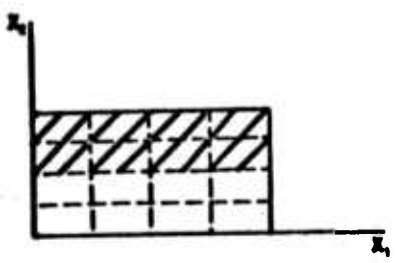

FIGURE 6. CHARACTERISTIC SET FOR FIRST BINARY BIT

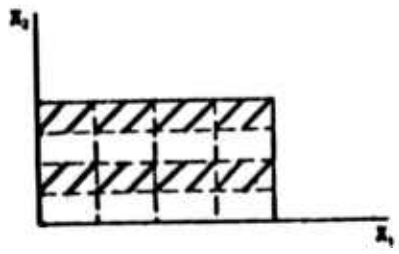

FIGURE 7. CHARACTERISTIC SET FOR SECOND BINARY BIT

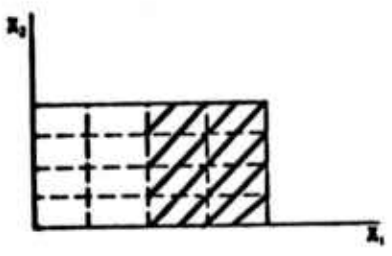

FIGURE 8. CHARACTERISTIC SET FOR THIRD BINARY BIT

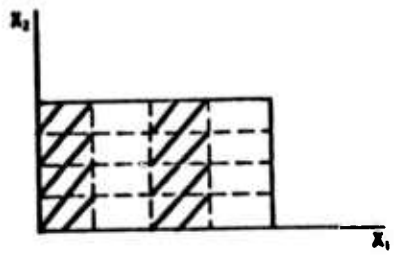

FIGURE 9. CHARACTERISTIC SET FOR FOURTH BINARY BIT

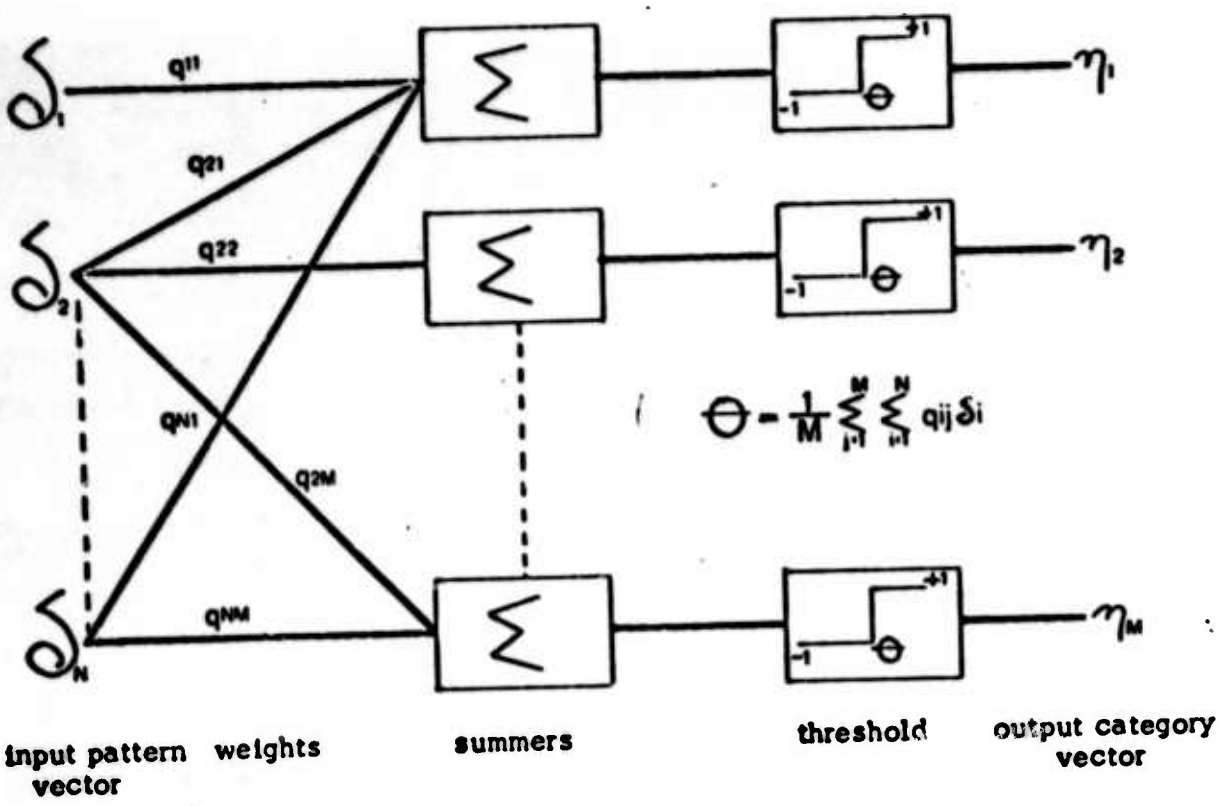

Figure 10. First Layer of Adaptive System

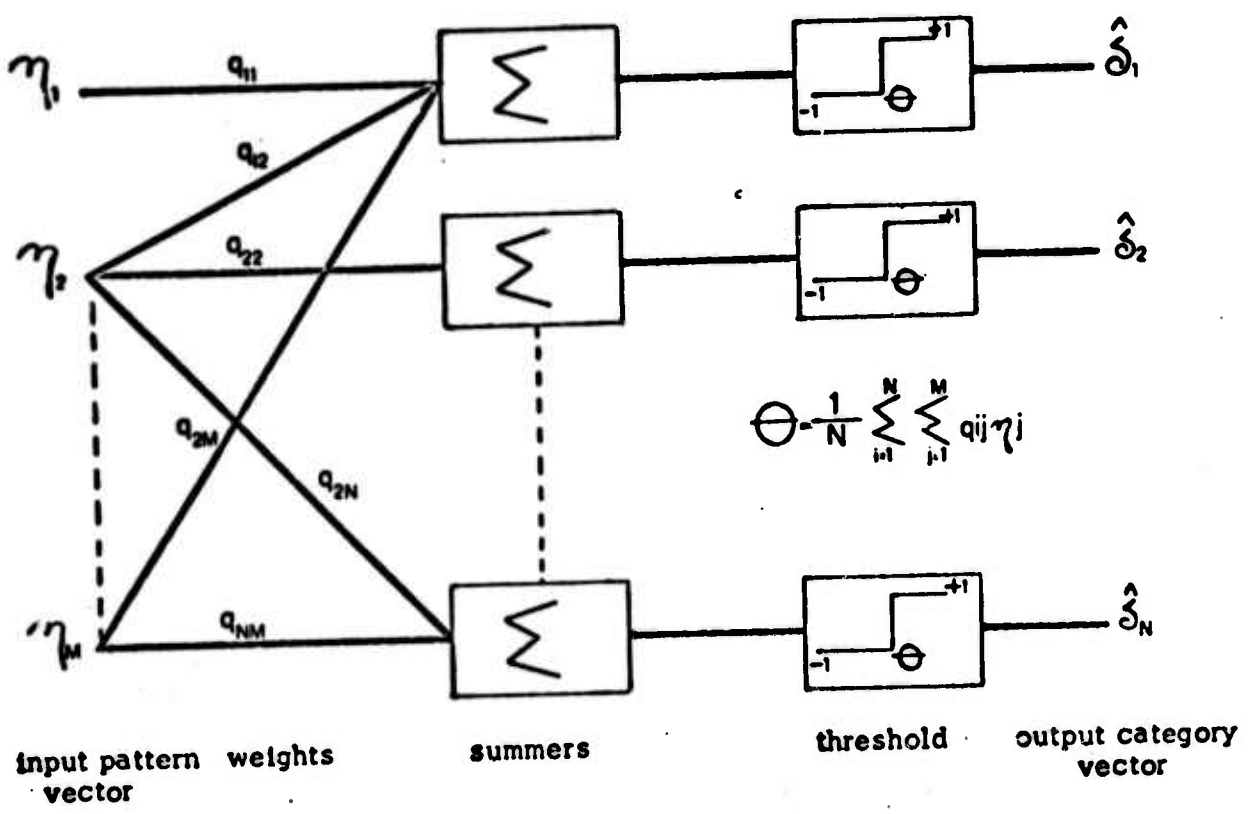

Figure 11. Second Layer of Adaptive System

δ_i	δ_i	η_j	CHANGE REQUIRED FOR η_j	CHANGE PRODUCED BY $\epsilon\delta_i\eta_j\lvert\delta_i-\delta_i\rvert$
1	1	1	none	0
1	1	-1	none	0
1	-1	1	increase	2ϵ
1	-1	-1	decrease	-2ϵ
-1	1	1	decrease	-2ϵ
-1	1	-1	increase	2ϵ
-1	-1	1	none	0
-1	-1	-1	none	0

Figure 12. Comparison of Change Required By and Change Produced By Reinforcement Statement

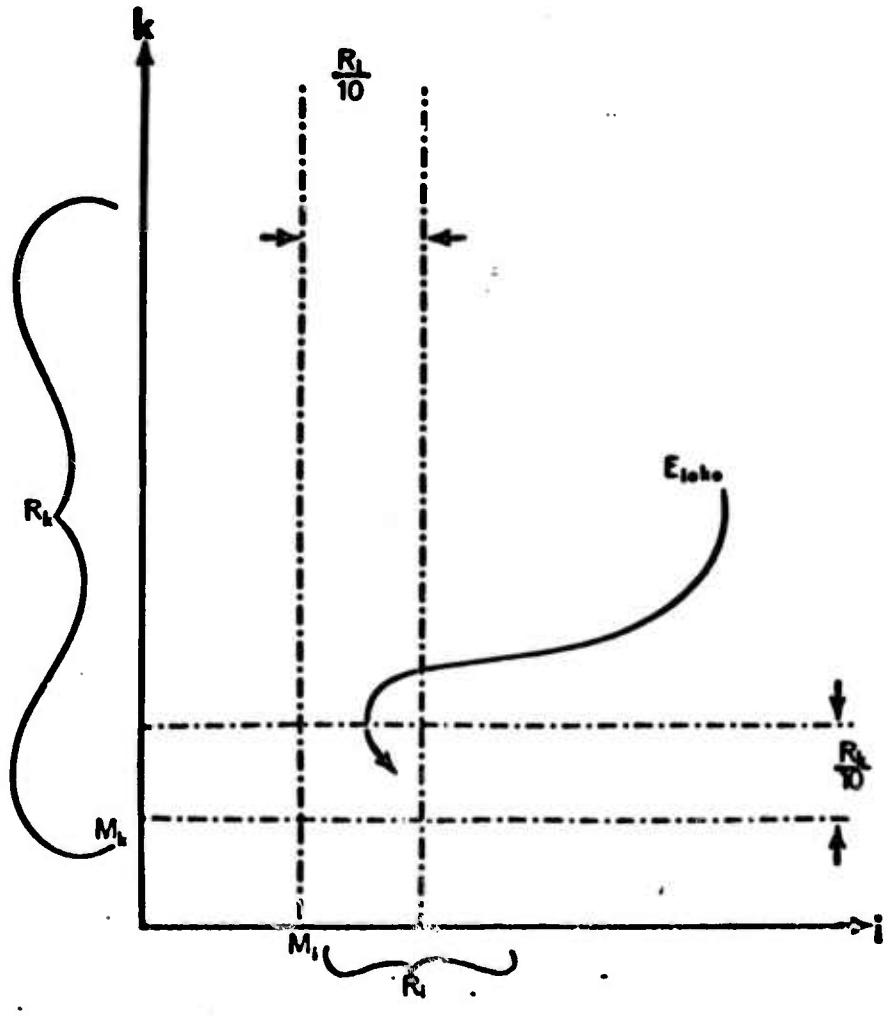

Figure 13. Geometric Configuration of a Typical Characteristic Set

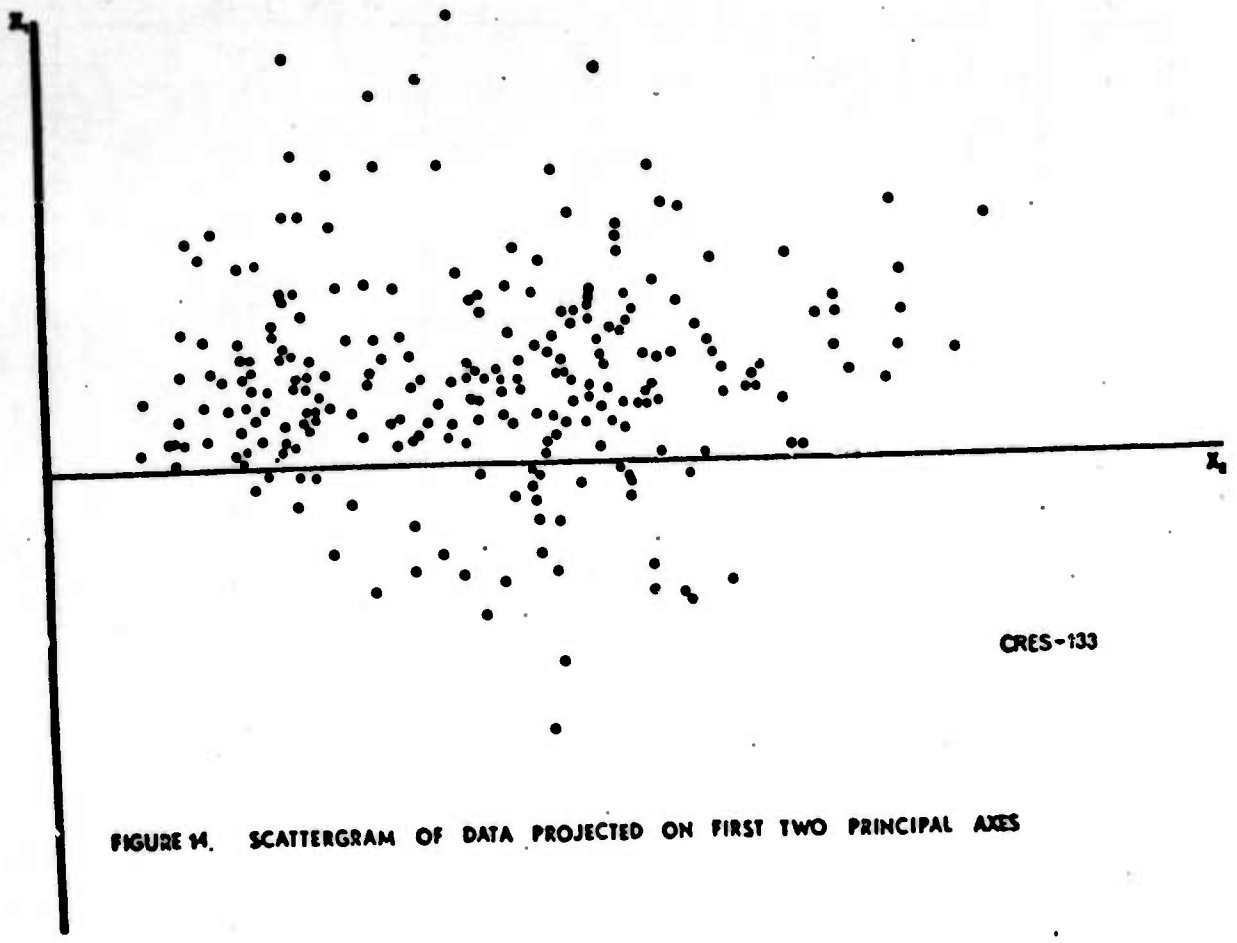

FIGURE 14. SCATTERGRAM OF DATA PROJECTED ON FIRST TWO PRINCIPAL AXES

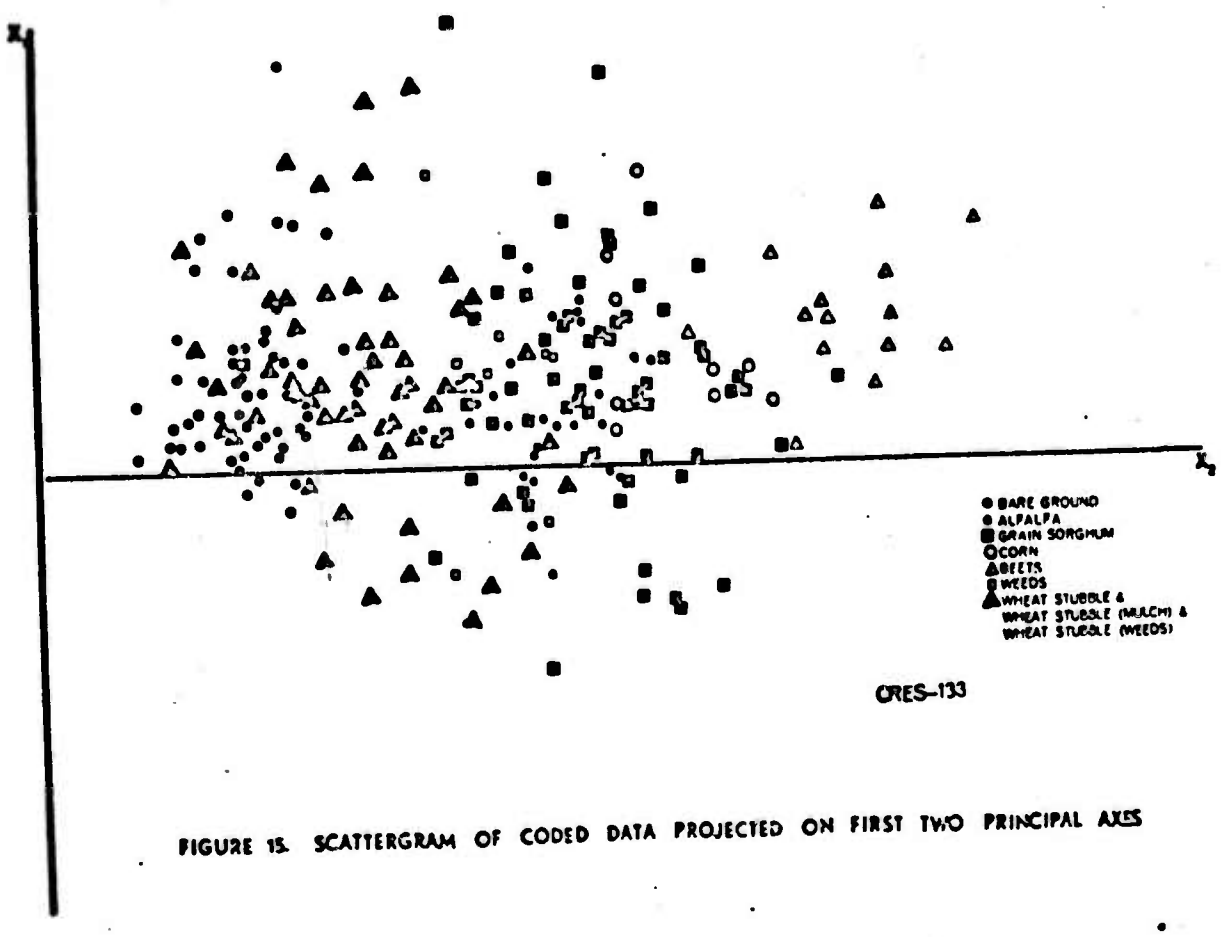

FIGURE 15. SCATTERGRAM OF CODED DATA PROJECTED ON FIRST TWO PRINCIPAL AXES

CATEGORY	I	SIMILARITY SET II	III	IV
BARE GROUND	52	3	0	0
CORN	0	0	7	2
WHEAT STUBBLE WEEDS	10	22	2	0
ALFALFA	0	14	15	0
GRAIN SORGHUM	1	22	47	1
WHEAT STUBBLE MULCH	9	3	0	0
WHEAT STUBBLE	9	5	0	0
WEEDS	0	5	4	0
PASTURE	1	3	2	0
SUGAR BEETS	0	0	3	11

FIGURE 16: CROSS TABULATION OF CATEGORY SIMILARITY SET FREQUENCIES

CATEGORY	I	SIMILARITY SET II + III	IV	
BARE GROUND	52	3	0	
CORN	0	7	2	
WHEAT STUBBLE WEEDS	10	24	0	
ALFALFA	0	29	0	
GRAIN SORGHUM	1	69	1	
WHEAT STUBBLE MULCH	9	3	0	
WHEAT STUBBLE	9	5	0	
WEEDS	0	9	0	
PASTURE	1	5	0	
SUGAR BEETS	0	3	11	

FIGURE 17: CROSS TABULATION OF CATEGORY AND SIMILARITY SET FREQUENCIES

CATEGORY	I	SIMILARITY SET II + III	V	
GROUP A BARE GROUND WHEAT STUBBLE (MULCH) WHEAT STUBBLE	70	11	0	
GROUP B CORN WS WEEDS ALFALFA GRAIN SORGHUM WEEDS PASTURE	12	143	3	
GROUP C SUGAR BEETS	0	3	11	

FIGURE 18: CROSS TABULATION OF CATEGORY GROUP SIMILARITY SET FREQUENCIES

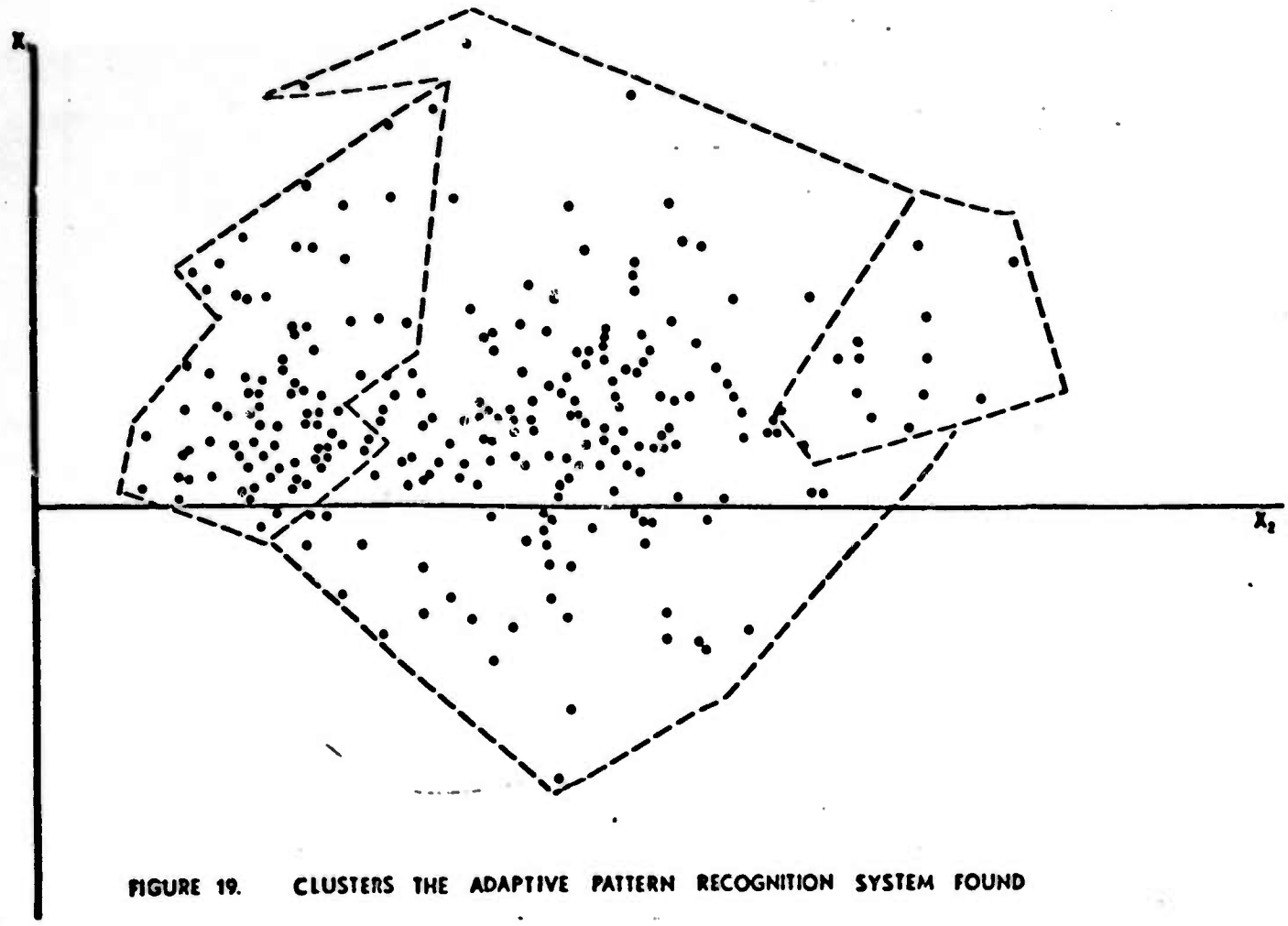

FIGURE 19. CLUSTERS THE ADAPTIVE PATTERN RECOGNITION SYSTEM FOUND

CATEGORY	SIMILARITY SET I	II + III	IV	
GROUP A BARE GROUND WHEAT STUBBLE MULCH WHEAT STUBBLE	.854	.070	0	
GROUP B CORN WS WEEDS ALFALFA GRAIN SORGHUM WEEDS PASTURE	.146	.910	.214	
GROUP C SUGAR BEETS	0	.02	.786	

FIGURE 20: CONDITIONAL PROBABILITY OF CATEGORY GROUP GIVEN SIMILARITY SET

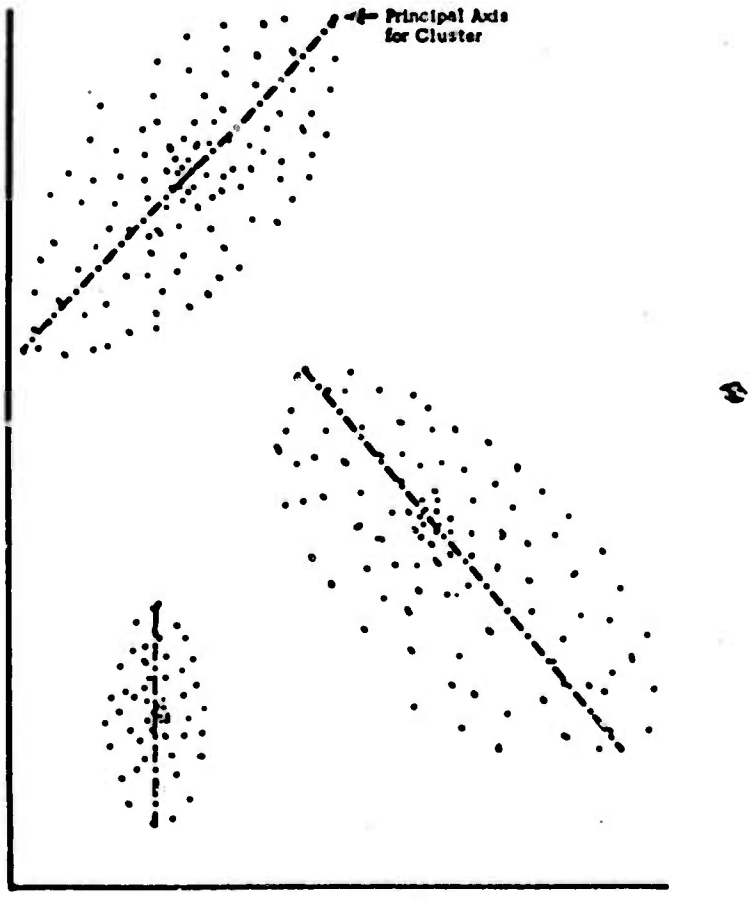

Figure 21. Clusters and Principal Axis Idea

Appendix E

A STATISTICAL AND CONDITIONAL PROBABILITY STUDY OF CROP DISCRIMINATION USING RADAR IMAGES

R. M. Haralick, F. Caspall,
R. K. Moore and D. S. Simonett

BLANK PAGE

Technical Memorandum 133-5
March 1968

A STATISTICAL AND CONDITIONAL PROBABILITY STUDY OF CROP DISCRIMINATION USING RADAR IMAGES

R. M. Haralick, F. Caspall,
R. K. Moore and D. S. Simonett

Remote Sensing Laboratory
Center for Research in Engineering Science
The University of Kansas
Lawrence, Kansas 66044

Abstract

A number of the constraints with which remote sensing must contend in crop studies are outlined. These include sensor, weather, and congruencing constraints; the nature of the answers demanded of the sensor system; and the complex spatial and temporal variances of both crops and cropping systems in areas of sub-continental dimensions. Attention is then focused on several methods which may be used in the statistical analysis of multi-dimensional remote sensing data.

Crop discrimination for radar K-band imagery is investigated by two methods. The first method uses spatial conditional probabilities in conjunction with a nearest-neighbor-probability approach, and the second method uses the standard statistical techniques of cluster analysis and principal axes representation.

Results indicate that crop type, height, and percent of cover significantly affect the strength of the radar return signal. Discrimination is better when the crops are mature. Sugar beets, corn and very bare ground are easily distinguishable, while sorghum, alfalfa and young wheat are harder to distinguish. Distinguishability will be improved if the imagery is examined in time sequence so that changes between times of planting, maturation and harvest provide additional discriminant tools.

Introduction

Agriculturalists, geographers and others are constrained in the study of crops with remote sensors by the kinds of agricultural characteristics that the sensors can in fact detect. The sensors used in the various portions of the electromagnetic spectrum are sensitive to dissimilar energy-matter interactions. They detect different characteristics and therefore convey different kinds of information. In the visible region, molecular absorptions produce the color effects which convey information about crop condition; in the infrared region, the cycle of thermal response under an insolation load may give information on moisture stresses within crops; in the radar region the backscattered return is primarily related to surface roughness and dielectric, which may be related to crop type, percent of cover, moisture content, and similar variables.

While at first sight radar cannot sense "color" for its information on crop condition, it may detect related changes in crop geometry and moisture and thus convey information about crop type and state which are not immediately obvious. Agriculturalists may wish radar and other remote sensors to:

(1) detect the presence of different crops--is the region entirely homogeneous or are there different crops,

(2) determine the crops actually present,

(3) determine the boundaries and acreages of different crops,

(4) determine the vigor (state) of crops,

(5) determine the agent responsible for any loss of crop vigor,

(6) predict yields.

This paper is concerned with the second of these items: determining the crops actually present. Studies on crop discrimination are now underway at Purdue University, The University of Kansas, the U.S. Department of Agriculture Experiment Station at Weslaco, Texas, and elsewhere, with a view to the ultimate use of remote sensor systems in automated or partially-automated data collection and analysis of crop type, condition and yields. Such data would be valuable in the United States and especially so in underdeveloped regions where adequate crop-yield and similar information is not available.

Because radar exhibits the combined advantages of fine resolution, virtual all-weather capability, and independence of the sun for illumination, and moreover is without serious degradation by the atmosphere, its abilities and shortcomings as a sensor of crops, pastures, and natural vegetation are matters of no small moment to the agricultural community. A great deal of research will be needed to clearly define these abilities and shortcomings, since little work has been carried out on radar as a sensor for agricultural purposes. The study reported here is one of a handful which explores these topics. All are concerned with a single frequency and one (less frequently two or four) polarization(s) only, and thus fall well short of an ultimate capability of multi-frequency, poly-polarization radars that are feasible for agricultural surveillance. The underlying concept behind synchronous data acquisition with multi-frequency polarization radars is that it represents the microwave equivalent of multiband spectral reconnaissance in the photographic and thermal IR region, which, as Hoffer (1967)* has shown, has produced some encouraging results in tests at Purdue University.

Temporal and Spatial Components of Crop Discrimination

Ideally, in the separation of crop types with a single sensor, we hope that there will be a narrow spread in the probability distribution of the radar reflectances for each crop: we also hope that the probability distributions for the radar reflectances of each crop will not overlap. This is of course not the case with radar or any sensor, the reason being that in that discrimination between crops, the attribute we are seeking--genetic difference between crops--must be approached through the surrogate of crop reflectance. The surrogate may be quite imperfectly correlated, in a discriminatory sense, with the defining genetic attributes. Furthermore, there is considerable natural variability in the time of planting, varieties planted, and conditions of crops as a function of time of planting, soil type and so on. Consequently no single sensor is able to effect clear-cut discrimination at a single time of all crops in all fields. It becomes

*Hoffer, R. M., Interpretation of Remote Multispectral Imagery of Agricultural Crops. Research Bulletin 831, Laboratory for Agricultural Remote Sensing, vol. 1, Purdue University Agricultural Experiment Station.

necessary, therefore, to increase the probability of correct discrimination of crops through the use of several frequencies and polarizations in concert, both synchronically and diachronically.

It is only through empirical testing of numerous sites in the United States (and elsewhere) at repeated intervals throughout a number of growing seasons (probably at least five) that we will be able to sufficiently define the time-sequential probability distributions of the radar returns for different crops. It is immediately apparent that if crops are spatially and temporally distributed, then the distribution of the reflectances within a single growing season and between growing seasons will demand a number of information channels to insure identification, which may become unmanageably large even if only a few looks through the growing seasons are available. This immediately creates a compromise in the amount of information obtained at any time and the number of times it is obtained. The various trade-offs between number and kind of sensors and number and timing of data collection by the sensors has yet to be worked on, but will be an essential ingredient of continuing studies in the U.S.

From this brief discussion it might intuitively be felt that multiple looks through time may turn out to be very important in remote sensing, and that through multiple looks it may be feasible to reduce the number of information channels needed at each time. Consider, for example, the condition of crops and their times of planting and harvesting in the United States. There are many differences in kinds of crops, growing season and growth patterns between west, center and east; between humid, subhumid, and irrigated; and between south, center and north, to name only the more obvious factors involved in crop geography. This means that from March through October, every week is a remote sensing week, since critical changes in the status of crops are occurring somewhere.

There are various degrees of crop identification accuracy which we may want from remote sensing systems. For example, we may wish (1) to positively identify the crops in every field in an area and to determine the acreages of each field with an error of 1% or less; or, less difficult, (2) to identify, with some acceptable error, the kind of crops in each field of a region, and to estimate total acreages of each crop in the region accurate to $\pm 5\%$.

If we want to determine the exact acreages of crop being grown in an area, either for statistical reporting purposes or for checking on wheat and feed grain program compliance, we have a situation described by the first case above. In such a circumstance, if ironclad identification cannot be made in a single pass, then multiple passes must be made, with the attendant problems of congruencing: storing spatial-reference coordinates for all points on the ground and of rendering time-separated, different-flight-path data in congruent planimetric geometry. This is no mean task! At present it is really an intolerable burden to place on a remote sensor system.

Alternatively, as in the second case above, we may be able to avoid the necessity for many passes by allowing modest errors in identification and by accepting regional average crop acreages with up to a 5% error. If we select this alternative, however, a more stringent requirement for spatial accuracy must be met.

As we have already mentioned, one of the major problems in obtaining high identification accuracy with any automated multi-sensor system is that of bringing the images into mutually congruent geometry. Each resolution cell of each image corresponds to a small area on the ground. The system must be able to determine the correspondence, in planimetric coordinates, between each resolution cell of each image and each resolution cell of every other image, and between each resolution cell and each small area on the ground. This correspondence must be established automatically if the system is to work quickly and effectively.

The problem of image congruence has been attacked by researchers investigating the visible and infrared region of the spectrum. Multiple wavelengths and mechanical rotating mirror-scanners have been developed in which the signal received is split into different wavelength bands, each with its own detector. The signals are then recorded simultaneously on different channels of a magnetic tape. A similar technique is feasible with radar systems operating with multiple polarizations and wavelengths, although direct recording of the video calls for a fairly wide-bandwidth recorder. The use of some form of intermediate storage so that only the

actual significant bandwidth of the signal need be recorded (sometimes hundreds of pulses are averaged to make one resolution cell) can reduce this problem.

A more severe problem of image congruence comes from multiple flights. If an aircraft or spacecraft carrying the radar could fly exactly the same path within a wavelength or so each time, the problem would not be difficult. Unfortunately, aircraft cannot repeat either horizontal or vertical location of the path to anything like wavelength precision; furthermore, operational conditions may require significant differences in altitude which result in distortions between images. Even the best-programmed flight lines sometimes deviate so that there are horizontal differences as well as vertical differences.

The need for automatic congruencing equipment is clearly urgent. Multiple recording during a single pass solves only the problem for that pass. No system known produces images on successive flights that are initially congruent. Digital correlation and subsequent linear or non-linear correction of scale could in theory solve the problem. The mass of information collected in any extensive aircraft flight program, however, prevents the use of these digital techniques for congruencing in the agricultural problem. For a geological problem, such techniques might be realistic because the flights need not be repeated so often, and a delay of a year or two in processing the data does not necessarily result in loss of its value. Some faster means must be found for the more timely problems in agriculture before the automated systems can be truly useful.

There is another approach to the image congruencing problem which relies on the fact that there are geographic boundaries which are relatively permanent. Homogeneous regions (determined by "natural" statistical classes) may be found on each image, independent of the other images. Boundaries must exist between homogeneous regions. Congruencing may be achieved by distorting the geometry of the images so that there is maximum correlation between the boundaries on each image with those on every other image. The distorted ("congruenced") images may now be used for classification purposes. The end product of the classification may be

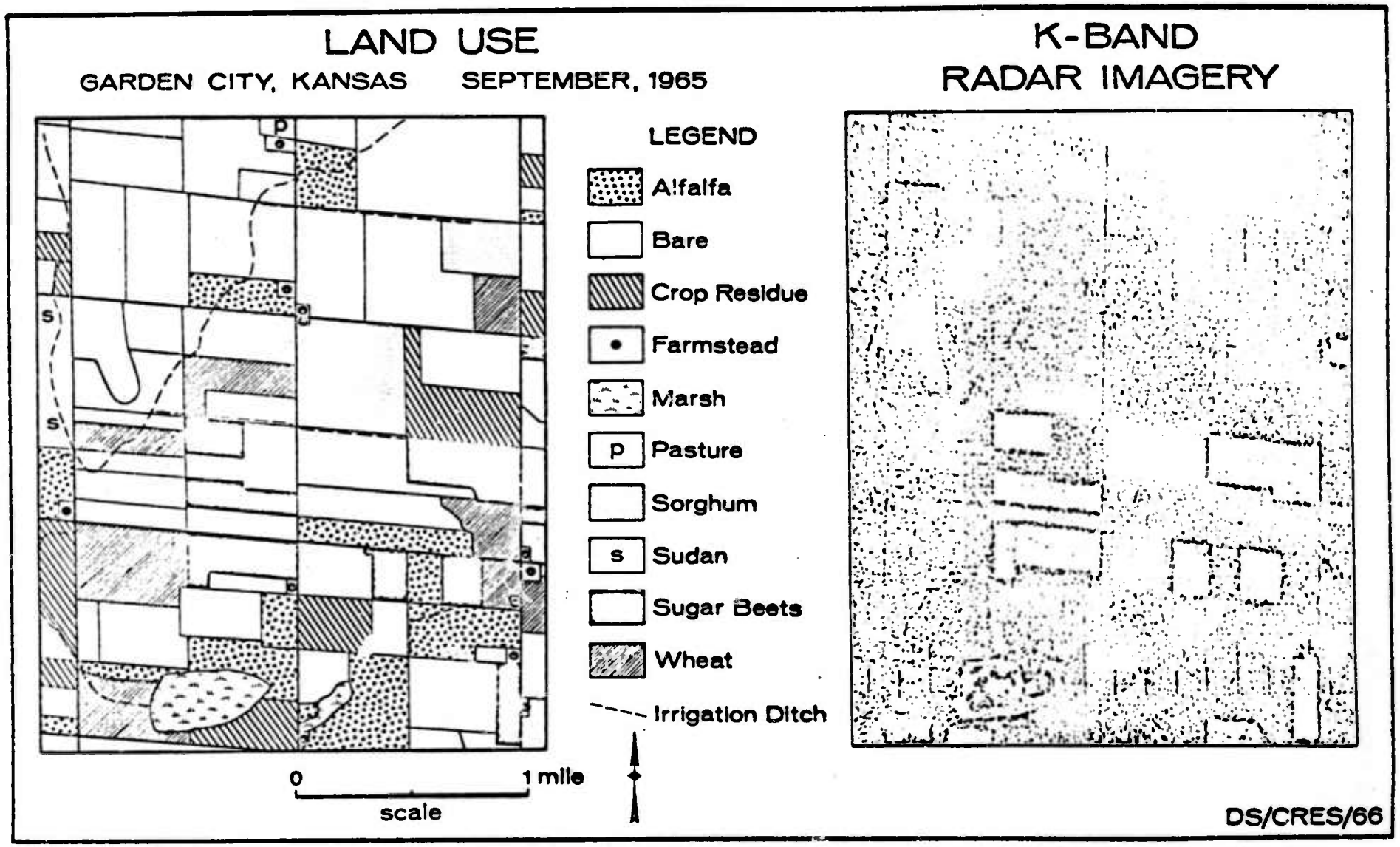

FIGURE 1. RADAR IMAGERY

brought to planimetric correspondence with the ground by examining the boundaries around the categories and distorting the geometry of the categorized image so that it matches the natural boundaries on a map.

If we did not need to know exactly where each crop occurred in a region, a relatively crude job of congruencing could be performed. Such unsophisticated congruencing would retain just enough statistical structure to tell us the acreage of each crop, independent of its spatial position, or the percentage of occurrence for each crop in the region. Little, if any, work has been done in this area, and we believe it warrants further thinking.

In the following sections of the paper we outline a number of ways of data manipulation of radar reflectances from crops with which we are experimenting at the University of Kansas. Before doing so, however, a few words are necessary about the area where the crop data has been obtained.

The region where the crop information is collected lies a few miles west of Garden City, in western Kansas (Figure 1). In this area there are over 400 fields for which data were collected at the time of radar overflights. The area was chosen because fields are generally large, slopes are extremely gentle, soils are uniform, both dryland and irrigated cropping is practiced, and there is some diversity of crop types, agricultural techniques, and moisture conditions. In this test area we can hold constant in an analysis such factors as topography, soil, and field size, and can obtain the maximum variations in soil and crop states, moisture levels, and so on, in order to quantitatively explore both crop discrimination and the contribution of different parameters to the radar backscatter.

Data Analysis

Sensor systems are designed to obtain information about an interesting statistical structure of an environment, where "interesting" is defined by the investigator. The sensor system must reflect or transmit this interesting environmental structure onto the data structure if anything

is to be gained using the sensor system. Thus, once a sensor system has been conceived and designed, the question that must be answered when it is tested is "what statistical structure of the environment is actually preserved through the sensor's 'eyes'--in particular, is the interesting structure preserved?"

In order to answer this question some way of examining the data, some way of determining the structure within the data, must be devised. Then the structure of the data may be compared with the known structure of the environment, and the question can be answered.

The most usual type of environmental structure which is defined as "interesting" is that of a classificatory nature. The investigator arranges the environment into a set of mutually exclusive categories. It is his hope that the sensor system will preserve enough of the environment's structure so that data obtained from the sensor system may also be categorized into a set of mutually exclusive classes, where each class corresponds to a unique category in the environment.

In order to determine the structure of the data, the following operations are valuable:

(1) the data set must be represented in some geometric way such as a scattergram, where the data structure is immediately apparent. This representation must be perceivable directly as a "picture."

(2) a statistically optimum classification of the data must be made, optimality being defined by the investigator.

(3) the natural classes of the data structure must be found and compared to the categories in the environment.

The information received in a "picture" of the data structure gives the investigator an immediate "feel" for what is actually happening. It gives him an intuitive base which he can expect to guide him to more sophisticated techniques. Further, it may quickly tell the investigator whether there have been faults in the sensor system while the system was gathering the present set of data. If so, then the data would not have to be further processed and the experiment could be rerun. The information

gained by the statistically optimum classification of a data set is, of course, most fundamental in the sensor system test. From it the investigator finds out how good the system really is in preserving the classificatory structure of the environment. Finally, by finding out the natural classes in the data structure, the investigator can learn "what language the sensor system speaks." If a natural class in the data structure actually corresponds to two environmental categories, then we would expect that regardless of the optimality of any statistical classifying rule, these two environmental categories are going to be confused, and the investigator can do nothing about it except search for a new sensor system. This confounding of categories must then be taken into account in any interpretation of data from the sensor system.

In the case where the sensors take data in a sequential way and it is known that observations which are close to each other in the sequence are likely to be in the same category, some effort should be made to preserve the similarity of neighboring data points in their classification. For imaging sensors in particular, this means that two neighboring resolution cells should not be classified independently. An exception to this occurs when the image data are like that of Figure 2, which has the kind of structure illustrated in the scattergram in Figure 3. Here there is complete isolation between the categories, with bare ground occupying the lower third of densities, grain sorghum occupying the middle third of densities, and corn occupying the upper third of densities.

Representing the data structure in a two- or three-dimensional scattergram is a problem when the measurements the sensor system takes are n-dimensional (n being more than three). Some criterion for choosing the representation must be determined. Suppose we decide that we would like to obtain the best representation possible by translating the data and then "squeezing it through a two-dimensional hole" with a linear transform. By "best" we will mean that the mean squared error of a least squares estimate of the original set of data, obtained from the data which have been squeezed through a two-dimensional hole, is minimized.

.11 BA	.15 BA	.09 BA	.80 CR
.08 BA	.10 BA	.71 CR	.75 CR
.41 GS	.47 GS	.77 CR	.74 CR
.51 GS	.50 GS	.53 GS	.45 GS

Key:
BA Bare ground
GS Grain sorghum
CR Corn

FIGURE 2. Simple image, where the density for each resolution cell is indicated by the number appearing in the top of each box and the category of surface cover which corresponds to the cell is indicated by the two letter code appearing at the bottom of each box.

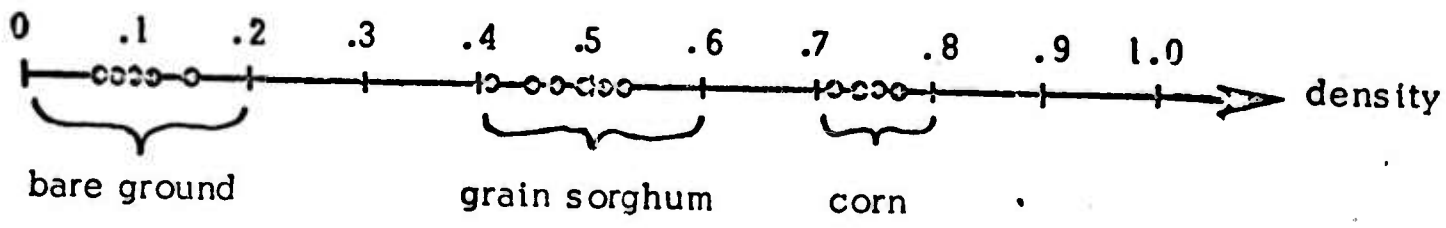

FIGURE 3 . Scatterograms of simple image data: The categories are all isolated.

It can be shown that this representation corresponds to finding a plane in n-dimensional space where the data projected onto this plane have maximum variance. Mathematically the situation can be represented as finding the projection operator P which has rank 2 and a translation vector t such that the mean squared error ϵ^2, defined by $\epsilon^2 = E\left[\left((x-t) - P(x-t)\right)' \left((x-t) - P(x-t)\right)\right]$, is minimized. The minimization is achieved when $t = E[x]$ and P projects onto the plane spanned by the two eigenvectors, v_1, v_2, with largest eigenvalues of $E\left[(x-E[x])\ (x-E[x])'\right]$, the covariance matrix, (see Kendall and Stuart 1964). We will call this representation the principal axes representation. The coordinates of any data vector relative to the principal axes' plane can be found easily as $(x-E[x])' v_1$ for the first component and $(x-E[x])' v_2$ for the second component.

Although there are many ways of classifying data, such as linear decision theory, which constructs hyperplanes boundaries, or nearest-neighbor search procedures, these are statistically admissable only under severly restrictive conditions. A Bayes' decision rule is almost always statistically admissable and optimal, in addition to allowing the use of a loss function which can weigh a correct classification more heavily on the more important categories. Therefore, to get information regarding the best possible classification which can be made, a Bayes' decision rule may be employed.

We used a Bayes' decision rule (see Middleton 1960) classifying each resolution cell of the radar imagery data independent of its neighboring cell. This was done because we did not have a Bayes' decision program taking into account the similarity of neighboring resolution cells. In order for the Bayes' decision rule to indicate the classificatory structure of the data rather than to merely "memorize" the data, the data set must be randomly divided in half; the first half must be used to generate the statistics for the Bayes' rule and the second half must be classified on the basis of this rule. A "goodness criterion" may be adopted, such as the total percentage of correct classification or the average percentage of overall categories of correct classification, where the percentages are properly weighed by the loss function adopted.

Finding the natural classes in the data structure, as seen through the sensor's eyes, is perhaps the hardest of the three operations suggested, since the problem is not well-defined. Certainly some information about the natural classes will be obtained from the principal axes representation and the Bayes' classification. Categories which are confused will definitely show up. However, it may be that parts of the environment which are categorized by the investigator as the same will show up in different natural classes, indicating that further distinctions may be made.

We will approach the natural-class problem of image data by two clustering methods. One sequentially forms clusters from data measurements, called centers, which have the highest probability in any small spatial region in the image (a spatial conditional-probability approach), and includes in each cluster those points which are sufficiently close to the center in measurement space and whose probabilities do not differ too much from the probability of the center point. The other forms clusters taxonomically on the basis of Euclidean distance in measurement space, using the multiple linkage model.

Clustering by Spatial Conditional Probability

The conditional probability approach first quantizes the data in the following way. Let the density in the ij^{th} resolution cell be $X^{ij} = (x_1^{ij}, x_2^{ij}, \ldots x_n^{ij})$ where x_k^{ij} is the output from the k^{th} sensor when the k^{th} sensor is observing the area represented by the ij^{th} resolution cell. Let R_k be the range for the k^{th} coordinate. The quantizing function Q is defined as $Q(X) = (i_1, i_2, \ldots, i_n)$ where $\frac{i_j - 1}{10} R_j \leq x_j < \frac{i_j R_j}{10}$.

In forming clusters, priority is given to the quantized measurement vectors for which the conditional probability of occurrence in an image spatial region is higher than the joint probability of its occurrence over the whole image. For example, a multi-spectral image may be partitioned into a number of connected spatial regions, as in Figure 4. The conditional probability distribution for each region is computed and compared with the

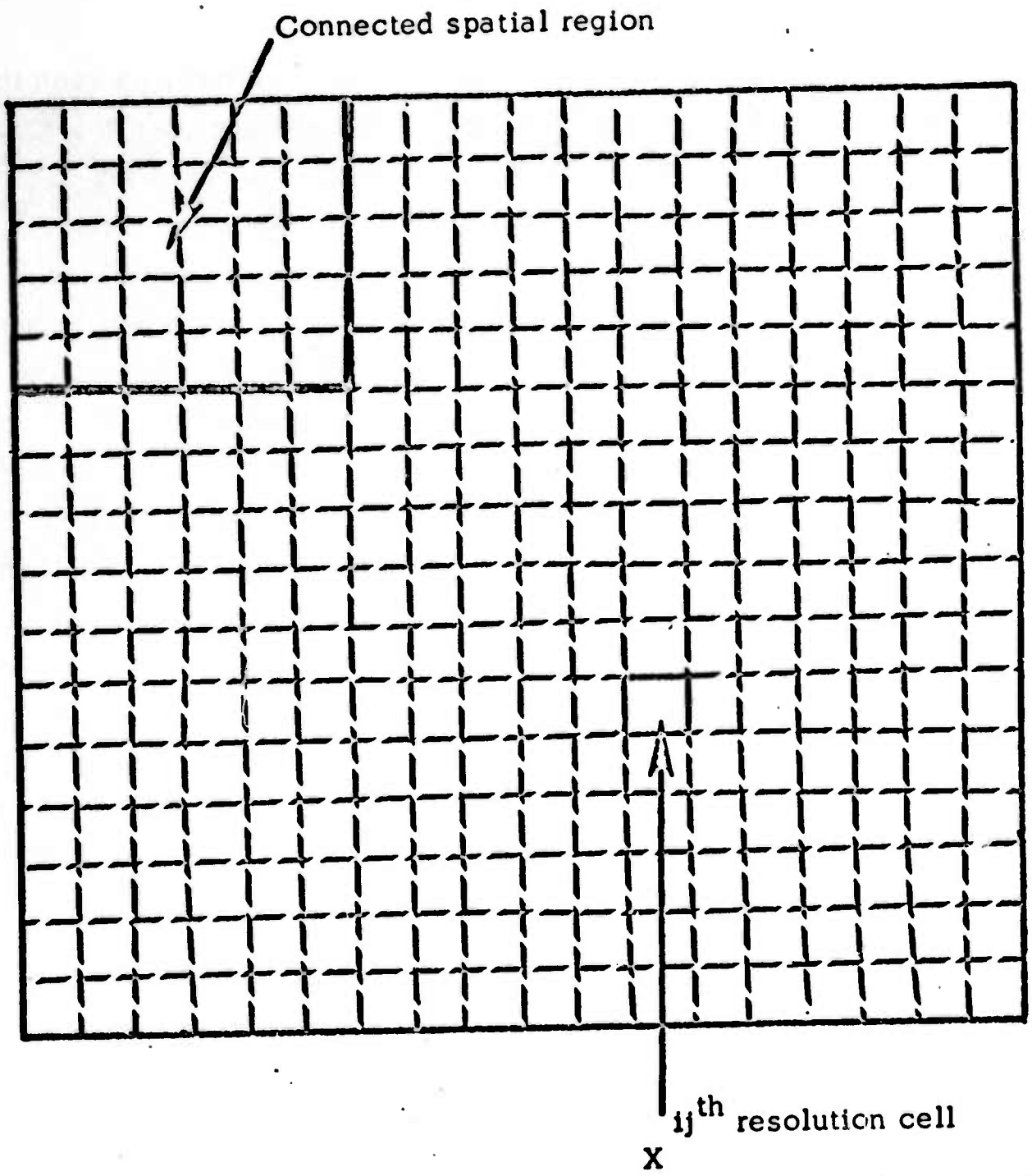

Figure 4. Multispectral image

joint probability distribution for the entire image. All the measurement vectors which have the highest conditional probability in the multi-spectral images are given priority in forming clusters. Each cluster is formed around a center--that is, a quantized measurement vector which is not yet in a cluster and which has the highest conditional probability for some spatial region. At any iteration, for a point X to be included in the cluster just being formed, there must exist a point Y already in the cluster such that:

(1) $|x_i - y_i| \leq 1$ for each i

(2) $P(X) \leq \epsilon_1 P(C)$ where C is the center and ϵ_1 is a prechosen parameter

(3) $P(X) \leq \epsilon_2 P(Z)$ where Z has the highest probability of any point already in the cluster and ϵ_2 is a prechosen parameter.

(4) $P(X) \leq \frac{1}{\epsilon_2} P(W)$ where W has the lowest probability of any point already in the cluster.

If there are any points which do not meet those criteria they are put into the cluster which is nearest to them.

Clustering by Multiple-Linkage Techniques

Multiple-linkage cluster analysis has been widely used as a numerical taxonomic technique in the biological sciences (see Sokal and Sneath, 1963). However, many of the assumptions made in classifying biota cannot be made in analyzing radar images, because there is no evolutionary relationship between the objects being categorized. Nevertheless, since the measurement vectors which can be clustered together are in some sense similar, the technique is worthwhile in finding the natural classes of a data set.

The clustering procedure takes the following form:

(1) a matrix of the similarity coefficients between each pair of measurement vectors is constructed. (For the multi-spectral images, these are the measurement vectors in each resolution cell.)

(2) the matrix is scanned and all pairs of measurement vectors which are mutually close are linked together.

(3) a new matrix is computed on the basis of the paired vectors and single vectors. This new matrix is scanned and all single vectors or paired

vectors which are mutually close are linked together. This is continued iteratively until all clusters are linked together.
Figure 5 illustrates the phenogram obtained from the multiple-linkage clustering.

The investigator may determine the natural class structure of the data by truncating the dendrogram at some distance, as illustrated by the vertical dashed line in Figure 5. Here a distance coefficient of .4 gives a reasonable picture and the natural classes are (b), (c), and (d), as indicated by the left margin. The dendrogram may also be used as a guide for further analysis. For example, the sugar beet field (202 BE) which linked with the corn field should be investigated in greater detail to determine why it is so different from the rest of the sugar beet fields.

There are some important differences between the conditional-probability clustering technique and the multiple-linkage cluster analysis. The multiple-linkage cluster technique analyzes the data microscopically, linking each observed measurement vector with other similar observed measurement vectors and simultaneously forming a set of clusters. In order to do this, an N x N matrix must be stored if there are N observed measurement vectors. The conditional probability clustering, a macroscopic technique, starts with the most important cluster, forms the clusters sequentially, and needs a storage of 2N places. These differences reflect themselves in the amount of data the techniques can handle. The conditional-probability clustering technique is quick and easily used with data sets containing thousands of measurement vectors, while the multiple-linkage clustering is slower, and data sets containing even hundreds of measurement vectors are at the limit of the procedure. However, the multiple-linkage clustering compensates for these disadvantages by giving a more detailed analysis of the data set.

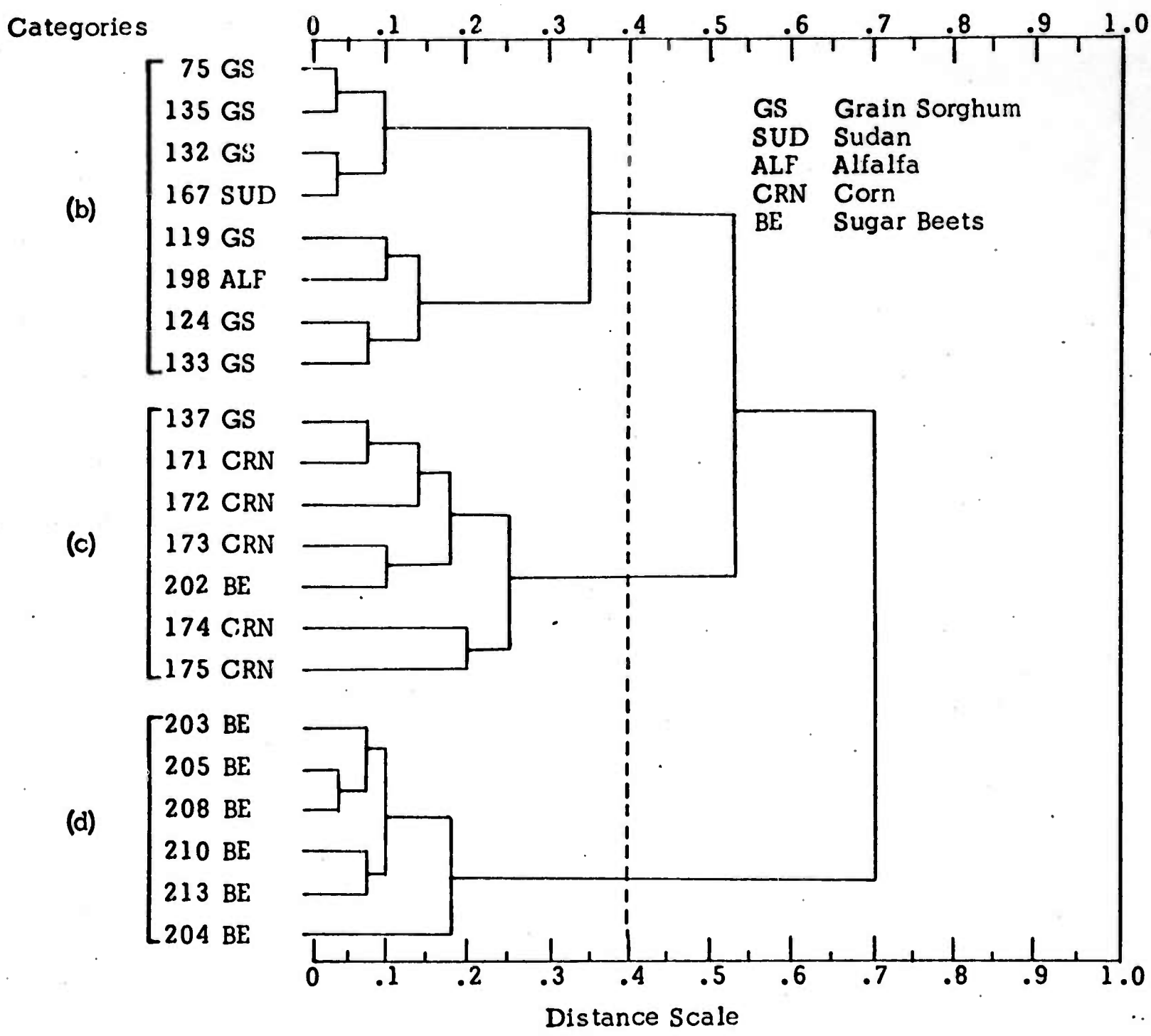

FIGURE 5. Section of a dendrogram showing graphically the results of cluster analysis. This is a section of the actual dendrogram used in categorizing the August and September data. The section of 21 data points was selected from the original 231 because it shows portions of three of the four major categories clustered. The dashed line shows the break point.

Statistical Crop Discrimination

We will illustrate this threefold approach to data analysis with two sets of data obtained from K-band radar imagery taken over agricultural areas in western Kansas. At the time the analysis was done, image digitization equipment was not available at the University of Kansas, and we had to satisfy ourselves with only the average radar return in each farming field. This field average was obtained by taking a few random scans over each field in the images with a microdensitometer and using the average of the scan lines as an estimate of the average radar return for the field.

The first set of images was obtained in a time-sequential fashion during the months of August and September in 1965. The August image had only one polarization, being horizontally transmitted and received, while the September images had two polarizations, being horizontally transmitted and both horizontally and vertically received. All three images were taken over the same test site near Garden City, Kansas. The second set of images, also taken over this area, was obtained during the month of July in 1966 and had all four polarization combinations. We wanted to find out:

(1) the agricultural type of environmental structures the radar imagery system did preserve, and
(2) whether more environmental structure could be preserved
    (a) if the data were taken in time sequence with few polarization combinations or
    (b) if the data were taken at the same time with all the polarization combinations.

Figures 6 and 7 illustrate scattergrams with the principal axes representation for these data. It may be noticed from the general pattern that as the agriculture becomes more intense (surface-cover or land-usage categories going from bare ground to sugar beets), the radar return becomes greater. This correlates most directly with the crop percent of cover. For both sets of data, we immediately see the overlapping of categories. In the July data the bare ground and wheat stubble overlap. Then the other part of wheat stubble overlaps with alfalfa, while the alfalfa overlaps with

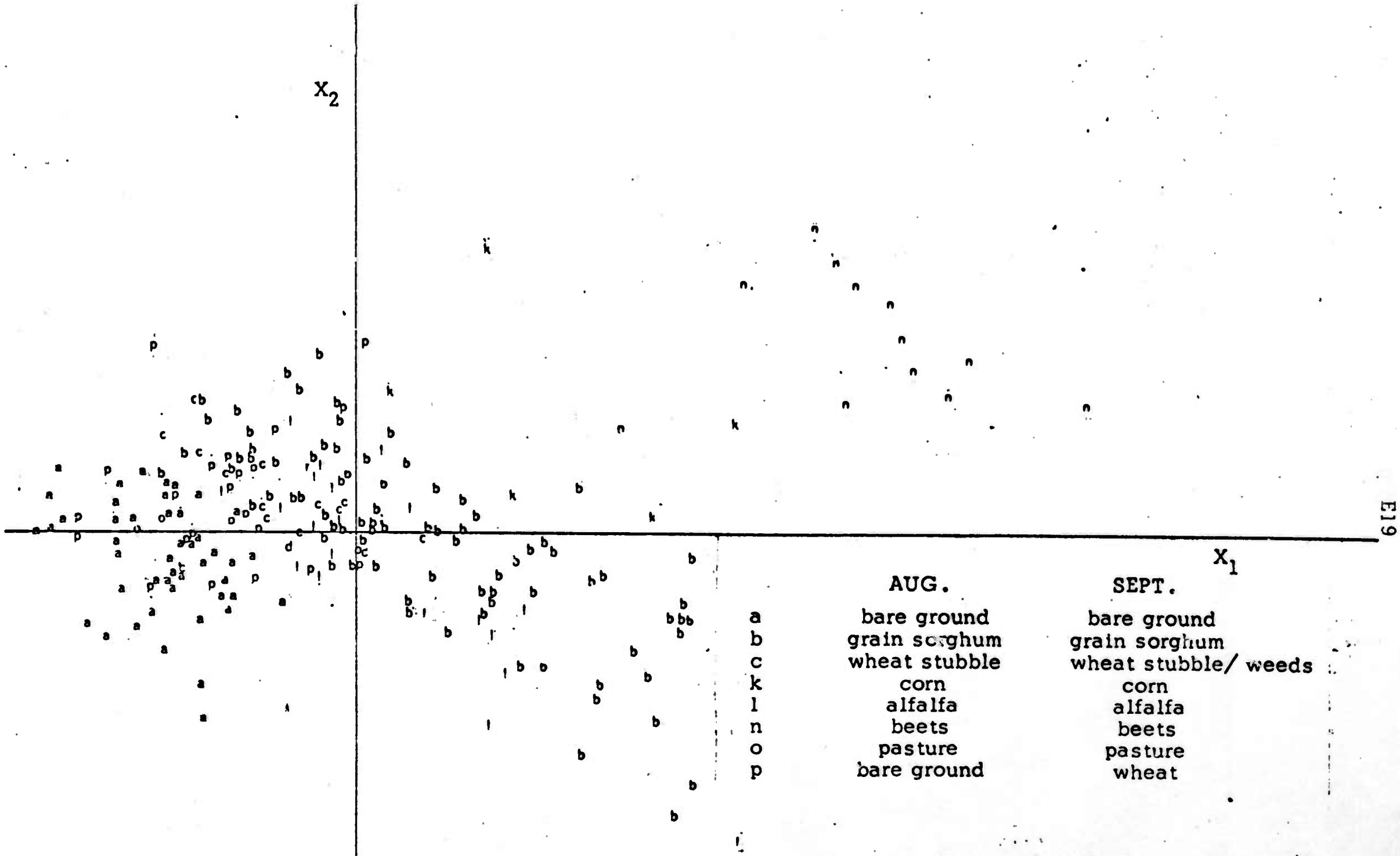

	AUG.	SEPT.
a	bare ground	bare ground
b	grain sorghum	grain sorghum
c	wheat stubble	wheat stubble/ weeds
k	corn	corn
l	alfalfa	alfalfa
n	beets	beets
o	pasture	pasture
p	bare ground	wheat

FIGURE 6. Scattergram of August - September 1965 Radar imagery field averages projected onto first two principal axes.

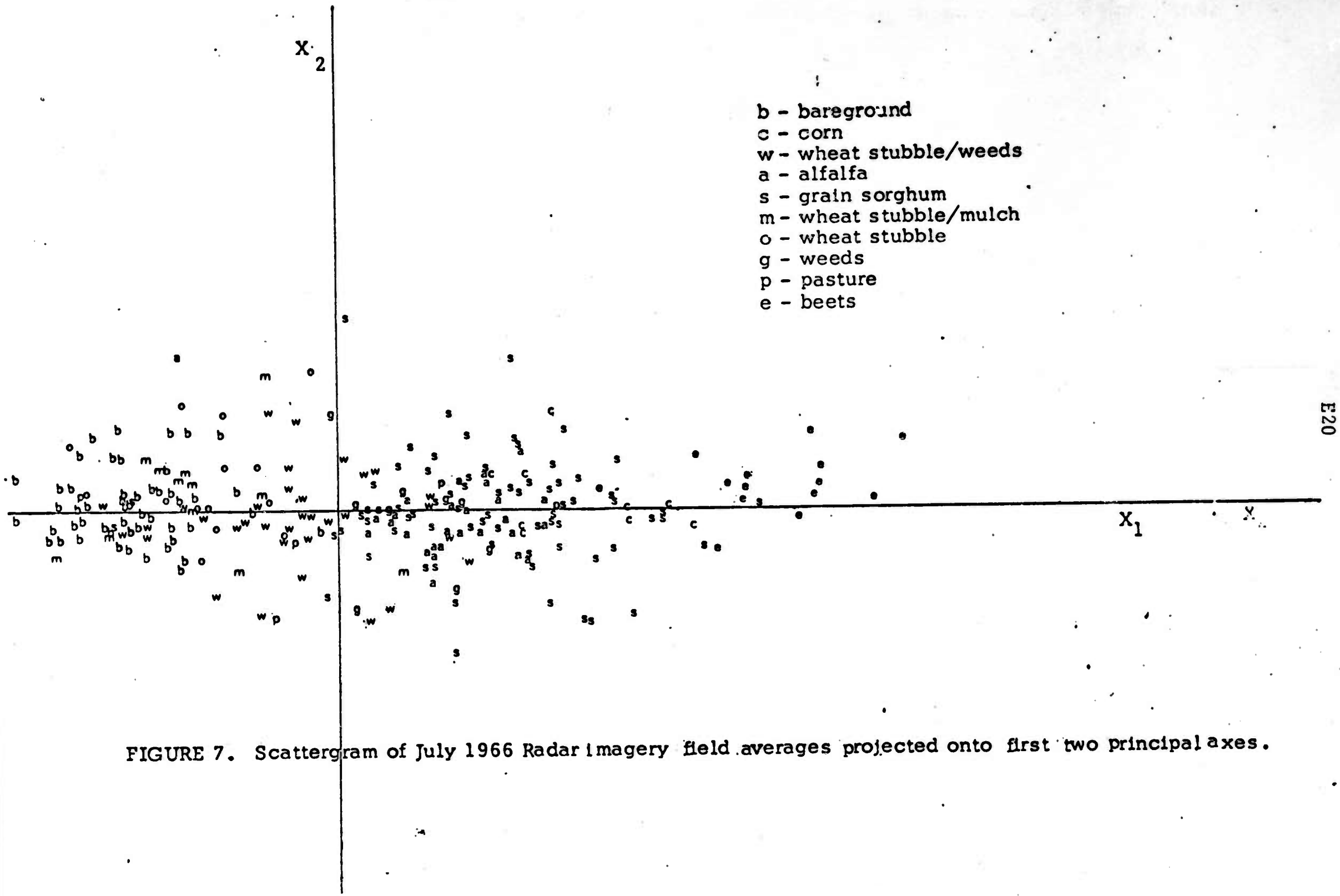

FIGURE 7. Scattergram of July 1966 Radar Imagery field averages projected onto first two principal axes.

the corn, and grain sorghum overlaps and covers both alfalfa and corn. Sugar beets stand almost isolated by themselves. In the time-sequential data bare ground stands out by itself, while wheat stubble overlaps with alfalfa and both overlap with the grain sorghum. The corn and sugar beets stand by themselves. This indicates that, for the July data, we would expect the Bayes' decision rule to confuse wheat stubble, alfalfa, corn, an and grain sorghum with each other, and to confuse bare ground and wheat stubble with each other while classifying sugar beets fairly well. For the time-sequential data we would expect the Bayes' decision rule to confuse wheat stubble, alfalfa, and grain sorghum with each other, while classifying bare ground, corn, and sugar beets fairly well. This is indeed true if we examine the tables in Figures 8 and 9, indicating the results of the Bayes' classification. For this problem the loss function was chosen to be an equal loss function; the same finite negative amount was lost for each correct classification and nothing was lost for an incorrect classification. Notice that 90% of the data grouped as shown were correctly classified for August-September, while only 78% of the July data were correctly classified. We would expect a natural class approach to show that the categories confused in the Bayes' classifying technique all belonged to the same natural class or cluster.

The spatial conditional-probability approach could not be fully utilized because of the lack of image-digitization equipment. However, a suitable approximation was tried. All field averages which were measurements of the same land usage category were lined up together. In this way the spatial closeness of similar types of fields in the data sequence could be utilized exactly as it would have been if the data sequence represented resolution cells of an image. Each spatial region consisted of a set of 10 sequential vectors in the sequence. The error from this approximation results mainly from the fact that clustering procedures of this type require large amounts of data to work well, and using field averages for resolution cells reduces the data size by two or three orders of magnitude. Despite this handicap, the conditional-probability clustering procedure indicates that the categories of vegetation which were confused in the Bayes' classifier do form fairly isolated clusters or similarity sets, as the tables in

Surface Cover Actually Measured:	Number of Measurements Identified as: (a) bare ground pasture	(b) grain sorghum, bare ground-wht., alfalfa wheat stubble-weeds	(c) corn	(d) sugar beets
(a) bare ground pasture	22 (91% cor. id.)	2	0	0
(b) grain sorghum, wheat stubble-weeds, alfalfa, bare ground-wheat	5	73 (91% cor. id.)*	2	0
(c) corn	0	0	2 (67% cor. id.)	1
(d) sugar beets	0	0	1	5 (83% cor. id.)

FIGURE 8. Identification accuracy for August-September 1965 radar imagery. A random sample of 113 measurements of field averages from a total set of 226 were used to train a Bayes' decision classifier, and the other 113 measurements of field averages were classified on the basis of the Baye's decision rule. Ninety per cent of the types of surface cover, grouped as shown, were correctly identified. Each field had the indicated type of surface cover for both the months of August and September, the exception being bare ground-wheat, which was bare ground in August and wheat in September.

*The 91% correct identification in groups (a) and (b) means that 91% of the measurements in each of these groups were actually identified as being in that group. In general the individual types of surface cover within each group were completely confused with one another.

Surface Cover Actually Measured:	Number of Measurements Identified as: (a) bare ground	(b) corn, alfalfa, grain sorghum, weeds, pasture, wheat stub.	(c) sugar beets
(a) bare ground	14 (52% cor. id.)	13	0
(b) corn, alfalfa, grain sorghum, weeds, pasture, wheat stubble	11	75 (85% cor. id.)*	2
(c) sugar beets	0	1	6 (86% cor.id.)

FIGURE 9. Identification accuracy for July 1966 radar imagery. A random sample of 129 measurements of field averages from a total set of 251 were used to train a Bayes' decision classifier, and the other 122 measurements of field averages were classified on the basis of the Bayes' decision rule. Of the types of surface cover shown, 78% were correctly identified in the above groupings.

*The 85% correct identification means that 85% of the measurements in group (b) were actually identified as being in group (b). In general, the individual types of surface cover in group (b) were completely confused with one another.

Figures 10 and 11 show. Although the Bayes' procedure categorized the August-September data better than the July data, the clusters found in the July data corresponded better to the surface cover categories than those clusters found in the August-September data. This was due to the fact that there was no physical separation between the confused surface cover categories as may be seen from the scattergrams. We should note that these clusters were formed without any information regarding "ground truth", i.e., knowledge concerning the vegetation category which each measurement vector actually represents.

The Euclidean distance-similarity coefficient from the multiple-linkage clustering technique were found to discriminate crop types nearly as well as the other methods of categorization (see Figures 12 and 13). Little discriminatory potential was indicated for the correlation coefficient, which suggests that reciprocity holds between the two radar cross-polarization returns and that depolarization of the radar signal from crop to crop is so slight that it cannot be used as a discriminating factor. The correlation similarity coefficient was not used in later analyses.

In an attempt to glean more information from the analysis of the August-September data, category (b) (see Figure 12) was subdivided into three separate categories (Figure 14). Note that category (b_3) contains mostly grain sorghum, category (b_2) contains mostly grain sorghum and alfalfa, and category (b_1) contains mostly grain sorghum and fall wheat, indicating that there is some discrimination even in the very complex portion of the data set. Comparing this grouping with Figure 6 shows that one would be hard pressed to discriminate regions of such quality from the scatterplot. Partial discrimination of this nature leads one to believe that if data were available in other wavelengths or through time, better discrimination could be achieved.

Obtaining data through time leads to the question of the best time to collect the data if better discrimination is desired. Looking again at Figure 14, we see that the problem lies in the b_1, b_2, and b_3 categories. To arrive at a solution to the problem of finding the optimum time to gather data for crop type discrimination, the curves in Figure 15 were constructed. The solid lines on the curves are based on actual average of the total data available at the University of Kansas (July, August, September, October, and November). We have based the dotted lines on crop growth patterns and maturity dates.

Surface Cover Actually Measured:	Number of Measurements Identified as: I	II	III
(a) bare ground sudan grain sorghum alfalfa bare ground– wheat wheat stubble– weeds	205	4	0
(b) corn	2	3	0
(c) sugar beets	0	1	11

FIGURE 10. Conditional probability clustering for August-September 1965 radar imagery. Six clusters were asked for, of which 4 were collapsed together since they had the most similar category distributions.

$\epsilon_1 = .27 \quad \epsilon_2 = .36$

Surface Cover Actually Measured:	Number of Measurements Identified as: I	II	III
(a) bare ground wheat stubble	99	17	0
(b) alfalfa grain sorghum corn weeds pasture	10	115	0
(c) sugar beets	0	3	11

FIGURE 11. Conditional-probability clustering for July 1966 radar imagery. Four clusters were asked for, 2 of which were collapsed together since they had the most similar category distributions.

$\epsilon_1 = .14 \quad \epsilon_2 = .36$

Number of Measurements Identified as:

Surface cover Actually Measured	(a) bare ground, pasture	(b) grain sorghum, bare ground-wheat, alfalfa wheat stubble-weeds	(c) corn	(d) sugar beets
(a) bare ground, pasture	47 (98% Correct Identification)	1	0	0
(b) grain sorghum, wheat stubble-weeds, alfalfa, bare ground-wheat	14	151 (90% Correct Identification)	1	0
(c) Corn	0	0	5 (100% Correct Identification)	0
(d) sugar beets	0	0	1	11 (92% Correct Identification)

E27

FIGURE 12. Identification accuracy for August-September radar imagery using complete linkage cluster analysis as the grouping technique: The data used were average image densities for monopolarization (HH) August 1965 imagery and for multiple polarization (HH, HV) September 1965 imagery. Multiple linkage clustering was applied using Euclidean distance as the similarity coefficient (see Sokal and Sneath, 1963 for details of the clustering procedure).

* The majority of these fields were young wheat fields very short and lacking complete cover.

Surface Cover Actually Measured	Number of Measurements Identified as: (a) bare ground	(b) corn, alfalfa, grain sorghum, weeds pasture, wheat stubble	(c) sugar beets
(a) bare ground	53 (94% Correct Identification)	3	0
(b) corn, alfalfa grain sorghum, weeds, pasture wheat stubble	25	159 (84% Correct Identification)	5
(c) sugar beets	0	1	13 (93% Correct Identification)

FIGURE 13. Identification accuracy for July 1966 radar imagery using complete linkage cluster analysis as the grouping technique: The data used were 259 measurement vectors each consisting of four multipolarization (HH, HV, VV, VH) image densities. Multiple linkage cluster analysis was used as the categorizing technique using Euclidean distance as the similarity coefficient (see Sokal and Sneath, 1963 for details of the clustering procedure).

* Mostly dry stubble

SIX CATEGORY BREAKDOWN USING MULTIPLE LINKAGE CLUSTER ANALYSIS

BASED ON THE EUCLIDEAN DISTANCE COEFFICIENT

Category	(a) Bare Ground and Wheat	(b_1) Grain Sorghum and Wheat	(b_2) Grain Sorghum and Alfalfa	(b_3) Grain Sorghum	(c) Corn	(d) Sugar Beets
Bare Ground	45	1				
Grain Sorghum	1	28	24	37	1	
Weeds and Wheat Stubble	2	6	8			
Fall Wheat	9	18	4			
Alfalfa	1	6	16	2		
Sudan	1			2		
Corn					5	
Pasture	2					
Sugar Beets					1	11
No. Correct/ Total	54/61	46/59	40/52	37/41	5/7	11/11
Percent Correct	89%	78%	77%	90%	71%	100%

FIGURE 14

Using the curves to determine when to collect data which would allow better discrimination of grain sorghum and winter wheat (category b_1), we see that data taken in April or May would allow us to achieve much better discrimination. During these spring months the grain sorghum fields are being prepared for the planting of the crop. On the other hand, winter wheat is in the process of rapid growth, and therefore would give a much higher radar return. Likewise, this same time period would allow much better discrimination between grain sorghum and alfalfa (category b_2). Alfalfa, like winter wheat, is in the early rapid growth stage during the early spring months. The discrimination of alfalfa from winter wheat appears difficult at first glance. However, the curve for winter wheat in Figure 15 is for the entire winter-wheat growing season, which starts in August. Many times winter wheat will not be immediately replanted in the crop rotation system; that is, winter wheat will be planted on a fallow field or will be followed by a fallow field. Even when a field of winter wheat is replanted after harvest, discrimination may be achieved by concentrated sensing in July and early August, during the bare-ground phase of the cycle.

While crop discrimination in this study was confined to radar imagery, the techniques could just as easily be applied to imagery from other remote sensing systems. It is probable that the best discrimination would be obtained by combining imagery of several congruent data sets from a number of sensing systems taking time sequential imagery rather than using all four polarizations in a single time period.

Possible Radar Systems and Their Problems

The results of the study presented above show an encouraging ability to discriminate crops with radar, especially in view of the paucity of data. The use of only a single-frequency multiple-polarization system at various times and for various polarizations and frequencies is urgently needed before an operational system for crop identification can be designed.

Radar systems flown to date for agricultural purposes have operated at K-band and at X-band. Only the K-band system has provided the multiple-

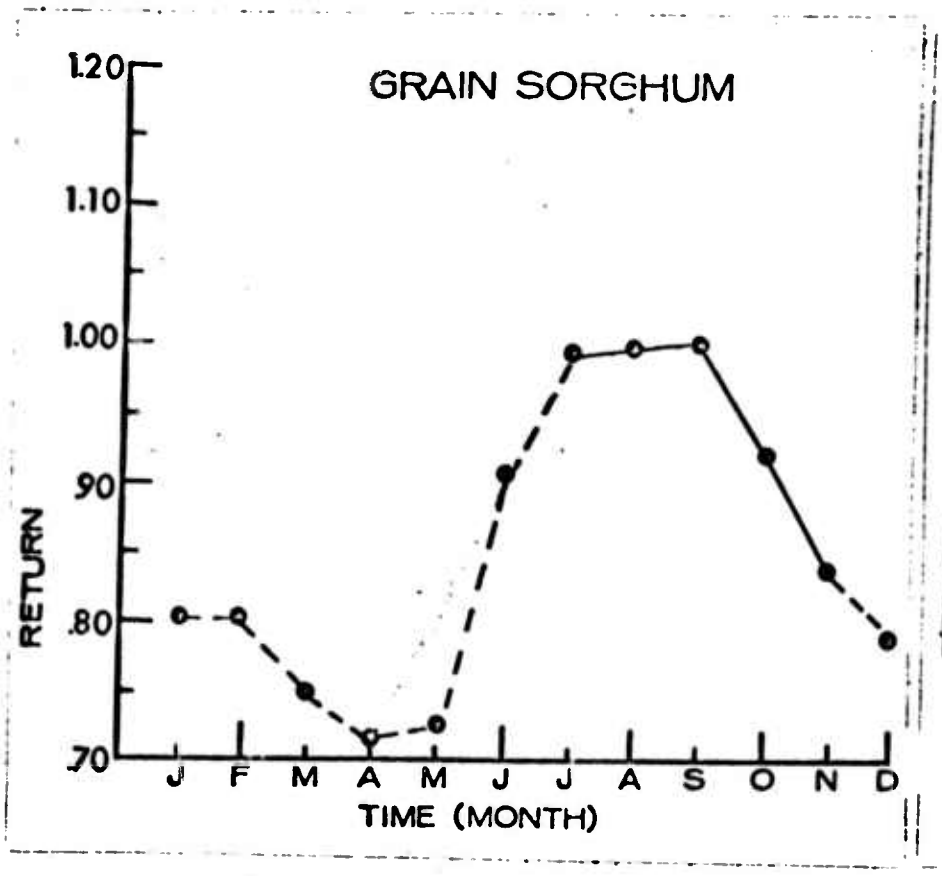

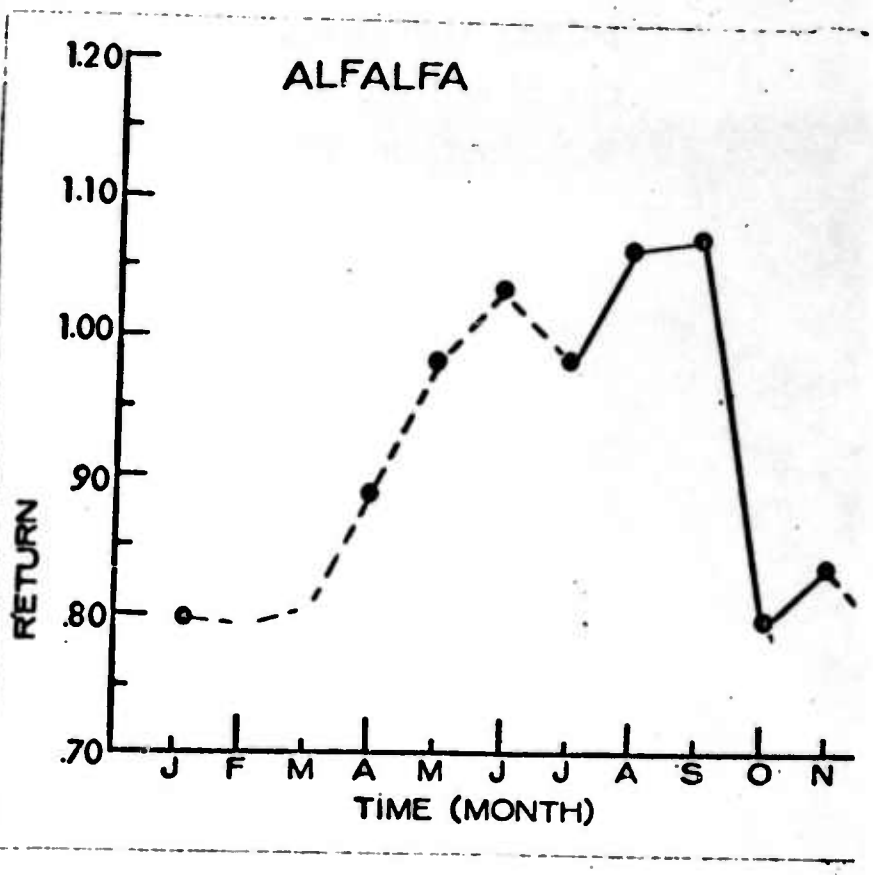

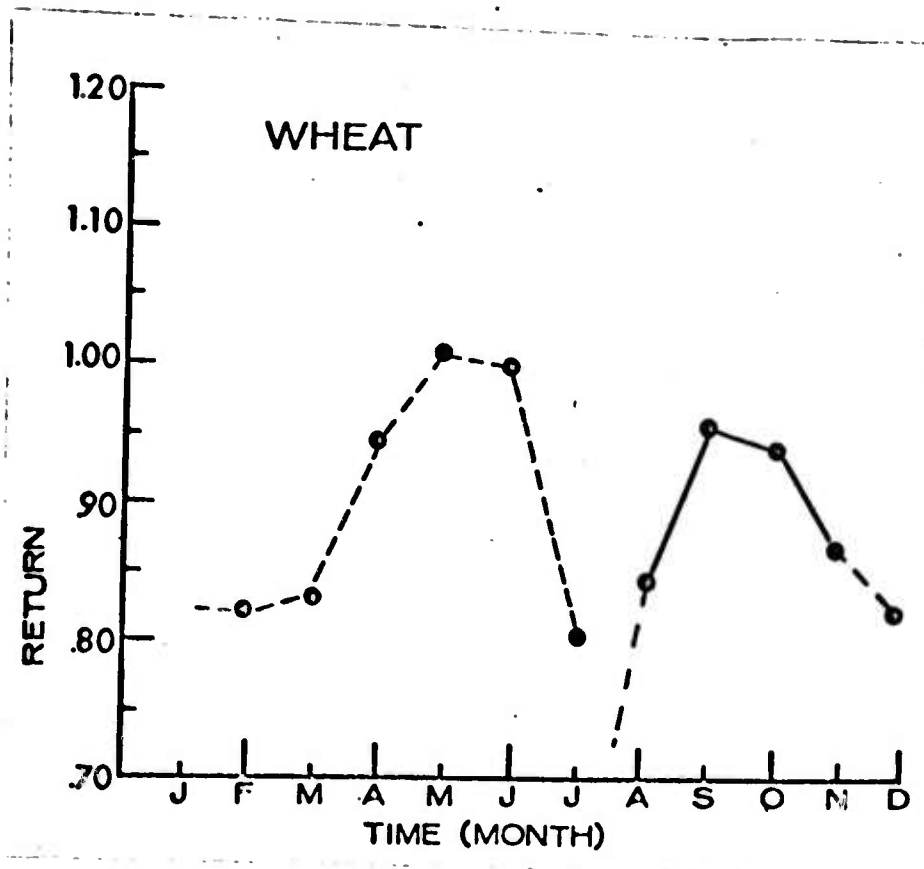

FIGURE 15. Relative radar return curves: The relative densities are based on HH polarization K-Band radar image densities. The solid lines are averages of the return for each crop type based upon the temporal data available. The images were obtained over a three year time period and therefore do not represent the average return for a given set of fields. The dashed lines were interpolated using known crop growth cycles, maturity dates and the average return from categories such as bare ground and wheat stubble.

polarization coverage that seems so useful. As indicated previously, the use of multiple frequencies should have many of the advantages for identification of crops found by the use of multiple wavelengths in the visible and infrared. The exact spread of frequencies required, however, cannot be determined on a purely theoretical basis, and many more measurements will be necessary before a full specification can be produced.

Clearly both K-band and X-band data are useful in crop discrimination. For crops with fairly large physical structure, such as corn, wavelengths longer than the 3 cm of X-band may also be valuable. Wavelengths as long as 10 or 20 cms may help in crop discrimination, and even longer wavelengths may be required for discrimination between soils or between trees in forest land. Research is required to determine both the spread and number of frequencies that can be effectively used.

The images studied here were produced with a real-aperture system. At the longer wavelengths, a synthetic aperture system will be necessary to achieve the type of resolution needed in crop studies from aircraft. Spacecraft platforms operating at any reasonable frequency will require synthetic aperture systems to produce imagery of usable resolution.

Synthetic-aperture images, like photographs made with pure laser light, have a speckled appearance, because each point is likely to be governed by a Rayleigh distribution and to be only one element of that distribution. Averaging over many points produces the mean value which is most significant in the recognition systems. These averages may be achieved spatially, but they may also be achieved in frequency by transmitting a continuous spectrum in the vicinity of each of the frequencies of a multi-frequency system. In fact, it may be desirable to sweep across an entire band of frequencies--for example, from 8 to 12 GHz, if it turns out in the experiments that there is sufficient differentiation of crops within this band. This technique is being tested in the 4 to 8 GHz band at the University of Kansas at present, although no measurements have yet been made.

Although we clearly lack a scientific basis for describing a system that might not be operational for ten years, the meager evidence to date

indicates that the system might look something like this: an aircraft system carrying a radar operating at either fixed or continuously-swept frequencies over a range of perhaps 3 to 30 GHz. The radar would look to the side and produce synthetic-aperture images. Information would be recorded on a multi-channel tape recorder. The recorded signals would be processed by a suitable congruencing technique so that they could be compared not only with each other, but with signals from the same area taken in previous flights. The measurement vectors so produced would be processed through one of the techniques described here (or others to be developed) to produce outputs of value to the agriculturalist. The outputs would include maps in which individual fields would be located, along with their crops and perhaps some indication of the average measurement vector for each of the crops. In addition, the system would be capable of producing integrated outputs giving total areas of various crops and various stages of growth. Whether the system will ever be able to point to diseased crops and actually to give predictions of yields over major areas remains to be determined. That such a system could indeed discriminate crops seems plausible on the basis of evidence at hand, but this ability certainly has not been proven.

An aircraft system such as this could fly at perhaps 500 miles per hour to obtain continuous coverage in the United States in a reasonable length of time. The swath width might be 20 to 40 miles, and the area covered would be determined accordingly.

Small satellites can carry single-frequency, single-transmitted polarization systems at the present state of the art (Moore and Simonett, 1967)*. Such systems could give coverage over the entire world and would be capable of the sorts of discriminations described here, although repetitive coverage might improve the results over the rather meager coverage used in the present analysis. With larger spacecraft capable of supplying perhaps a kilowatt of power, the full broad-band multipolarization system could be carried in space. The swath width to be used in space will depend upon the antenna size and the power available, and will vary from a minimum of around 20 kilometers with the systems that could be

* CRES Technical Report 61-32 (see Bibliography, p. G4)

carried on a Nimbus-size satellite at present to much larger numbers possible if more power and space are available.

The potential of this technique is clearly high for crop studies the world over, but many of the predictions are based upon extreme extrapolations from rather limited data. Obviously, a great deal more experimentation is called for, particularly with radars operating in different wavelengths and with multiple coverage at frequent intervals throughout the growing season. Furthermore, extensive studies at present have been limited to one site in western Kansas and to another in the Phoenix area, where some work has been done by Goodyear Aerospace Corporation. These sites are representative of certain cropping practices and certain types of crops, but flights must obviously be arranged in other areas of the world where the crops, agricultural practices, or both are different from those observed in the United States.

Concluding Remarks

From the preceding discussion the following conclusions emerge.

(1) In any remote sensing system concerned with the detection of and discrimination between crops, there is a severe fall-off in the ability of the system to provide the answers requested of it, when constraints of increasing severity are placed on the sensor, the timeliness of data collection, the congruencing of data sets through time, or the spatial or data-discrimination requirements of the system. Thus, rather than asking too much of a sensor system and suffering disappointment because it cannot provide the required information, it is appropriate to define for each remote sensing problem various alternative-constraints strategies and loss functions so that rational choices may be made.

(2) Though only a small amount of data were available, we have clearly shown that identification accuracies in the ninetieth percentile can be attained by using the methods illustrated in this paper. Further work needs to be done on clustering techniques which can analyze data in as detailed a fashion as the multiple-linkage clustering procedure, yet with

the ability of the conditional-probability clustering method to handle large amounts of data quickly. No attempt has been made here to associate crop type with the spatial texture distribution it produces on the image, yet this might well allow for identification accuracies approaching 99%.

Acknowledgements

Financial support for this study was provided by the following contracts: Project Themis (DOD), DAAK02-68-C-0089; USGS Contract 14-08-0001-10848; and NASA Contract NAS 9-7175. The support of the University of Kansas Computation Center is also gratefully acknowledged.

Appendix F

OBSERVATIONS ON THE GEOMORPHOLOGY AND LAND USE OF PART OF THE WASATCH RANGE, UTAH

R. Peterson

Technical Memorandum 133-4

March 1968

OBSERVATIONS ON THE GEOMORPHOLOGY AND LAND USE OF PART OF THE WASATCH RANGE, UTAH

R. M. Peterson

AN/APQ-97 multiple polarization radar imagery obtained in October, 1965 on NASA flight number 90 was examined to document its potential for obtaining the following types of information: physiography, surface material, geomorphic history, mineralized areas, drainage, land use, and transportation.

Both HH and HV radar polarizations were examined with the naked eye and with a 5 power microscope. 2X enlargements of the radar imagery were also examined; sometimes with a reading glass.

Thorough study of the radar imagery resulted in a wealth of information, much of which is new and which does not appear in reports or maps of the area. Examples are some ancestral stream patterns with resultant information on the origin of the Wasatch Range, fracture zones and possibly undiscovered mineralized areas.

After a study of the radar, information obtained from the imagery was compared with data on topographic maps, geologic maps, and 1:63,360 scale aerial photo mosaics. It is significant that even though the scale of the radar imagery is only approximately 1:160,000, it was necessary to consult maps of 1:24,000 scale to observe some of the same features. In some cases comparison of first-round radar data with published data gave clues to more features to search for on radar imagery and resulted in new discoveries. Examples are two previously unreported major fracture zones and a joint set that appear to control location of mineral deposits in the Park City area.

The following maps were prepared by tracing information from the radar imagery onto transparent overlays: physiographic maps (2 types), landform classification maps, surface material, ancestral drainage,

present drainage, land use, and transportation.

The study area is a rectangle approximately 12 by 30 miles extending east from Salt Lake City to the east side of Rhodes Valley, Utah (see Fig. 1). The major portion of the study area is occupied by the Wasatch Mountains whose steep escarpment overlooks Salt Lake City.

The Wasatch Range, the westernmost range of the Middle Rocky Mountains, trends north and south and lies at the east side of the Great Basin. The local relief between the Great Salt Lake Valley and the highest part of the range, which is about two miles from the Wasatch Front, is over 6,800 feet (the highest peaks in this area are Mt. Olympus at 9,026 feet and Twin Peaks at 11,330 feet), (Fig. 1). The drainage divide lies approximately 10 miles east of the front and at a lower elevation than peaks near the front. There is a gentle eastward slope of the Wasatch Range from near the front to the broad valleys of Parleys Park and Rhodes Valley, which are in the Wasatch-Uinta transition area.

Rhodes Valley (also known as Kamas Valley or the Kamas Sag) lies at the extreme western end of the Uinta Range and is a wide, flat-floored valley at an elevation of approximately 6,400 feet. To the west of Rhodes Valley the low, rolling West Hills are covered predominately by sagebrush and scrub oak and are usable primarily for grazing. The only other flat areas in the study area are Parley's Park, at an elevation of 6,600 feet, and the narrow flood plains and terraces along the Provo and the Weber Rivers and their tributaries.

Natural Vegetation

The natural vegetation on the floors of Parleys Park and Rhodes Valley was grass; cottonwood, river birch, willow and box elder trees grew along streams. The lower hills are covered by sagebrush and some juniper, June grass and remnants of the native Indian rice grass. Scrub oak and sagebrush with snowberry and some maple grow between 7,000 and 8,000 feet. At 8,000 to 10,000 feet are coniferous forests of Engleman spruce with some Alpine fir, Douglas fir, and lodgepole pine. The higher

parts of the study area are above timber line which ranges from 9,500 to 10,500 feet (Hawkes, 1959, pp. 9-11).

Drainage

Several streams have cut scenic canyons into the Wasatch. Within the study area most of these stream valleys and the higher parts of the range are covered by dense forests and have snow for several months each year. Because of the spectacular alpine scenery, snow cover and proximity to Salt Lake City, three nationally famous ski resorts are located within the study area. These are the Alta at the head of Little Cottonwood Canyon, Brighton at the head of Big Cottonwood Canyon, and the Park City ski area near the mining town of Park City, (see Fig. 1).

Drainage of the entire study area is to the Great Salt Lake. Several canyons, cut through the Wasatch Front by westflowing streams, are visible on the imagery. From north to south these are Parleys, Mill Creek, Neffs, Big Cottonwood, Little Cottonwood, and Bells Canyons. The heads of most of these canyons contain cirques from which Pleistocene valley glaciers advanced down the canyons, in cases as far as the Wasatch Front.

The east side of the region is drained by two rivers that head in the Uinta Mountains. The Weber River has its origin on the north side of the Uintas and flows west across the north side of Rhodes Valley, then in its northward course it receives tributaries which drain most of the central part of the study area. The Provo River heads on the south flank of the Uintas, flows through the south end of Rhodes Valley, through the narrow Upper Provo Canyon across Heber Valley and then to Great Salt Lake via Utah Lake and the Jordon River.

Land Use

The land use in this area depends, to a large extent, on elevation, slope of the land, availability of water, and location of mineral deposits. Land use of the study area is shown in Figure 2 which was prepared from radar imagery. Mountainous areas here serve five main uses: One is the

function of watershed and storage area for water. This is especially important for the arid Wasatch Oasis which extends along the west side of the Wasatch Range. Bailey (1941, p. 194) states that at least 80% of the usable stream flow in Utah comes from mountain lands over 7,000 feet in altitude and that each acre of irrigated land is dependent upon water from approximately seven acres of watershed land. The Wasatch Oasis, which contains most of Utah's farms, cities, and population, would not exist if there were no watersheds such as those in this study area. Grazing is a second use of the mountain land. Large herds of sheep and some beef cattle are grazed in many parts of the area although the hills between Rhodes Valley and Parleys Park are most heavily grazed. Forestry is a third use of these mountains although this is not as important as it was in earlier times. Mining, a fourth land use, has been conducted near Park City and in Little Cottonwood Canyon since 1868. Over 450 million dollars of gold, silver, copper, lead, and zinc have been mined in the Park City Mining District, although many mines have closed in recent years. A fifth land use in the mountainous areas is recreation. Ski resorts here draw large numbers of people from all over the United States each year. In the canyons east of Salt Lake City there are many weekend cottages and summer homes in addition to numerous camps and picnic facilities.

The predominant use of land in the valleys is for agriculture. The majority of the farmers live in nucleated settlements which are readily apparent on the radar imagery. In Rhodes Valley farmsteads not in the villages tend to be on the main north-south road. The imagery shows the relationship between well drained land and the location of the villages and farms; most of the farms are on the better drained sides of Rhodes Valley and Parleys Park. The lower sides of the valleys have stronger return from the wet land covered with marsh grass.

Inspection of the radar imagery shows many clusters of cottages, mine buildings and mine dumps. Examination of both HH and HV polarizations reveals more cultural features than either one polarization alone. For example, several mine dumps appear on the imagery. Near Keatley south of Park City, mine dumps and railroads leading to the mines are visible on

imagery. South of Parleys Park the waste dumps on Quarry Mountain can be seen.

By comparing both polarizations and combining information from each, it is possible to prepare a transportation map from radar imagery (Fig. 3). Shown are only the hard-surface main roads, not jeep roads which are visible in many places.

Geomorphic history. The geomorphology of the present Wasatch Range is the result of a fairly complex history. As summarized by Granger et al., (1952) and Threet (1959) the following sequence occurred. At the beginning of the Laramide orogeny, in middle and late Cretaceous time, north-south compression formed the east-west folds of the Central Wasatch. Thrust sheets from the west overrode the site of the present Wasatch and clastics eroded from highlands were deposited in adjacent basins. After a quiet period the Cretaceous folds were further compressed in Paleocene or Eocene time; at about the same time the Little Cottonwood, Alta, Clayton Peak and Park City stocks were intruded.

The Wasatch Range was first elevated by folding along north-south axes, which began in the late Eocene or Oligocene. At this time the major relief features were formed, the courses of the Weber and Provo Rivers were established and lavas and andesitic pyroclastics were extruded.

Regional warping along old trends in late Oligocene or early Miocene was followed by erosion of broad surfaces. One of these broad erosional surfaces, the Weber Valley surface, may be preserved in Big Cottonwood Canyon (Granger, et al. 1952, p. 36) where there are elevated, broad valley profiles. The former erosion surface, represented by an extension of the spurs on the sides of Big Cottonwood Canyon has been dissected. This erosion probably began before Pleistocene glaciation, possibly in late Pliocene time (Granger et al., 1952, p. 36).

Block faulting and broad warping, which began in late Miocene or Pliocene, was continued in late Pliocene and Pliestocene. Associated with the uplift was dissection of old erosional surfaces, diversion and capture of streams, and erosion of Parleys Park and Rhodes Valley. During the Pleistocene

the high parts of the Wasatch were glaciated and Lake Bonneville, the fresh water ancestor of Great Salt Lake, filled part of the Great Basin.

Geomorphic Regions. The area studied can be divided into the following regions: (1) The small portion of the Great Basin where Salt Lake City is situated, (2) The mountainous terrain of the complex Wasatch Range, (3) The valleys of Parleys Park and Rhodes Valley, and (4) The Andesite Hills. The Uinta Range is not discussed in this paper because only the western tip of this range is shown on the imagery.

1. The Salt Lake City Area. Shown on the radar imagery is part of Salt Lake City and small neighboring cities. Several stream terraces are visible where the distributaries from Big and Little Cottonwood Canyons have deepened their channels. Much of Salt Lake City is built on the floor of Pleistocene Lake Bonneville. The waves of Lake Bonneville, which was approximately the size of present day Lake Superior, cut terraces along the Wasatch Front. A delta built into Lake Bonneville at the mouth of Big Cotton-wood Canyon is seen on the imagery. Also shown is a lateral moraine at the mouth of Little Cottonwood Canyon and an end moraine at the mouth of Bells Canyon. Fault scarps are shown which cut across the moraines and delta between Bell and Big Cottonwood Canyons.

2. The Wasatch Range. This subregion includes the Wasatch Range from the Wasatch Front to Parleys Park and the spur of the Wasatch Range south of Park City and east to the Provo River.

The complex structure consists mostly of sediments folded along east-west axes; these folds are truncated on the west by the Wasatch fault. On the south side of the study area a series of plutons has intruded a large east-west anticlinal fold which seems to be the continuation of the Uinta fold. Thrust faults and high angle faults occur throughout the area.

The topography of the Wasatch Range is youthful. Most slopes are near the angle of repose. Stream valleys are characterized as having V-shaped profiles in the non-glaciated portions, steep gradients, and valley floors barely wider than the streams in them. Road building in these canyons has always been a problem because of the narrowness of the canyons and

the almost vertical cirque walls at the heads of canyons. Hard surfaced roads extend up the canyons on the west side of the range, but, other than jeep roads, no roads (or railroads) cross the area shown on this imagery.

The radar imagery shows that the drainage of the Wasatch Range is well developed. No uplands remain other than the narrow ridge divides. Several stream patterns with a variety of controls can be recognized on the imagery. The drainage pattern of the major west-flowing streams is basically dendritic but some angularity, caused by faults and joints, can be distinguished in stream orientations. The attitude of strata influences some stream orientations; this is especially evident in Thaynes Canyon, Iron Canyon, and Dutch Draw south of Parleys Park.

The influence of structure on drainage is evident by the stream pattern around the Alta Stock and Clayton Peak stock.

The topography of the higher parts of the Wasatch can best be described as alpine. The high Wasatch Range is glaciated to such an extent that one of the most striking features observable on radar imagery, or on geologic maps, is the large proportion of the area covered by glacial moraine. Glacial moraine is conspicuous on radar imagery because of its characteristic graytone and speckled texture. Moraine covers the cirque floors, and in some cases extends for miles down the canyons.

Shown on the imagery are many slpine features such as U-shaped valleys, end moraines, lateral moraines, ground moraines, cirques, tarns, horns, cols, and truncated spurs. Several hanging valleys can be seen in Big Cottonwood Canyon. A landslide is shown on the imagery in Big Cottonwood Canyon.

3. Parleys Park and Rhodes Valley. Parleys Park is an alluvial-filled valley at approximately 6,600 feet elevation. The valley is almost level with a gentle slope to the northeast. Much of the valley, especially the east side, is swampy and covered with marsh grass as indicated by dark gray tone on the radar imagery. On Quarry Mountain at the south side of the valley, waste dumps from large quarries can be seen on the imagery.

Rhodes Valley is a wide alluvial valley with several nucleaded farming villages. River terraces are visible along both the Provo River and the Weber

River. The andesite Hills, locally called the West Hills, lie to the west of Rhodes Valley.

4. The Andesite Hills. The Andesite Hills lie in the eastern part of the study area between Parleys Park and Rhodes Valley and south of Rhodes Valley. The higher hills lie at about 7,800 feet elevation compared with 6,400 in Rhodes Valley. Most slopes are moderate, although in the western portion there are many gentle slopes. Local relief is generally moderate; less than 500 feet. The region is characterized as being in a mature stage of an erosion cycle.

The andesitic pyroclastic rock of early Tertiary age (Geologic Map of Northeastern Utah, 1961, compiled by Stokes and Madsen) has a characteristic graytone and texture on radar imagery plus a characteristic erosional pattern. The vegetation cover of grass, sagebrush and scrub oak, characteristic of these hills, seems to be responsible for some of the signal return.

The West Hills (generally the region west of Rhodes Valley and east of Parleys Park, Richardson Flat and Keetly) have a drainage divide near the west side of the region so the streams flowing east are long and have gentle gradients compared with the streams on the west side of the region. The drainage pattern, generally dendritic, is an indication of the homogeneous andesite.

Rock Units

Rocks within the study area range in age from Precambrian to Quaternary. Following is a generalized list of stratigraphic units in the Wasatch Mountains and vicinity.

Igneous Rocks

Early Tertiary? Andesitic pyroclastic rocks
Diorite porphyry; Park City stock
Diorite; Clayton Peak stock
Granodiorite; Alta stock
Quartz monzonite; Little Cottonwood stock

Quaternary

Alluvial deposits
Glacial deposits

Tertiary

Fowkes Formation
Knight Conglomerate
Crazy Hollow Formation

Cretaceous

Echo Canyon Conglomerate
Wanship Formation
Frontier Sandstone
Aspen Shale
Bear River Formation
Kelvin Conglomerate

Jurassic

Preuss Sandstone
Twin Creek Limestone
Nugget Sandstone

Triassic

Ankareh Formation
Thaynes Formation
Woodside Shale

Permian

Park City Formation

Pennsylvanian

Weber Quartzite
Round Valley Limestone

Mississippian

Douglinut Formation
Humbug Formation
Deseret Limestone
Gardison Limestone
Fitchville Formation

Cambrian

Maxfield Limestone
Ophir Formation
Tintic Quartzite

Precambrian

Mutual Formation
Mineral Fork Tillite
Big Cottonwood Formation

Many of the above rock units can be recognized and traced on radar imagery. Examples are the Weber Quartzite, the Thaynes Formation, Ankareh Formation, the Nugget Sandstone, and various igneous rocks.

An extensive area of volcanics south and west of Rhodes Valley which are mapped as early Tertiary? andesitic pyroclastics (Geologic Map of Utah, compiled by Stokes and Madsen, 1961) are recognizable on radar imagery by characteristic gray tones and textures, plus the group of characteristics one would use to recognize the same type of rocks on aerial photographs.

An especially interesting feature of imaging radar is its ability to delineate glacial moraines. Not only is ground moraine readily apparent, but so also are lateral moraines (in Bonanza Flats, for example) and terminal moraines (examples in Thaynes Canyon, Dutch Draw, and at the mouth of Bells Canyon). The interface between moraines and alluvium is very apparent (for example in Thaynes Canyon and Dutch Draw). General boundaries of the alluvium which fills river valleys and small basins (as at Parley Park, Rhodes Valley, and the valley of the Provo River) can be readily mapped from radar imagery.

Figure 4, which is a generalized map showing surface materials, was prepared by tracing boundaries of alluvium, moraine, and rock classes from the radar imagery onto a transparent overlay.

Structure

In the west part of the study area the major folds of the Wasatch have east-west axes. The north limb of the large anticlinal fold that appears to be the westward extension of the Uinta Arch can be seen in Mill Creek Canyon and Big Cottonwood Canyon. The south limb of this anticline is now mostly part of the Little Cottonwood stock. Steep northward dips and northeast-striking beds are visible on the imagery north of Big Cottonwood Canyon. Inasmuch as Little Cottonwood Canyon lies at the outer range of the radar scan where the radar beams had a low incident angle, the high north wall of Little Cottonwood Canyon caused a radar shadow in the lower end of the canyon making this portion of the imagery unusable. A few miles up the canyon, however, the imagery shows rock that has erosional characteristics of massive, igneous rock. This agrees with geologic maps which show the Little Cottonwood granitic stock at this location.

In addition to the Little Cottonwood granite stock, already mentioned, the Alta stock, the Clayton Peak stock, and the Park City stock are discernable on the imagery. Since these are mineralized regions which have had considerable economic importance, the ability to recognize such regions on radar is very significant.

Many of the folds in the study area can be observed on radar imagery. Because the attitudes of strata can be ascertained from radar imagery, the orientation of major folds can be determined from imagery. An example is the northeast trending anticline of Park City.

Several faults in the Wasatch Range can be detected by methods similar to those used for fault detection on aerial photographs. In some cases abrupt changes in gray tones and textures characteristic of rock units suggest faulting. When lithologic units are recognized on radar, offsetting, abrupt termination, or abrupt changes in altitudes of rock units can be used as evidence for faulting. Faults with physiographic expression are most easily detected.

The most conspicuous feature on the Wasatch Range is the Wasatch Front fault escarpment. There is relative relief at the front of 6810 feet (4520 feet elevation near Sandy, opposite the mouth of Little Cottonwood

Canyon; 11,330 feet at Twin Peaks north of Little Cottonwood Canyon). In addition to the numerous faceted spurs along the front, the imagery also shows recent fault scarps that cut across terraces and deltas associated with Lake Bonneville.

Along the Wasatch Front in Parleys Canyon and Mill Creek Canyon the imagery shows sediments striking generally northeast and dipping steeply north. In Neffs Canyon changes in strike that are discernable on radar correspond to faults shown on the geologic map by Granger et al. (1952). Attitudes of beds are apparent at many other places on the imagery.

In a geomorphic study of a mountainous region such as the Wasatch Range; structure is a chief element in the development of the geomorphology. It is therefore necessary to know the location and nature of at least the major faults and the dominant joint patterns in order to understand the geomorphology. A few other examples of faults detectable by radar are given below.

In the upper part of Mill Creek's Porter Fork the Lower Strand Mountain branch of the Mount Raymond thrust fault can be discerned by a change in altitude of beds and by lineation along the fault

To the east the Mount Raymond thrust can be traced by the position of the Weber Quartzite thrust slices, which lie above the thrust planes, and by lineations along the faults. The Silver Fork normal fault is very apparent where it terminates the Thaynes and Arkereh Formations and the Nugget Sandstone in Reynolds Gulch north of Big Cottonwood Canyon. This fault can be traced on the imagery north to the Mount Raymond thrust which was offset by the Silver Fork fault. Ground truth confirming this observation is reported by Granger et al., (1952, p. 24).

In Mill D Canyon, a Big Cottonwood tributary of Reynolds Gulch, the imagery shows a zone of north-south faulting that terminates the Paleozoic sediments to the east. The sediments east of Mill D Canyon, which are for the most part of Mississippian Deseret and Madison Limestones, exhibit an east-west joint pattern that is very pronounced on radar.

Possible faults or fracture zones which do not appear on published geologic maps are suggested by lineations on the radar imagery. South of Parleys Park a lineation, trending generally northeast-southwest, extends from the west side of Quarry Mountain southward up the west side of Iron Canyon and along the west side of the intrusion immediately east of Brighton. Dikes, mines and prospect pits north of this intrusion lie along this zone. Another possible fault or fracture zone, suggested by a lineament on the imagery, lies along the east side of the aforementioned stock. This lineament extends from the west side of Clayton Peak northeastward near the east side of the Alta Stock.

The Park City Mining District

Park City is one of the great base metal mining districts of Utah (Wilson, 1954, p. 182) and has been one of the most important mining districts in the United States. Silver, gold, lead, zinc and copper are the chief minerals mined there. The large mine dumps are visible on radar imagery, especially when HH and HV polarizations are compared.

The mineralized zones at Park City are related to the intrusive stocks of quartz monzonite which caused contact metamorphism in the adjacent sediments, especially in the limestones. (Lindgren, 1933, p. 584).

Lode deposits are often between limestone and quartzite, but may be in quartzite. Bedded ores are sulphides that have replaced limestones (the Park City Formation or Thaynes Formation).

An examination of the Park City West Geologic Map (Crittenden, et al., 1966) shows that mines tend to be at contacts between the Woodside shale and Thaynes Formation or between the Weber Quartzite and the calcareous Park City Formation. The mineralizing solutions apparently moved along channels formed by faults and joints. The Park City West geologic map shows a set of parallel faults (shown on geologic maps by both continuous and dashed lines) trending east-northeast and another set trending north-northeast.

A set of lineaments that may be faults or joints, visible on radar but not shown on the geologic map, trends northwest-southeast.

It is very significant that the large mines (shown on radar by the large waste dumps) tend to be located (1) at the contact of a calcareous formation and a relatively impermeable formation and (2) where the lineaments visible on radar intersect a fault. It might be possible to locate new mineral deposits with a knowledge of the new lineaments shown on this radar imagery.

Ancestral Drainage

A significant feature of radar imagery is its ability to depict former stream courses. The imagery shows distinctly the former courses of the tributaries in Upper Provo Canyon (Figures 5 and 6). The angles at which these streams join the Provo River form acute angles that point eastward, or up the present course of the Provo. Through almost the entire length of the Upper Provo Canyon the streams apparently flowed east to Rhodes Valley and northward to the Weber River. Rhodes Valley is a grossly oversized valley for Beaver Creek which flows through its central portion. This example of stream piracy has been known since Anderson described it in 1915 and it was chosen by Longwell and Flint in their physical geology text to illustrate stream piracy, but it is so striking on radar imagery that it suggests radar's value as a useful tool for mapping ancestral stream patterns.

The radar imagery shows a well-developed dendritic stream pattern in the headwaters of Mill Creek. The present stream divide transects the upper part of this stream pattern which results in an abnormal appearing drainage pattern east of the headwaters of Mill Creek. It is postulated that water from Parleys Park may have formerly drained westward through Mill Creek and possibly other westward flowing streams. It should be noted that the streams at the head of Mill Creek Canyon flow at high angles to the strike of the Paleozoic and Mesozoic sediments which have been folded and thrust-faulted. There is also a possibility, suggested by drainage shown on radar imagery, that other westward-flowing streams, such as Big Cottonwood, formerly had tributaries that extended farther eastward (Figures 5 and 6). To illustrate the comparative value of radar

in detecting old stream courses an air photo mosaic of upper Mill Creek, with a scale larger than the scale of the radar imagery was examined; the ground clutter on the photo obscured the ancestral drainage pattern.

There has been much speculation as to why the Weber and Provo Rivers, which drain the eastern Wasatch and the western Uintas, flow across the Wasatch Range. One explanation is Powell's antecedence hypothesis of a river maintaining its course while cutting through a slowly rising mountain range. A later hypothesis was that of superposition, whereby the river courses were superimposed from Tertiary strata which unconformably covered the Laramide structures. However, in the Wasatch Range there are no remnants of the Tertiary cover near the cross drainage of the Weber and Provo Rivers.

Hunt, in his 1956 report on the Colorado Plateau, used a combination of Powell's antecedence and Gilbert's superposition in what he called anteposition.

Hinze (1913) and others postulated that consequent streams on the west side of the Wasatch might have cut across the range to capture streams which drained to such lowlands as the Uinta or Bridger Basins. According to this concept rivers, such as the Weber and Provo, that captured sufficient drainage were able to cut gorges through the Wasatch Range.

Eardley believes that the Weber and Provo Rivers were established by Oligocene time and that they maintained their courses as the Wasatch Range was elevated first by folding, then by faulting. He believes that the Wasatch Range has been tilted by uplift of the range along the Wasatch Front. An absolute upward movement on the east side of the Wasatch Fault would have tilted the Wasatch some 3° or 4° along a hingeline. Eardley believes an axis of tilt lies at the head of the Provo Canyon; that below this axis the Provo has cut a gorge and above the axis the Heber Valley is filled with alluvium.

Threet (1959) questions the location of the hinge and its existence, because (1) Eardley's axis of tilt coincides with the intersection of the present profile of the Provo River and the hard Oquirrh Quartzite and (2) it is not known that Heber Valley is deeply alluviated.

The postulated reversal of drainage in upper Mill Creek Canyon supports Eardley's hypothesis regarding uplift and tilting of the

Wasatch Range and the location of the hingeline. It is postulated that Mill Creek was a consequent westward flowing stream; that at that time Parleys Park was still filled by the Tertiary conglomerates and andesites which today cover hills adjacent to Parleys Park. Uplift of the Wasatch Range caused tilting along an axis which is located at or near the present drainage divide between Mill Creek and east-flowing streams. This locality is 20 miles north-northwest of Eardley's Provo Canyon locality and the same distance east from the Wasatch Front.

When the area east of the hinge was lowered by tilting, drainage in the headwaters of ancestral Mill Creek was reversed. That the ancestral stream pattern has been altered by glaciation indicates that the tilting was prePleistocene. Since the tilting, according to this hypothesis, the level of Parleys Park has been lowered by erosion of Tertiary conglomerates and andesites which formerly must have filled the lowland.

Landform Classification

Radar imagery appears to have value as a tool in studying genetic landscape evoluation and for quantitative geomorphic classification. Although much research reamains to be done in this area findings to date are encouraging.

As part of a study on integrated landscapes in Puerto Rico, David Schwarz and Major Roland Mower compared landforms discernable on radar imagery with the quantitative landform classification of the island by Young (1953). Young's classification was based on three parameters represented by three digits. The digits show local relief, percentage of steep land, and percentage of flat land. With this criteria for classification, shown in Table 1, Young devised the classification of major landforms shown in Table 2. In many respects Young's classification resembles that of Hammond (1964).

Young's landform classification was developed specifically for Puerto Rico and was based on topographic maps. In their study of Puerto Rico with classified radar imagery, Schwarz and Mower superposed Young's landform regions on the radar imagery. They found that they could identify Young's landform regions on the radar imagery and in some cases were

able to add detail to them. For example, in an area described by Young as rugged hill land (classified 233) with one corner of the region described as rolling hills (213), Schwarz and Mower distinguished two different types of topography, rather than one, in the larger part of the region.

They also found that Young's classification, which was based on topographic maps, was generalized and in many places missed much detail shown on radar. For example, in Schwarz and Mower's regions C-2, C-3, and C-4, the imagery shows many lowland areas between the rugged hills and the rolling hills which were not included in Young's classification. Other examples can be seen in this part of Puerto Rico where the geomorphic classification based on topographic maps generalized much more than a classification based on radar imagery.

Schwarz and Mower concluded that radar imagery could be used to refine and add detail to Young's classification and that radar imagery is adequate for some aspects of regional generalization. Discrimination between landform regions such as flat lowlands and low hills could be accomplished with relative ease. They did experience difficulty in differentiating between various degrees of slopes in mountainous areas.

Included in this paper (Fig. 7) is a landform map of part of the Wasatch Range using Hammond's 1964 classification, for which criteria are given in Table 3. Hammonds classification is included here in Table 4. Although some difficulty was experienced in adapting Hammonds' broad classification to the small study region, with modifications the classification was found to be workable.

Hammond based his classification on the three parameters of slope, local relief, and profile type. The symbols B3b, according to Hammond's classification, describe an area which is 50-80% gently sloping (B); has 300-500 feet of local relief (3); and 50-75% of the gentle slope is in lowland (b). Hammond, who considered areas of about six square miles as the smallest units to be classified, stated that since his map is small scale and is based upon a simple classification, it is a highly abstract version of reality.

Because the Wasatch Range map is drawn to a much larger scale than Hammond's maps, some modifications in the classifications were made.

The local relief and profile type classes remain the same, but the slope classes were changed. Hammond selected the value of eight per cent inclination as the upper limit of "gentle" slope, but for the Wasatch Range, where little of the area is gently sloping, slope was modified to refer to relative slope rather than to any absolute slope gradient. Therefore, in this context, C slopes are steeper than B slopes and not as steep as D slopes; areas characterized as B generally have gentle slopes and D values have extremely steep slopes.

Physiographic Maps from Radar

Radar imagery portrays terrain features in such a way that the imagery is a generalized, shaded, relief map. Not only is there no symbolization problem, as on topographic and physiographic maps, but there are continuous graytone values on the radar imagery to convey a fairly detailed representation of terrain over large areas. With the addition of some place names a print of radar imagery portrays general physiography.

The two physiographic maps in this paper (Figures 8 and 9) portray the same area in the wasatch Range. Figure 8 was drawn by William Brooner who used a quill pen and India ink to sketch topography on tracing paper laid over the radar imagery.

Figure 9, was drawn by Mrs. William Brooner from a 2X enlargement of radar imagery. Various graytones were achieved by using a brush and different dilutions of India ink. Some features, such as ridge crests, were drawn with pen and ink. Although this illustration incorporates details from the radar imagery, it is more of an artist's concept than Figure 8.

It is necessary to emphasize that both of these physiographic diagrams are first attempts by persons with only limited cartographic experience to show that the technique of tracing generalized terrain maps from radar is feasible and may have potential. It may be that generalized terrain maps could be produced quicker and for less cost from radar, or a combination of radar and space-borne photography, than from large scale aerial photographs and topographic maps.

Acknowledgement: This work was supported by Project Themis (USAETL Contract DAAK02-68-C-0089, ARPA order No. 1079) and NASA Contract NAS9-7175.

TABLE 1

Criteria for Young's Classification of Landforms

First Digit: local relief in meters

1: 0 - 112

2: 112 - 242

3: 242 - 770

Second Digit: percent of steep slope*

1: 1 - 5

2: 5 - 25

3: 25 - 100

Third Digit: percent of flat land+

1: 100 - 60

2: 60 - 3

3: 3 - 0

* Steepland - slopes greater than 59%

\+ Flatland - slopes less than 3%

TABLE 2

Major Landform Classification by Young

LOWLANDS

(111) Flat lowlands

(112) Rolling lowlands with some flat land

(113) Rolling lowlands

(122) Rough lowlands with some flat land

HILL LANDS

(212) Rolling hill land with some flat land

(213) Rolling hill lands

(223) Rough hill lands

(232) Rugged hill lands with some flat land

(233) Rugged hill lands.

MOUNTAIN LANDS

(313) Rolling mountain lands

(323) Rough mountain lands

(333) Rugged mountain lands

TABLE 3

Criteria for Hammond's Classification of Landforms

First Letter: percent of area gently sloping*

A	> 80
B	50 - 80
C	20 - 50
D	< 20

Second letter: local relief in feet

1:	0 - 100
2:	100 - 300
3:	300 - 500
4:	500 - 1000
5:	1000 - 3000
6:	3000 - 5000

Third letter: profile type - percent of gentle slope in lowland or on upland

a	> 75 (in lowland)
b	50 - 75 (in lowland)
c	50 - 75 (on upland)
d	< 75 (on upland)

* Gentle slope - 8% or less slope

TABLE 4

Major Landform Classification by Hammond

PLAINS

- A1 Flat plains
- A2 Smooth plains
- B1 Irregular plains, slight relief
- B2 Irregular plains

TABLE LANDS

- B3c,d Tablelands, moderate relief
- B4c,d Tablelands, considerable relief
- B5c,d Tablelands, high relief
- B6c,d Tablelands, very high relief

OPEN HILL AND MOUNTAINS

- C2 Open low hills
- C3 Open hills
- C4 Open high hills
- C5 Open low mountains
- C6 Open high mountains

HILLS AND MOUNTAINS

- D3 Hills
- D4 High hills
- D5 Low mountains
- D6 High mountains

Summary

The observations in this report are preliminary. Much work remains to be done in the way of regional description and analysis which will be followed by field checks.

However, this report indicates that radar imagery has utility for regional geomorphic analysis and description and for land use studies. The lack of ground clutter on radar allows one to see geomorphic features that are often obscured on aerial photographs.

The topography of the Wasatch Range is well displayed on radar imagery. Especially striking are glacial features, some fault scraps, and stream patterns. Radar shows unmapped lineaments, possibly representing faults, that control development of certain landforms and apparently deposition of mineral deposits. A postulated ancestral stream pattern with reversal of drainage in the headwaters seems to yield fundamental data on the origin of cross cutting rivers and tilting in the Wasatch Range.

The 8 thematic maps prepared from radar imagery used in this study are: land use, transportation, surface materials, landform classification, present drainage, ancestral drainage, and 2 physiographic maps. In the next phase of research other maps, such as vegetation maps, will be prepared, regional descriptions will be expanded, and field checks will be performed.

TABLE 4

Major Landform Classification by Hammond

PLAINS

- A1 Flat plains
- A2 Smooth plains
- B1 Irregular plains, slight relief
- B2 Irregular plains

TABLE LANDS

- B3c,d Tablelands, moderate relief
- B4c,d Tablelands, considerable relief
- B5c,d Tablelands, high relief
- B6c,d Tablelands, very high relief

OPEN HILL AND MOUNTAINS

- C2 Open low hills
- C3 Open hills
- C4 Open high hills
- C5 Open low mountains
- C6 Open high mountains

HILLS AND MOUNTAINS

- D3 Hills
- D4 High hills
- D5 Low mountains
- D6 High mountains

Summary

The observations in this report are preliminary. Much work remains to be done in the way of regional description and analysis which will be followed by field checks.

However, this report indicates that radar imagery has utility for regional geomorphic analysis and description and for land use studies. The lack of ground clutter on radar allows one to see geomorphic features that are often obscured on aerial photographs.

The topography of the Wasatch Range is well displayed on radar imagery. Especially striking are glacial features, some fault scraps, and stream patterns. Radar shows unmapped lineaments, possibly representing faults, that control development of certain landforms and apparently deposition of mineral deposits. A postulated ancestral stream pattern with reversal of drainage in the headwaters seems to yield fundamental data on the origin of cross cutting rivers and tilting in the Wasatch Range.

The 8 thematic maps prepared from radar imagery used in this study are: land use, transportation, surface materials, landform classification, present drainage, ancestral drainage, and 2 physiographic maps. In the next phase of research other maps, such as vegetation maps, will be prepared, regional descriptions will be expanded, and field checks will be performed.

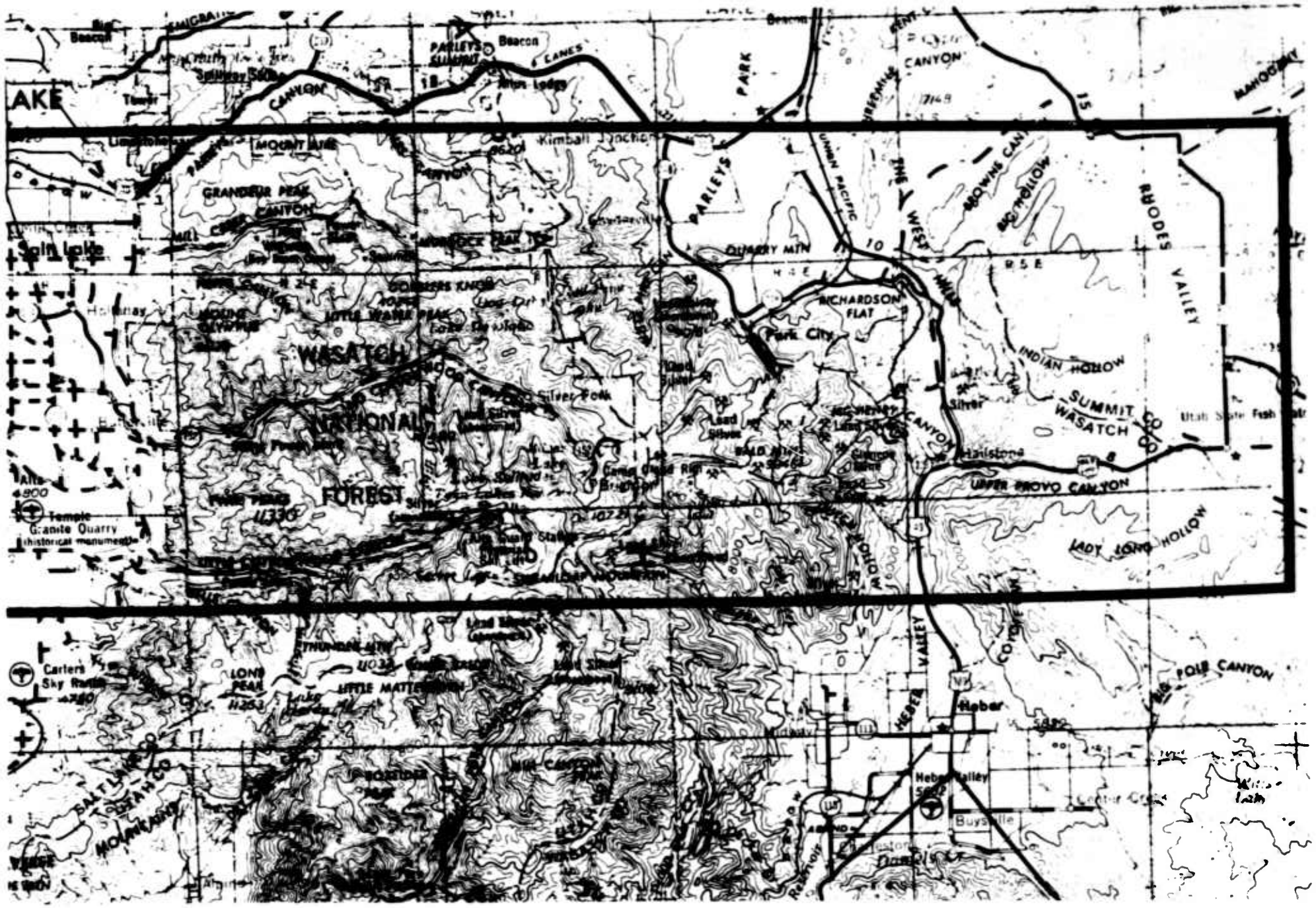

Figure 1. A portion of the 1:250,000 Salt Lake City, Utah Quadrangle showing the location of the study area in the Wasatch Range.

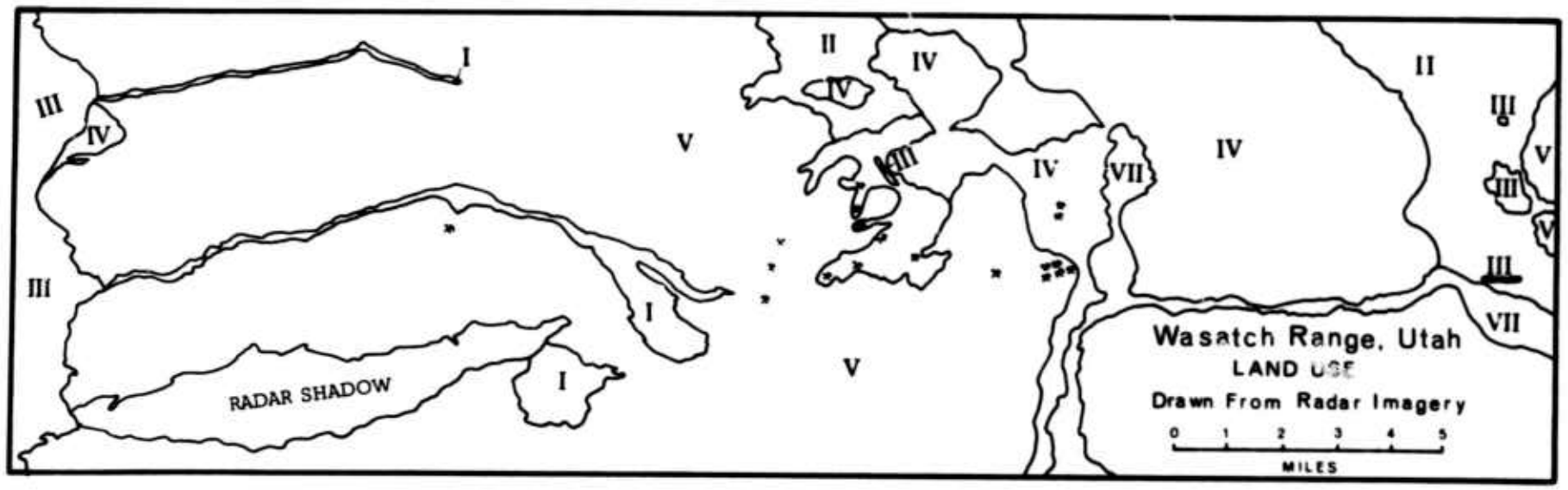

Figure 2. Land Use Map drawn from K-band radar imagery of the Wasatch Range, Utah. I. Recreation, II. Irrigated agriculture, III. Urban, IV. Grazing, V. Forestry, VI. Mining ⚒, VII. Wooded floodplains used for pasture and agriculture.

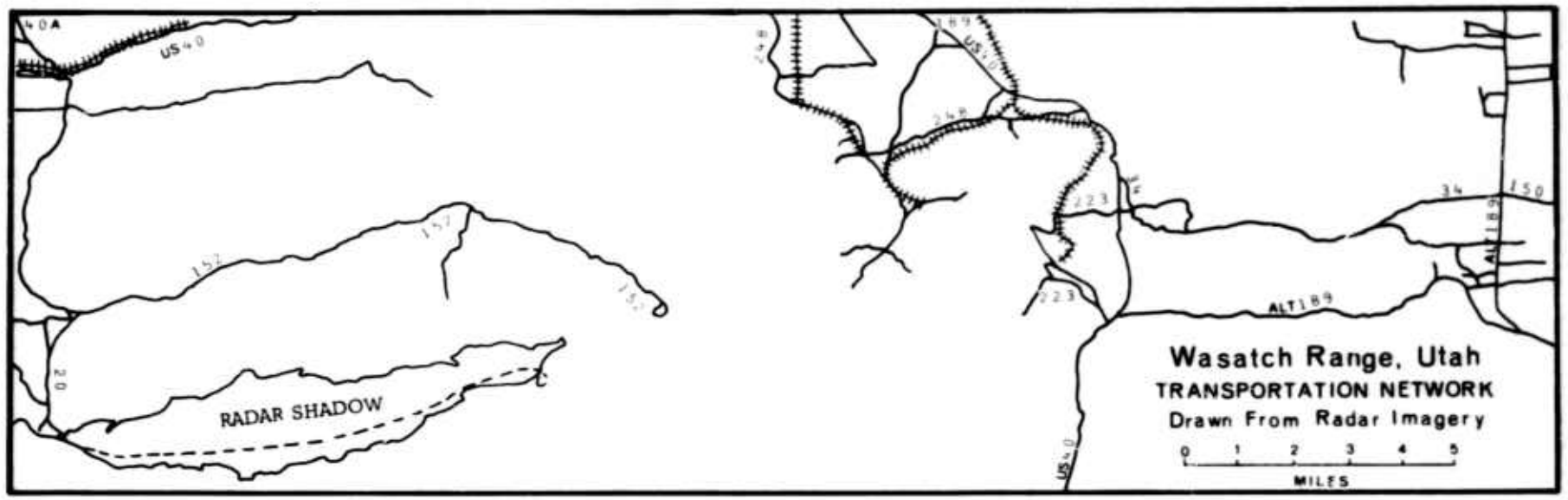

Figure 3. Transportation map drawn from K-band radar imagery of the Wasatch Range, Utah.

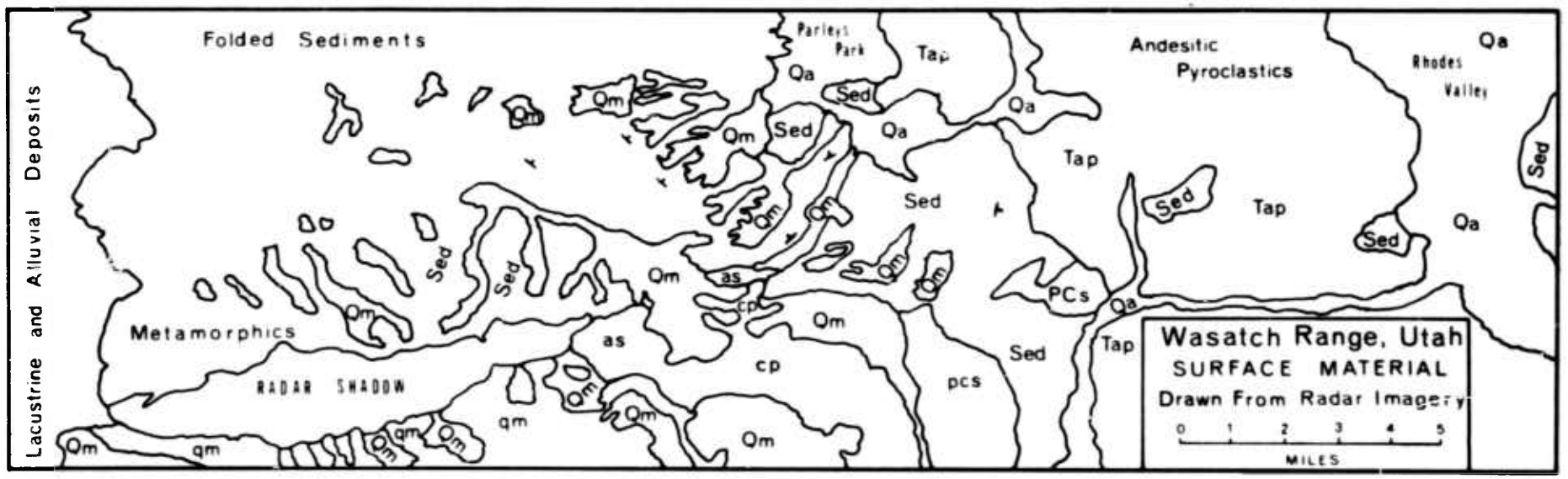

Figure 4. Surface materials as interpreted from K-band radar imagery of the Wasatch Range, Utah. as: Alta stock; cp: Clayton Peak stock; pcs: Park City stock; qm: quartz monzonite of Little Cottonwood stock; Qa: Quaternary alluvium; Qm: Quaternary moraines; Sed: Sedimentary rocks; Tap: Tertiary andesitic pyroclastics.

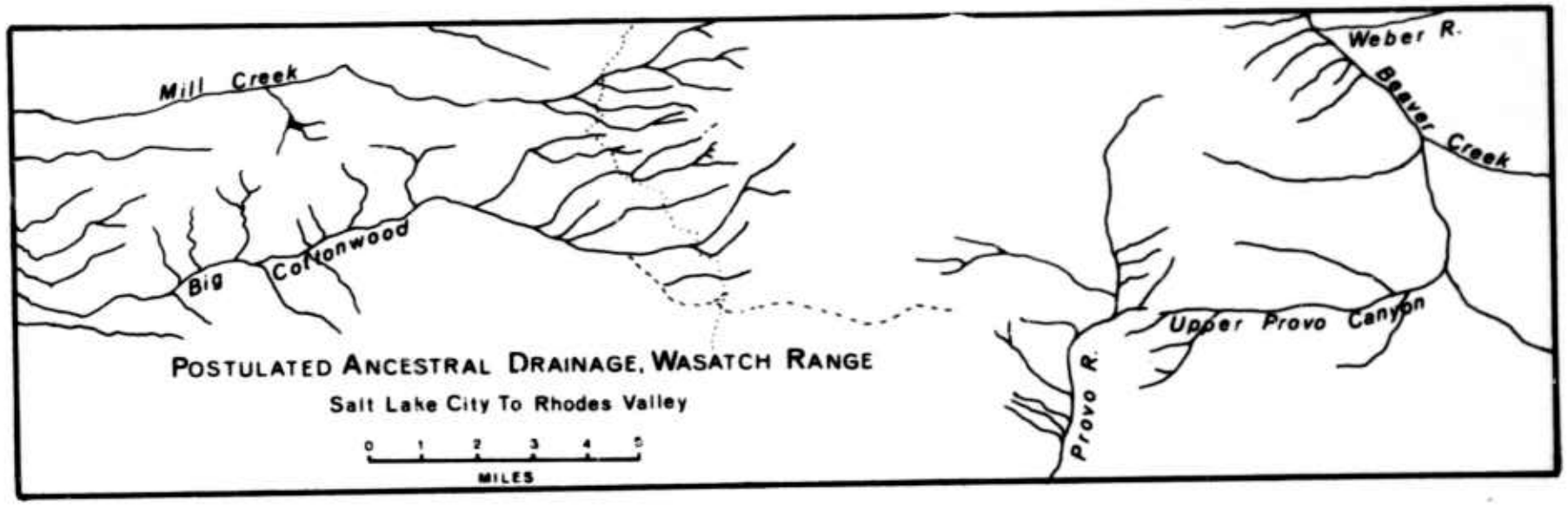

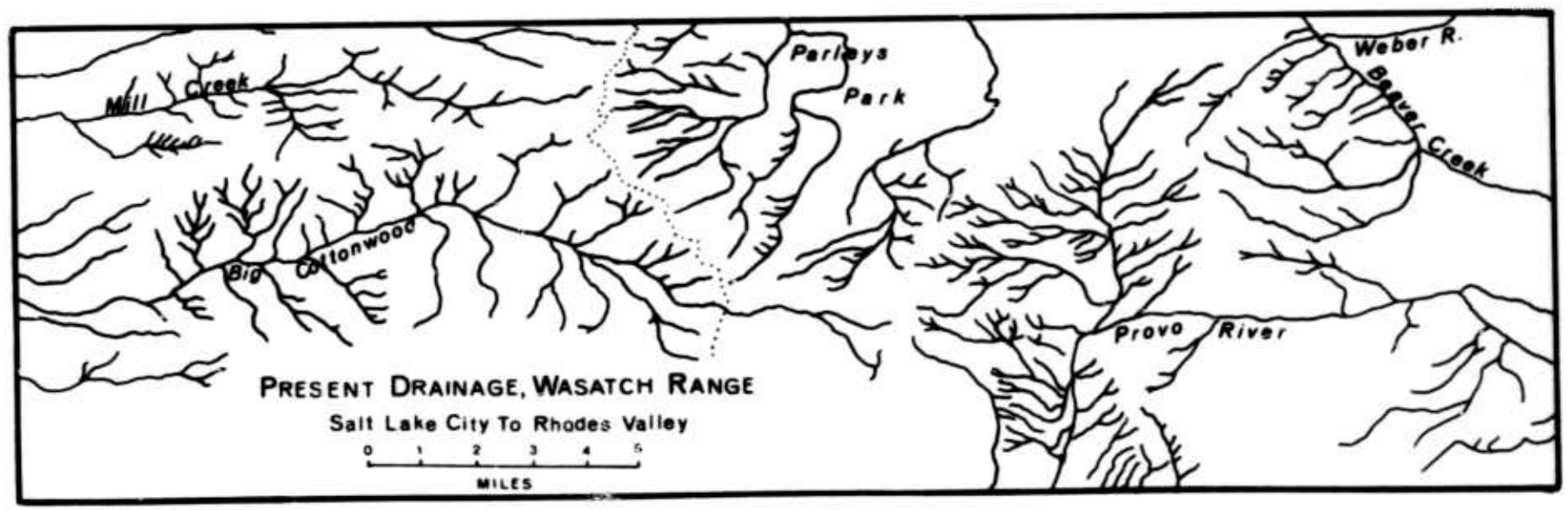

Figures 5 (top) and 6 (bottom). Ancestral and present drainage of the Wasatch Range, Utah. Drawn from K-band radar imagery.

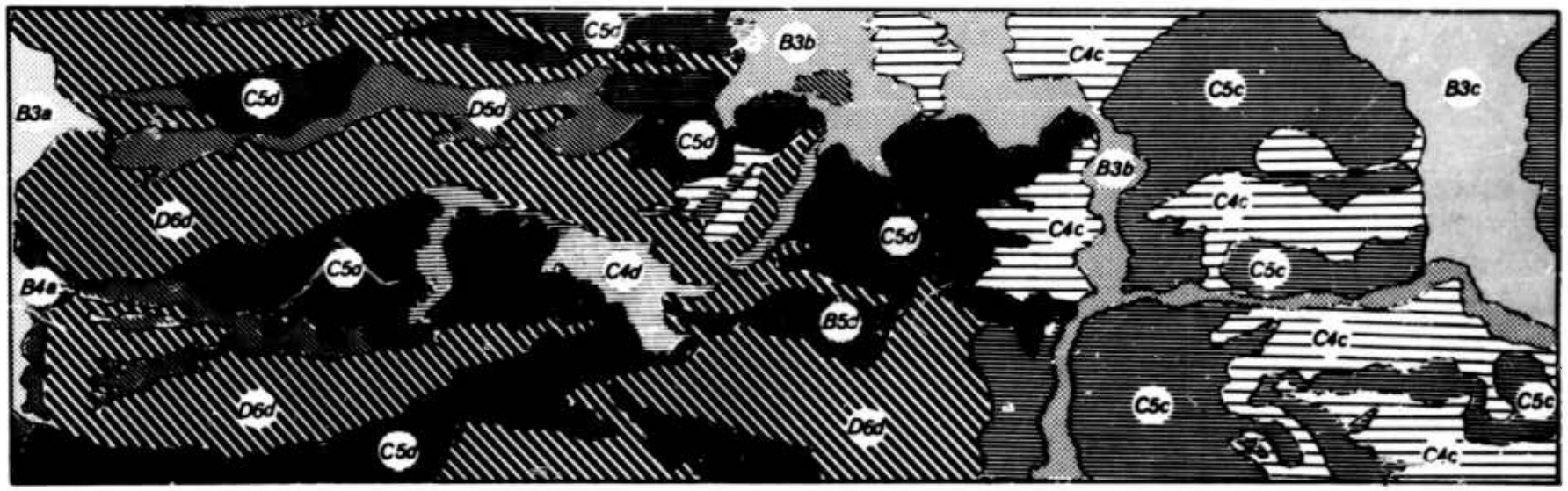

Wasatch Range, Utah -- Landform Classification*

From AN/APQ-97 Radar

B3a - Gently sloping lowland with 0-100 foot relief
B3b - Gently sloping lowland with 300-500 foot relief
B3c - Gently sloping upland with 300-500 foot relief
B4a - Gently sloping lowland with 500-1000 foot relief
B5d - Gently sloping upland with 1000-3000 foot relief
C4c - Gentle to medium sloping upland with 500-1000 foot relief
C4d - Medium to steep sloping upland with 500-1000 foot relief
C5c - Gentle to medium sloping upland with 1000-3000 foot relief
C5d - Medium to steep sloping upland with 1000-3000 foot relief
D5d - Steeply sloping upland with 1000-3000 foot relief
D6d - Steeply sloping upland with 3000-5000 foot relief

*Based on a modification of Hammond's classification.

WGU/CRES/68

Figure 7. Landform classification map of the Wasatch Range, Utah. Derived from K-band radar imagery except for elevations.

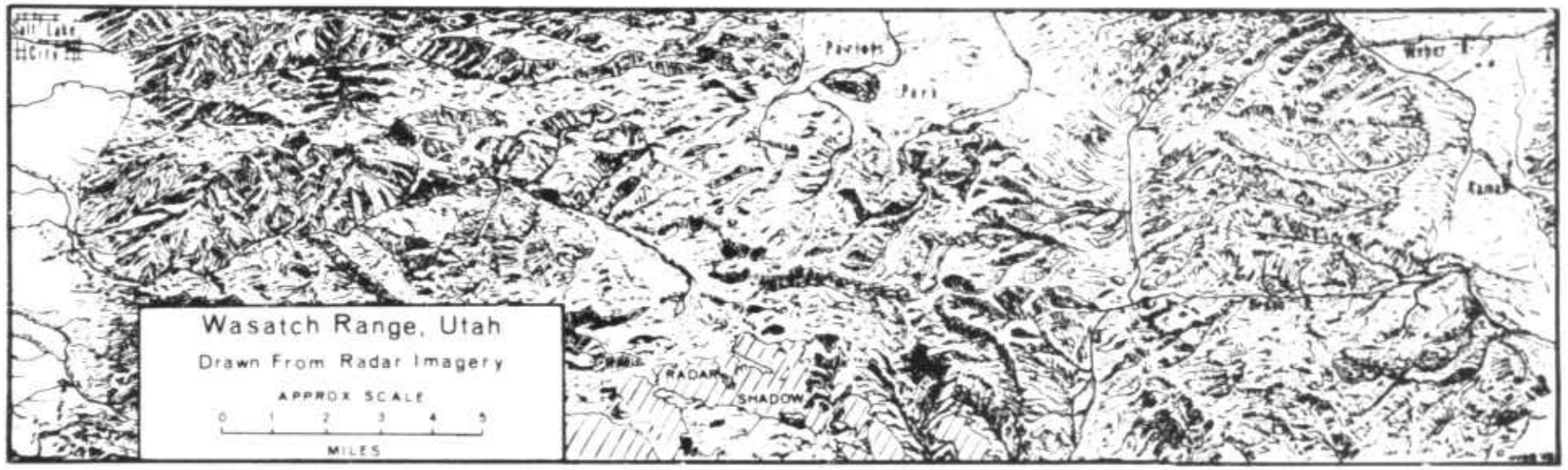

Figure 8. Physiographic Map of the Wasatch Range, Utah.

Figure 9. Physiographic Map of the Wasatch Range, Utah.

REFERENCES

Publications

Anderson, G. E., 1915, Stream Piracy of the Provo and Weber Rivers, Utah, Am. Jour. Sci., 4th ser., Vol. 40, pp. 314-316.

Bailey, R. W., 1941, Climate and Settlement of the Arid Regions, in Yearbook of Agriculture, pp. 188-196. U.S. Govt. Printing Office.

Eardley, Armand J., 1933, Strong Relief Before Block Faulting in the Vicinity of the Wasatch Mountains, Utah, Journal of Geology, Vol. XLI, No. 3, April-May 1933, p. 243-267.

_____, 1939, Structure of the Wasatch-Great Basin region, Geol. Soc. America Bull., Vol. 50, No. 8, p. 1277-1310.

_____, 1944, Geology of the North-Central Wasatch Mountains, Utah, Bull. Geol. Soc. America, Vol. 55, p. 819-894.

_____, 1952, Wasatch Hinterland, in Guidebook to the Geology of Utah, No. 8, pp. 52-60, 1 map, Utah Geological Society.

Granger, A. E., Crittenden, M. D., Sharp, B. J., and Calkins, F. C., 1952, Geology of the Wasatch Mountains east of Salt Lake City, Utah Geol. Soc. Guidebook 8, 1. 1-37.

Hammond, E. H., 1964, Analysis of Properties in Land Form Geography: An Application to Broad Scale Land Form Mapping. Annals Assoc. Amer. Geog., Vol. 54, pp. 11-19.

Hawkes, B. W., 1959, The Back Valleys of Summit and Wasatch Counties, in Guidebook to the Geology of the Wasatch and Uinta Mountains Transition Area, pp. 8-18. Intermountain Assoc. of Petrol. Geol. 10th Annual Field Conference.

Hintze, F. F., 1913, A Contribution to the Geology of the Wasatch Mountains, Utah, New York Acad. Sci. Annals, Vol. 23, pp. 85-143.

Hunt, C. B., 1956, Cenozoic Geology of the Colorado Plateau, U.S. Geol. Survey. Prcf. Paper 279, pp. 65-67.

Lindgren, W., 1933, Mineral Deposits. New York: McGraw Hill Book Co., 930 pp.

Longwell, C. R., and Flint, R. F., 1962, Introduction to Physical Geology. New York: John Wiley & Sons, Inc. 504 pp.

Marsell, R. E., 1964, The Wasatch Fault Zone in North Central Utah, in Guidebook to the Geology of Utah, No. 18, pp. 1-14, 1964, Utah Geological Society.

_____, 1964, The Wasatch Fault Zone in Salt Lake County, idem, pp. 31-52.

Threet, R. L., 1959, Geomorphology of the Wasatch-Uinta Mountains Junction, in Guidebook to the Geology of the Wasatch and Uinta Mountains Transition Area, pp. 24-35. Intermtn. Assoc. Petrol. Geol. 10th Annual Field Conference.

Young, R. N., 1955, A Geographic Classification of Landform Types of Puerto Rico, in Symposium on the Geography of Puerto Rico, pp. 27-45, ed. by C. F. Jones and Pico Rafael. Rio Piedras, P. R: Univ. of Puerto Rico Press., 503 pp.

Wilson, C. L., 1959, Park City Mining District: Intermtn. Assoc. Petrol. Geol., 10th Annual Field Conference Guidebook.

Maps

Baker, Arthur A., Caulkins, S. C., Crittenden, Max E. Jr., and Broomfield, V. S., Geologic Map of the Brighton Quadrangle, Utah. 1966. U.S. Geological Survey.

Crittenden, Max E. Jr., Geologic Map of the Dromedary Quadrangle, Utah. 1965. U.S. Geological Survey.

_____, Geologic Map of the Mount Aire Quadrangle, Salt Lake County, Utah. 1965. U.S. Geological Survey.

_____, Caulkins, S. C., Sharp, B. S., Geologic Map of the Park City West Quadrangle, Utah. 1966. U.S. Geological Survey.

Geologic Map of Northwestern Utah. Compiled by W. L. Stokes, 1963. College of Mines and Mineral Industries, University of Utah.

Geologic Map of Northwestern Utah. Compiled by W. L. Stokes and James H. Madsen, Jr., 1961. College of Mines and Mineral Industries, University of Utah.

Appendix G

CRES BIBLIOGRAPHY

TECHNICAL REPORTS

CRES Technical Report 61-1 "Fresnel Zone Processing of Synthetic Aperture Radar Data," M. Buchanan, June 1965. Supported by NASA Contract NSR 17-004-003.

CRES Technical Report 61-2 "Plane Wave Scattering from a Rough Surface with Correlated Large and Small Scale Orders of Roughness," H. S. Hayre and D. E. Kaufman, May 1965. Supported by NASA Contract NSR 17-004-003.

CRES Technical Report 61-3 "Some Applications of Radar Return Data to the Study of Terrestrial and Oceanic Phenomena," W. J. Pierson, B. B. Scheps, D. S. Simonett, March 1965. Presented at the Third Goddard Memorial Symposium on Scientific Experiments for Manned Orbital Flights, Washington, D. C., March 1965, Published in Vol. 4, Scientific Experiments for Manned Orbital Flight, American Astronautical Society, p. 87-137. Supported by NASA Contract NSR 17-004-003.

CRES Technical Report 61-4 "Spacecraft Radar as a Means for Studying the Antarctic," D. S. Simonett, D. A. Brown, September 1965. Presented to VII Congress International Quaternary Assoc., Boulder, Colorado, September 1965. Published in the Proceedings. Supported by NASA Contract NSR 17-004-003.

CRES Technical Report 61-5 "Remote Sensing from Spacecraft as a Tool for Investigating Arctic Environments," D. S. Simonett, S. A. Morain, September 1965. Presented to VII Congress International Quaternary Assoc., Boulder, Colorado, September 1965, Published in the Proceedings. Supported by NASA Contract NSR 17-004-003.

CRES Technical Report 61-6 "Imaging Radars on Spacecraft as a Tool for Studying the Earth," R. D. Ellermeier, D. S. Simonett, November 1965. Presented at the International Symposium on Electromagnetic Sensing of the Earth from Satellites, Miami Beach, Florida, November 22-24, 1965. Published in the Proceedings, p. L1-L20. Supported by NASA Contract NSR 17-004-003.

CRES Technical Report 61-7 "Radar as a Remote Sensor," R. K. Moore, January 1966. Supported by NASA Contract NSR 17-004-003.

CRES Technical Report 61-8 "Use of Orbital Radars for Geoscience Investigations," J. W. Rouse, Jr., W. P. Waite, R. L. Walters, January 1966. Presented at the Third Space Congress Meeting, Cocoa Beach, Florida, March 1965. Published in the Proceedings, p. 77-94. Supported by NASA Contract NSR 17-004-003.

CRES Technical Report 61-9 "Vegetation Analysis with Radar Imagery," S. A. Morain, D. S. Simonett, April 1966. Presented at the Fourth Symposium on Remote Sensing of the Environment, University of Michigan, Ann Arbor, Michigan, April 1965. Published in the Proceedings, p. 605-622. Supported by NASA Contract NSR 17-004-003.

CRES Technical Report 61-10 "Some Empirical and Theoretical Interpretations of Multiple Polarization Radar Data," R. D. Ellermeier, A. K. Fung, D. S. Simonett, April 1966. Presented at Fourth Symposium on Remote Sensing of the Environment, University of Michigan, Ann Arbor, Michigan, April 1966. Published in the Proceedings, p. 657-670. Supported by NASA Contract NSR 17-004-003.

CRES Technical Report 61-11 "Radar Scatterometry--An Active Remote Sensing Tool," R. K. Moore, April 1966. Presented at Fourth Symposium on Remote Sensing of the Environment, University of Michigan, Ann Arbor, Michigan, April 1966. Published in the Proceedings, p. 339-375. Supported by NASA Contract NSR 17-004-003.

CRES Technical Report 61-12 "Future and Present Needs of Remote Sensing in Geography," D. S. Simonett, April 1966. Presented at Fourth Symposium on Remote Sensing of the Environment, University of Michigan, Ann Arbor, Michigan, April 1966. Published in the Proceedings, p. 37-49. Supported by NASA Contract NSR 17-004-003.

CRES Technical Report 61-13 "The Geological Value of Simultaneously Produced Like- and Cross-Polarized Radar Imagery," L. F. Dellwig, R. K. Moore, July 1966. Published in Journal of Geophysical Research, vol. 71, no. 4, July 15, 1966, p. 3597-3601. Supported by NASA Contract NSR 17-004-003.

CRES Technical Report 61-14 "The Potential of Low Resolution Radar Imagery in Regional Geologic Studies," L. F. Dellwig, J. N. Kirk, R. L. Walters, July 1966. Published in Journal of Geophysical Research, Letters, vol. 71, no. 20, October 15, 1966, p. 4995-4998. Supported by NASA Contract NSR 17-004-003.

CRES Technical Report 61-16 "Automatic Processing of Multi-Spectral Images," G. W. Dalke, September 1966. Supported by NASA Contract NSR 17-004-003.

CRES Technical Report 61-17 "Identification of Remote Objects by Means of Scatterometry Data and Application to Pisgah Crater," G. W. Dalke, February 1967. Supported by NASA Contract NSR 17-004-003.

CRES Technical Report 61-18 "Use of Radar for Mapping Information-Gathering in Cloudy Environments," D. S. Simonett, S. A. Morain (being completed). Supported by NASA Contracts NSR 17-004-003 and NAS 9-7175.

CRES Technical Report 61-19 "The Use of Multi-Parameter Radar Imagery for the Discrimination of Terrain Characteristics," R. D. Ellermeier, D. S. Simonett, L. F. Dellwig. Presented at IEEE International Convention, New York, March 1967. Published in the 1967 IEEE International Convention Record, Part 2, p. 128-135. Supported by NASA Contract NSR 17-004-003 and NASA Grant NsG-298.

CRES Technical Report 61-20 "Evaluation of Multiple Polarized Radar Imagery for the Detection of Selected Cultural Features," A. Lewis. (Classified Report). Supported by NASA Contracts NSR 17-004-003 and NAS 9-7175.

CRES Technical Report 61-21 "The Potential of Radar as a Remote Sensor in Agriculture: 1. A Study with K-Band Imagery in Western Kansas," D. S. Simonett, J. E. Eagleman, A. B. Erhart, D. C. Rhodes and D. E. Schwarz, March 1967. Supported by NASA Contract NSR 17-004-003 and NASA Grant NsG-298.

CRES Technical Report 61-22 "Field Studies on Vegetation at Horsefly Mountain, Oregon and Its Relation to Radar Imagery," S. A. Morain, January 1967. Supported by NASA Contract NSR 17-004-003 and NASA Grant NsG-298.

CRES Technical Report 61-23 "K-Band Radar in Vegetation Mapping," S. A. Morain and D. S. Simonett. Presented at the Annual Convention of the American Society of Photogrammetry, Washington, D. C., March 1967. Published in Photogrammetric Engineering, vol. 33, no. 7, July 1967, p. 730-740. Supported by NASA Contract NSR 17-004-003 and NASA Grant NsG-298.

CRES Technical Report 61-24 "Geologic Evaluation by Radar of NASA Sedimentary Test Site," H. C. MacDonald, P. A. Brennan, and L. F. Dellwig. Published in IEEE Transactions on Geoscience Electronics, vol. GE-5, no. 3, December 1967, p. 72-78. Supported by NASA Contract NSR 17-004-003 and NASA Grant NsG-298.

CRES Technical Report 61-25 "Investigation of Cross-Polarized Radar on Volcanic Rocks," E. Gillerman, February 1967. Supported by NASA Contract NSR 17-004-003.

CRES Technical Report 61-26 Deleted

CRES Technical Report 61-27 "Application of Color-Combined Multiple-Polarization Radar Images to Geoscience Problems," D. S. Simonett, December 1966. Presented at the Colloquium on Classification Procedures: Computer Applications in the Earth Sciences, Kansas Geological Survey, Lawrence, Kansas, December 1966. Published as Computer Contribution 7, State Geological Survey, University of Kansas, Lawrence, Kansas, December 1966, p. 19-24. Supported by NASA Contract NSR 17-004-003.

CRES Technical Report 61-28 "Implementation of Pattern Recognition Techniques as Applied to Geoscience Interpretation," G. W. Dalke, December 1966. Presented as the Colloquium on Classification Procedures: Computer Applications in the Earth Sciences, Kansas Geological Survey, Lawrence, Kansas, December 1966. Published as Computer Contribution 7, State Geological Survey, University of Kansas, Lawrence, Kansas, December 1966, p. 24-29. Supported by NASA Contract NSR 17-004-003.

CRES Technical Report 61-29 "Orbital Remote Sensors--Data Processing for Geoscience Investigations," G. W. Dalke and J. W. Rouse, Jr. Presented at the American Astronautical Society Symposium, Huntsville, Alabama, June 1967. Published in the Transactions, vol. II, p. MM-23-1 to MM-23-20. Supported by NASA Contract NSR 17-004-003.

CRES Technical Report 61-30 "Radar Bibliography for Geosciences," R. L. Walters. (being completed). Supported by NASA Contract NSR 17-004-003, NASA Grant NsG-298, USGS Contract 14-08-0001-10848, and NASA Contract NAS 9-7175.

CRES Technical Report 61-31 "An Evaluation of Radar Imagery as a Tool for Drainage Basin Analysis," R. M. McCoy, August 1967. Supported by NASA Contract NSR 17-004-003, NASA Grant NsG-298, and NASA Contract NAS 9-7175.

CRES Technical Report 61-32 "Potential Research and Earth Resource Studies with Orbiting Radars: Results of Recent Studies," R. K. Moore and D. S. Simonett. Presented at the 4th Annual Meeting of the American Institute of Aeronautics and Astronautics (AIAA), Anaheim, California, October 23-27, 1967. Published as AIAA Paper no 67-767, 21 pp. Supported by NASA Contract NSR 17-004-003, NASA Contract NAS 9-7175, USGS Contract 14-08-0001-10848, NAVOCEANO Contract N62305-67-C-0044, and NSF Grant GK-1153.

CRES Technical Report 118-1 "A Medial Transformation of Two-Dimensional Data with Applications to Data Compression and Noise Reduction," P. Youngberg, August 1967. Supported by NASA Contract NAS 9-7175.

CRES Technical Report 118-2 "Analysis of Scatterometry Data from Pisgah Crater," J. Lundien, August 1967. Supported by NASA Contract NAS 9-7175.

CRES Technical Report 118-3 "Scatterometer Data Analysis Techniques," H. Masenthin (in press). Supported by NASA Contracts NSR 17-004-003 and NAS 9-7175.

CRES Technical Report 118-4 "Pattern Recognition Ideas," R. Haralick (being completed). Supported by NASA Contract NAS 9-7175.

CRES Technical Report 118-5 "Adaptive Pattern Recognition by Similarity Set Construction," R. Haralick, October 1967. Supported by NASA Contracts NSR 17-004-003 and NAS 9-7175.

CRES Technical Report 118-6 "A Survey of Some Pattern Recognition Techniques," Jess O. Betlack (being completed). Supported by NASA Contract NAS 9-7175.

CRES Technical Report 118-7 "The Influence of Radar Look-Direction on the Recording of Geologic Lineament Patterns," J. Kirk, L. Dellwig and L. Jefferis (being completed). Supported by NASA Contract NAS 9-7175.

TECHNICAL MEMORANDA

CRES Technical Memorandum 61-2 "Multi-Frequency Acoustical Simulation System," M. Buchanan, September 1964. Supported by NASA Contract NSR 17-004-003.

CRES Technical Memorandum 61-3 "A Method of Analyzing NRL Flight Radar Return," J. W. Rouse, Jr., September 196[illegible] Supported by NASA Contract NSR 17-004-003.

CRES Technical Memorandum 61-4 "Color Theory," G. W. Dalke, October 1964. Supported by NASA Contract NSR 17-004-003.

CRES Technical Memorandum 61-5 " Initial Design Considerations for the Multi-Color Display," G. W. Dalke, J. E. Rathke, J. W. Rouse, Jr., December 1964. Supported by NASA Contract NSR 17-004-003.

CRES Technical Memorandum 61-6 "Establishment of the Criteria for Determining the Pulse Repetition Frequency, the Beam Length, Beam Width and Pulse Length on the Ground," J. Butler, October 1964. Supported by NASA Contract NSR 17-004-003.

CRES Technical Memorandum 61-8 "Synthetic Aperture Power Requirements," R. K. Moore, J. Butler, November 1964. Supported by NASA Contract NSR 17-004-003.

CRES Technical Memorandum 61-9 "Satellite Altimeter Using Two Antennas," J. Butler, R. K. Moore, March 1965. Supported by NASA Contract NSR 17-004-003.

CRES Technical Memorandum 61-11 "Possible Lunar Analogs for Use by the Waterways Experiment Station, Vicksburg, Mississippi," D. A. Brown, December 1964. Supported by NASA Contract NSR 17-004-003.

CRES Technical Memorandum 61-12 "Considerations for Proposed NRL Modification to Add Synthetic Aperture Imaging Capability," J. W. Rouse, Jr., January 1965. Supported by NASA Contract NSR 17-004-003.

CRES Technical Memorandum 61-13 "Synthetic Aperture Antenna," J. W. Rouse, Jr., May 1965. Supported by NASA Contract NSR 17-004-003.

CRES Technical Memorandum 61-14 "Calculation of Tristimulus Coefficients for the CRES Multicolor Display," G. W. Dalke, May 1965. Supported by NASA Contract NSR 17-004-003.

CRES Technical Memorandum 61-15 "Modifications Made on Photovolt 520-A Densitometer," M. Buchanan, May 1965. Supported by NASA Contract NSR 17-004-003.

CRES Technical Memorandum 61-16 "Unfocused Synthetic Aperture Antenna Radar Power Requirements," J. W. Rouse, Jr., June 1965. Supported by NASA Contract NSR 17-004-003.

CRES Technical Memorandum 61-17 "Theory of Synthetic Aperture," M. Buchanan, June 1965. Supported by NASA Contract NSR 17-004-003.

CRES Technical Memorandum 61-18 "Remote Sensor Studies of the Pisgah Crater Area, California: A Preliminary Report," L. F. Dellwig, M. E. Bickford, N. Kirk, R. Walters, December 1965. Supported by NASA Contract NSR 17-004-003.

CRES Technical Memorandum 61-19 "Technique for Producing a Pseudo Three-Dimensional Effect with Monoscopic Radar Imagery," L. F. Dellwig, H. C. MacDonald, J. N. Kirk, December 1965. Supported by NASA Contract NSR 17-004-003.

CRES Technical Memorandum 61-21 "Reduction of Like-Images to Space Correlated Data Lists," G. W. Dalke, M. O. Vichellich, May 1966. Supported by NASA Contract NSR 17-004-003.

CRES Technical Memorandum 61-22 "The [3 x 3] Matrix Unit," F. Welter, May 1966. Supported by NASA Contract NSR 17-004-003.

CRES Technical Memorandum 61-23 "Pattern Recognition Problem," R. M. Haralick, June 1966. Supported by NASA Contract NSR 17-004-003.

CRES Technical Memorandum 61-24 "Photographic Color Combination Procedures and Equipment Available at CRES," D. Egbert, June 1966. Supported by NASA Contract NSR 17-004-003.

CRES Technical Memorandum 61-25 "Radar Bibliography for Geoscientists," R. L. Walters, June 1966. Supported by NASA Contract NSR 17-004-003.

CRES Technical Memorandum 61-26 "Radar Linears not Related to Geology," H. D. MacDonald, E. Gillerman, L. F. Dellwig, J. N. Kirk, July 1966. Supported by NASA Contract NSR 17-004-003.

CRES Technical Memorandum 61-27 "Radar Fundamentals," J. W. Rouse, Jr., W. P. Waite (being completed). Supported by NASA Contract NSR 17-004-003.

CRES Technical Memorandum 61-28 "Image Reproduction with Color Television Receiver," R. L. Knuckey, July 1966. Supported by NASA Contract NSR 17-004-003.

CRES Technical Memorandum 61-30 (Deleted)

CRES Technical Memorandum 61-31 "Automatic Acuteness Measurements for Multiple Images," G. W. Dalke, August 1966. Supported by NASA Contract NSR 17-004-003.

CRES Technical Memorandum 61-32 "Automatic Measurement and Reduction of Drainage Basin Data," G. W. Dalke, August 1966. Supported by NASA Contract NSR 17-004-003.

CRES Technical Memorandum 61-33 "Automatic Measurements of Texture and Detection of Lines in a Flying-Spot Scanner System," G. W. Dalke, August 1966. Supported by NASA Contract NSR 17-004-003.

CRES Technical Memorandum 61-34 (Deleted)

CRES Technical Memorandum 61-35 "Pattern Recognition and Similarity," R. M. Haralick, August 1966. Supported by NASA Contract NSR 17-004-003.

CRES Technical Memorandum 61-36 "Design System for Flying-Spot Scanner," J. E. Rathke, August 1966. Supported by NASA Contract NSR 17-004-003.

CRES Technical Memorandum 61-37 "The CRES Data Handling System," J. E. Rathke, August 1966. Supported by NASA Contract NSR 17-004-003.

CRES Technical Memorandum 61-38 "Photomultiplier, Compensated Video Amplifier and Video Amplifier Circuits," J. E. Rathke, September 1966. Supported by NASA Contract NSR 17-004-003.

CRES Technical Memorandum 61-39 "The 3-Channel Flying-Spot Scanner," J. E. Rathke, August 1966. Supported by NASA Contract NSR 17-004-003.

CRES Technical Memorandum 61-40 "The Tri-Color Display Unit," J. E. Rathke, September 1966. Supported by NASA Contract NSR 17-004-003.

CRES Technical Memorandum 61-41 (Deleted)

CRES Technical Memorandum 61-42 "Multi-Color Presentation of Images with Edge Enhancement," R. L. Knuckey, October 1966. Supported by NASA Contract NSR 17-004-003.

CRES Technical Memorandum 61-43 "Synthetic-Aperture Signal Film Quantity Calculations," J. W. Rouse, Jr., October 1966. Supported by NASA Contract NSR 17-004-003.

CRES Technical Memorandum 61-44 "An Analog to Digital to Paper Tape Converter," J. Betlack, April 1966. Supported by NASA Contract NSR 17-004-003.

CRES Technical Memorandum 61-45 "Terrain Discrimination by Radar Image Polarization Comparison," R. K. Moore, L. F. Dellwig, October 1966. Published in Proceedings IEEE, vol. 54, no. 9, September 1966, p. 1213-1214. Supported by NASA Contract NSR 17-004-003.

CRES Technical Memorandum 61-46 "Analog to Digital Converter for Low Frequency Sampling," R. Field, April 1967. Supported by NASA Contract NSR 17-004-003.

CRES Technical Memorandum 61-47 "Evaluation of Geoscience Information as a Function of Radar Resolution," R. McCoy (Classified-internal distribution only). Supported by NASA Contract NSR 17-004-003.

CRES Technical Memorandum 61-48 "Electronic Processing for Synthetic Aperture Array Radar," R. K. Moore, J. W. Rouse, Jr., Published in Proceedings IEEE, vol. 55, no. 2, February 1967, p. 233-234. Supported by NASA Contract NSR 17-004-003.

CRES Technical Memorandum 61-49 (Deleted)

CRES Technical Memorandum 61-50 "Radar Imagery, a New Tool for the Geologist," J. W. Kirk, R. L. Walters. Published in The Compass of Sigma Gamma Epsilon, vol. 43, no. 2, January 1966, p. 85-93. Supported by NASA Contract NSR 17-004-003.

CRES Technical Memorandum 61-51 Not assigned.

CRES Technical Memorandum 61-52 Not assigned.

CRES Technical Memorandum 61-53 Not assigned.

CRES Technical Memorandum 61-54 "Use of the Numerical Taxonomy System," R. Haralick, July 1967. Supported by NASA Contracts NSR 17-004-003 and NAS 9-7175.

CRES Technical Memorandum 61-55 "LGP-30 Autocorrelation Program," P. Youngberg, July 1967. Supported by NASA Contracts NSR 17-004-003 and NAS 9-7175.

CRES Technical Memorandum 61-56 "IBM Paper Tape Punch Program for the LGP-30 Computer," P. Youngberg, August 1967. Supported by NASA Contracts NSR 17-004-003 and NAS 9-7175.

CRES Technical Memorandum 61-57 "Analog to Digital to Paper Tape Data Printer for the LGP-30 Computer," P. Youngberg, August 1967. Supported by NASA Contracts NSR 17-004-003 and NAS 9-7175.

CRES Technical Memorandum 118-1 "Pattern Recognition of Multi-Spectral Photographs Using a Conditional Probability Method," R. Haralick, September 1967. Supported by NASA Contract NAS 9-7175.

CRES Technical Memorandum 118-2 "Line Driving Amplifier," J. Bryant, November 1967. Supported by NASA Contract NAS 9-7175.

CRES Technical Memorandum 118-3 "Synthetic Aperture Radar Acoustic Simulator," L. Fromme, December 1967. Supported by NASA Contract NAS 9-7175.

CRES Technical Memorandum 118-4 "Preliminary Mission Analysis Report; NASA/MSC Mission No. 47, Site 93, Pt. Barrow, Alaska," J. Rouse, Jr., October, 1967. Supported by NASA Contract NAS 9-7175.

CRES Technical Memorandum 118-5 "Preliminary Report on Radar Lineaments in the Boston Mountains of Arkansas," J. Kirk and R. Walters. Published in The Compass of Sigma Gamma Epsilon, vol. 45, no. 2, January 1968, p. 122-127. Supported by NASA Contract NSR 17-004-003 and NASA Grant NsG-298.

CRES Technical Memorandum 118-6 "On the Feasibility of Imaging Radar for Small Spacecraft," J. Rouse, Jr., (being completed). Supported by NASA Contract NAS 9-7175.

OTHER PUBLICATIONS

Moore, R. K. and W. J. Pierson, "Measuring Sea State and Estimating Surface Winds from a Polar Orbiting Satellite," Presented at the International Symposium on Electromagnetic Sensing of the Earth from Satellites, Miami Beach, Florida, November 22-24, 1965. Published in the Proceedings, p. R1-R28. Supported by NASA Contract NSR 17-004-003.

Moore, R. K. and D. S. Simonett. Contribution to several chapters in the National Academy of Science-National Research Council Publication entitled Multi-Spectral Sensing of Agricultural Resources. The contributions summarize the present status of knowledge of radar as a remote sensor in agriculture. (To be published). Supported by NASA Contract NSR 17-004-003, NASA Grant NsG-298, NASA Contract NAS 9-7175, and USGS Contract 14-08-0001-10848.

Moore R. K. and D. S. Simonett, "Radar Remote Sensing in Biology," Bioscience, vol. 17, no. 6, June 1967, p. 384-394. Supported by NASA Contract NSR 17-004-003.

Rouse, J. W., Jr. "Preliminary Mission Analysis Report, NASA/MSC Mission No. 47, Site 93, Pt. Barrow, Alaska, "October 1967. Supported by NASA Contract NAS 9-7175.

TECHNICAL MEMORANDA

CRES Technical Memorandum 112-1 "Acoustic Scattering from Surfaces with Controlled Wave Spectra: Part I," R. Knuckey, March 1967. Supported by NAVOCEANO Contract No. NOO N62306-67-C-0044.

CRES Technical Memorandum 112-2 "Acoustic Scattering from Surfaces with Controlled Wave Spectra: Part II," R. Knuckey, June 1967. Supported by NAVOCEANO Contract No. NOO N62306-67-C-0044.

CRES Technical Memorandum 112-3 "Range Error Statistics for Split-Gate Altimeter: Part I, Square Law Detection," H. Lee, October 1967. Supported by NAVOCEANO Contract No. NOO N62306-67-C-0044.

CRES Technical Memorandum 112-4 "Range Error Statistics for Split-Gate Altimeter: Part II, Linear Detection," H. Lee, October 1967. Supported by NAVOCEANO Contract No. NOO N62306-67-C-0044.

TECHNICAL MEMORANDA

CRES Technical Memorandum 121-1 "Ice Type Identification by Radar; Earth Resources Survey Program, Mission Analysis Report, NASA/MSC Mission 47," J. Rouse, Jr., February 1968. Supported by AINA Contract No. ONR-394.

TECHNICAL REPORTS

CRES Technical Report 121-1 "Ice Type Identification by Radar," J. Rouse, Jr. (being completed). Supported by AINA Contract No. ONR-394.

TECHNICAL MEMORANDA

CRES Technical Memorandum 137-1 "Orbit Considerations for Radar Imagery of Arctic Sea Ice," R. Gerchberg, March 1968. Supported by NOL Contract No. NOO N62306-67-C-0044.

CRES Technical Memorandum 137-2 "Unfocused Synthetic Aperture Radar: Basic System Requirements," R. Gerchberg, March 1968. Supported by NOL Contract No. NOO N62306-67-C-0044.

TECHNICAL REPORTS AND OTHER PUBLICATIONS

CRES Technical Report 48-1 "Exact Solution to the Scattering of Waves From a Rough Surface," A. K. Fung, June 1964. Supported by NSF Grant GP-2259 and NASA Grant NsG-298.

CRES Technical Report 48-3 "Scattering Theories and Radar Return," A. K. Fung, May 1965. Supported by NSF Grant GP-2259 and NASA Grant NsG-298.

CRES Technical Report 48-4 "The Omnidirectional Scattering of Acoustic Waves from Rough Surfaces with Application to Electromagnetic Scattering," B. E. Parkins, June 1965. Supported by NSF Grant GP-2259 and NASA Grant NsG-298.

CRES Technical Report 48-5 "Scattering and Depolarization of Electromagnetic Waves by Rough Surfaces," A. K. Fung, November 1965. Supported by NSF Grant GP-2259 and NASA Grant NsG-298.

CRES Technical Report 48-6 "Frequency Dependence of Waves Scattered from Rough Surfaces," A. K. Fung, December 1965. Supported by NSF Grant GP-2259 and NASA Grant NsG-298.

CRES Technical Report 48-7 "Literature Survey on Scattering from Layered Media," T. Leovaris, July 1966. Supported by NSF Grant GP-2259 and NASA Grant NsG-298.

CRES Technical Report 48-8 "Polarized and Depolarized Powers Returned from a Dielectric Rough Surface," A. K. Fung, July 1966. Supported by NSF Grant GP-2259 and NASA Grant NsG-298.

CRES Technical Report 48-9 "Omnidirectional Measurements of Acoustic Waves Scattered from a Known Rough Surface at Various Angles of Incidence," W. D. Boles, August 1966. Supported by NSF Grant GP-2259 and NASA Grant NsG-298.

CRES Technical Report 48-10 "Theory of Radar Scatter from Rough Surfaces, Bistatic and Monostatic with Application to Lunar Radar Return," A. K. Fung, March 1964. Published in Journal of Geophysical Research, vol. 69, no. 6, March 1964, p. 1063-1073. Supported by NSF Grant GP-2259 and NASA Grant NsG-298.

CRES Technical Report 48-11 "Effects of Structure Size on Moon and Earth Radar Returns at Various Angles," A. K. Fung and R. K. Moore, March 1964. Published in Journal of Geophysical Research, vol. 69, no. 6, March 1964, p. 1075-1081. Supported by NSF Grant GP-2259 and NASA Grant NsG-298.

CRES Technical Report 48-12 "Notes on Backscattering and Depolarization by Gently Undulating Surfaces," A. K. Fung, R. K. Moore and B. E. Parkins, March 1965. Published in Journal of Geophysical Research, vol. 70, no.6, March 1965, p. 1559-1562. Supported by NSF Grant GP-2259 and NASA Grant NsG-298.

CRES Technical Report 48-13 "Scattering and Depolarization of EM Waves from a Rough Surface," A. K. Fung, March 1966. Published in Proceedings IEEE Letters, vol. 54, no. 3, March 1966, p. 395-396. Supported by NSF Grant GP-2259 and NASA Grant NsG-298.

CRES Technical Report 48-14 "The Correlation Function in Kirchhoff's Method of Solution of Scattering of Waves from Statistically Rough Surfaces," A. K. Fung and R. K. Moore, June 1966. Published in Journal of Geophysical Research, vol. 71, no. 12, June 1966, p. 2939-2943. Supported by NSF Grant GP-2259 and NASA Grant NsG-298.

CRES Technical Report 48-15 "On Depolarization of Electromagnetic Waves Backscattered from a Rough Surface," A. K. Fung, July 1966. Published in Planetary Space Science, vol. 14, July 1966, p. 563-568. Supported by NSF Grant GP-2259 and NASA Grant NsG-298.

CRES Technical Report 48-16 "Vector Scatter Theory Applied to Moon and Venus Radar Return," A. K. Fung, July 1966. Published in Proceedings IEEE, vol. 54, no. 7, July 1966, p. 996-998. Supported by NSF Grant GP-2259 and NASA Grant NsG-298.

CRES Technical Report 48-17 "Frequency Dependence and Surface Roughness," A. K. Fung, October 1966. Published in Proceedings IEEE, vol. 54, no. 10, October 1966. p. 1482-1483. Supported by NSF Grant GP-2259 and NASA Grant NsG-298.

CRES Technical Report 60 N-1 "Radar Astronomy Usage" R. K. Moore, April 1966. Published in IEEE Spectrum Correspondence, vol. 3, no. 4, April 1966, p. 156-159. Supported by NSF Grant GP-2259 and NASA Grant NsG-298.

CRES Technical Report 37-1 "A Study of Earth Radar Returns from Alouette Satellite," R. C. Chia, H. H. Doemland, and R. K. Moore, April 1967. Supported by NASA Grant NsG-477.

CRES Technical Report 105-1 "Rough Surface Scattering and its Application to Earth and Moon Radar Returns," A. K. Fung, January 1967. Supported by NSF Grant GK-1153.

CRES Technical Report 105-2 "Scattering and Depolarization of Electromagnetic Waves by a Horizontally Weakly Inhomogeneous Medium," A. K. Fung, May 1967. Supported by NSF Grant GK-1153.

CRES Technical Report 105-3 "Scattering of Electromagnetic Waves from a Slightly Rough Dielectric Layer," A. K. Fung, May 1967. Presented at Spring URSI Meeting, May 22-25, 1967, Ottawa, Ontario, Canada. Supported by NSF Grant GK-875.

CRES Technical Report 105-4 "Wave Propagation Across an Irregular Interface Between a Homogeneous and an Inhomogeneous Medium," A. K. Fung and C. M. Tu, July 1967. Supported by NSF Grant GK-1153.

CRES Technical Report 105-5 "Transducer Design," T. Leovaris, N. Boles, and A. Fung, March 1968. Supported by NSF Grant GK-875 and GK-1153.

Fung, A. K., "Theory of Radar Scatter from Rough Surfaces, Bistatic and Monostatic, with Application to Lunar Radar Return," Journal of Geophysical Research, vol. 69, no. 6, March 16, 1964, p. 1063-1073. Supported by NSF Grant GP-2259 and NASA Grant NsG-298.

Fung, A. K. and R. K. Moore, "Effects of Structure Size on Moon and Earth Radar Returns at Various Angles," Journal of Geophysical Research, vol. 69, no. 6, March 15, 1964, p. 1075-1081. Supported by NSF GP-2259 and NASA Grant NsG-298.

Chia, R. C., A. K. Fung and R. K. Moore, "High Frequency Backscatter from the Earth Measured at 1000 km Altitude," Proceedings IEEE Letters, vol. 52, no. 11, November 1964, p. 1384-1385. Supported by NASA Grant NsG-477.

Fung, A. K., R. K. Moore, and B. E. Parkins, "Notes on Backscattering and Depolarization by Gently Undulating Surfaces," Journal of Geophysical Research, vol. 70, no. 6, March 15, 1965, p. 1559-1562. Supported by NSF Grant GP-2259 and NASA Grant NsG-298.

Chia, R. C., A. K. Fung and R. K. Moore, "High Frequency Backscatter from the Earth Measured at 1000 km Altitude," Radio Science, Journal of Research NBS/USNC-URSI, vol. 69D, no. 4, April 1965, p. 641-649. Supported by NASA Grant NsG-477.

Fung, A. K., "Scattering and Depolarization of EM Waves from a Rough Surface," Proceedings IEEE Letters, vol. 54, no. 3, March 1966, p. 395-396. Supported by NSF Grant GP-2259 and NASA Grant NsG-298.

Fung, A. K., "On Depolarization of Electromagnetic Waves Backscattered from a Rough Surface," Planetary Space Science, vol. 14, July 1966, p. 563-568. Supported by NSF Grant GP-2259 and NASA Grant NsG-298.

Fung, A. K. and R. K. Moore, "The Correlation Function in Kirchhoff's Method of Solution of Scattering of Waves from Statistically Rough Surfaces," Journal of Geophysical Research, vol. 71, no. 12, July 15, 1966. Supported by NSF Grant GP-2259 and NASA Grant NsG-298.

Fung, A. K., "Vector Scatter Theory Applied to Moon and Venus Radar Return," Proceedings IEEE, vol. 54, no. 7, July 1966, p. 996-998. Supported by NSF Grant GP-2259 and NASA Grant NsG-298.

Moore, R. K. and B. E. Parkins, "Omnidirectional Scattering of Acoustic Surfaces of Known Statistics," Journal of the Acoustical Society of America, vol. 40, no. 1, July 1966, p. 17-175. Supported by NSF Grant GP-2259 and NASA Grant NsG-298.

Fung, A. K., "Frequency Dependence and Surface Roughness," Proceedings IEEE, vol. 54, no. 10, October 1966, p. 1482-1483. Supported by NSF Grant GP-2259 and NASA Grant NsG-298.

Fung, A. K. and C. M. Tu "Reflection of Electromagnetic Waves from a Two-Dimensionally Inhomogeneous Medium," Presented at Southwestern IEEE Conference (SWIEEECO), April 19-21, 1967, Dallas, Texas. Published in the SWIEEECO Record, IEEE Catalog No. F-72, p. 12-4-2 to 12-4-7. Supported by NSF Grant GK-1153.

Fung, A. K. "A Note on the Wiener-Khintchine Theorem for Autocorrelation," Proceedings IEEE Letters, vol. 55, no. 4, April 1967, p. 594-595. Supported by NSF Grant GK-1153.

Fung, A. K. and P. Beckmann "Surface Current of a Locally Flat Conductor and Depolarized Backscatter," Proceedings IEEE, vol. 55, no. 7, July 1967, p. 1235. Supported by NSF Grant GK-1153.

Parkins, B. E., "Omnidirectional Scattering of Acoustic Waves by Rough, Imperfectly Reflecting Surfaces," Journal of the Acoustical Society of America, vol. 51, no. 1, July 1967, p. 126-134. Supported by NSF Grant GP-2259 and NASA Grant NsG-298.

Fung, A. K. "Theory of Cross-Polarized Power Returned from a Random Surface," Applied Science Research, vol. 18, August 1967, p. 50-60. Supported by NSF Grant GP-2259 and NASA Grant NsG-298.

Fung, A. K. "Comments on Electromagnetic Scattering from Rough Finitely Conducting Surfaces," Radio Science, Journal of Research NBS/USNC-URSI, vol. 2, no. 12, December 1967, p. 1525. Supported by NSF Grant GK-1153.

Fung, A. K. "Character of Wave Depolarization by a Perfectly Conducting Rough Surface and its Application to Earth and Moon Experiments," Planetary Space Science, vol. 15, 1967, p. 1337-1347. Supported by NSF Grant GK-1153.

Fung, A. K. "Mechanisms of Polarized and Depolarized Scattering from a Rough Dielectric Surface," Journal of the Franklin Institute, vol 285, no. 2, February 1968, p. 125-133. Supported by NSF Grant GK-875 and GK-1153.

Fung, A. K. "Backscattering of Waves by Composite Rough Surfaces," Presented at Spring URSI Meeting, Washington, D. C., April 9-12, 1968. Supported by NSF Grant GK-875 and GK-1153.

Moore, R. K., A. Zachs and R. C. Chia "Radar Scattering from the Ocean--Theory, Simulation and Experiment," Presented at Spring URSI Meeting, Washington, D. C., April 9-12, 1968. Supported by NSF Grant GK-1153.

TECHNICAL REPORTS

CRES Report 122-1 "Multi-Image Correlation Systems Study for MGI Study Plan," G. Dalke, July 1967. Supported by USAETL Contract No. DAAK0.. -67-C-0435.

CRES Report 122-2 "Multi-Image Correlation Systems Study for MGI, Phase I Technical Report," G. Dalke, December 1967. Supported by USAETL Contract No. DAAK02-67-C-0435.

TECHNICAL REPORTS

CRES Report 133-1 "Project THEMIS: A Center for Remote Sensing Study Plan (U)," R. D. Ellermeier, January 1968. Supported by THEMIS Contract No. DAAK02-68-C-0089.

CRES Report 133-2 "Project THEMIS: A Center for Remote Sensing Semi-Annual Technical Report (U)," R. D. Ellermeier, April 1968. Supported by THEMIS Contract No. DAAK02-68-C-0089.

CRES Technical Report 133-3 "Adaptive Pattern Recognition of Agriculture in Western Kansas by Using a Predictive Model in Construction of Similarity Sets," R. M. Haralick, March 1968. Supported by THEMIS Contract No. DAAK02-68-C-0089.

TECHNICAL MEMORANDA

CRES Technical Memorandum 133-1-1 "Antenna and Power Output Considerations for the Polypanchromatic Radar," W. Waite, January 1968. Supported by THEMIS Contract No. DAAK02-68-C-0089.

CRES Technical Memorandum 133-1-2 "Preliminary Systems Analysis of the Polypanchromatic Radar," W. Waite (in press). Supported by THEMIS Contract No. DAAK02-68-C-0089.

CRES Technical Memorandum 133-2 "Broad Spectrum Backscatter Acoustic System," J. W. Rouse, Jr., March 1968. Supported by THEMIS Contract No. DAAK02-68-C-0089 and NASA Contract NAS 9-7175.

CRES Technical Memorandum 133-3 "IDECS System Development," G. Kelly and G. Dalke, March 1968. Supported by THEMIS Contract No. DAAK-2-68-C-0089.

CRES Technical Memorandum 133-4 "Observations on the Geomorphology of Part of the Wasatch Range, Utah," R. Peterson, March 1968. Supported by THEMIS Contract No. DAAK02-68-C-0089 and NASA Contract NAS 9-7175.

CRES Technical Memorandum 133-5 "A Statistical and Conditional Probability Study of Crop Discrimination Using Radar Images," R. Haralick, F. Caspall, R. Moore and D. Simonett. Presented at IEEE International Convention, March 18-21, 1968, New York, To be published in the Convention Record. Supported by THEMIS Contract No. DAAK02-68-C-0089, USGS Contract No. 14-08-0001-10848 and NASA Contract NAS 9-7175.

RECENT OR PENDING PAPERS

Dellwig, L. F. "What's New in Radar for the Geologist," Presented to the Highway Research Board of the National Research Council, January 19, 1968, Washington, D. C. Supported by NASA Contracts NSR 17-004-003 and NAS 9-7175 and NASA Grant NsG-298.

Moore, R. K. and A. W. Biggs "Research in Radar Scatterometry and Altimetry," Presented at the Ninth Meeting of the Ad Hoc Spacecraft Oceanography Advisory Group, January 23-24, 1968, Texas A & M University, College Station, Texas. Supported by NAVOCEANO Contract NOO N62306-67-C-0044.

Dellwig, L. F., H. C. MacDonald, and J. N. Kirk "The Potential of Radar in Geologic Exploration," Presented at the Fifth Symposium on Remote Sensing of Environment, April 16-18, 1968, University of Michigan, Ann Arbor, Michigan. To be published in the Proceedings. Supported by NASA Contract NAS 9-7175.

Schwarz, D. and F. Caspall "The Use of Radar in the Discrimination and Identification of Agricultural Land Use," Presented at the Fifth Symposium on Remote Sensing of Environment, April 16-18, 1968, University of Michigan, Ann Arbor, Michigan. To be published in the Proceedings. Supported by USGS Contract USGS 14-08-0001-10848.

Simonett, D. S. "Land Evaluation Studies with Remote Sensors in the Infrared and Active and Passive Microwave Regions," To be presented at the Land Evaluation Symposium, a joint CSIRO-UNESCO symposium, August 1968, Canberra, Australia. Supported by USGS Contract USGS 14-08-0001-10848.

Simonett, D. S. "Potential of Radar Remote Sensors as Tools in Reconnaissance Geomorphic, Vegetation and Soil Mapping," To be presented at the 9th Congress, International Soil Science Society, August 1968, Adelaide, Australia. Supported by USGS Contract USGS 14-08-0001-10848.

Unclassified

Security Classification

DOCUMENT CONTROL DATA - R & D

(Security classification of title, body of abstract and indexing annotation must be entered when the overall report is classified)

1. ORIGINATING ACTIVITY (Corporate author) Center for Research, Inc. University of Kansas	2a. REPORT SECURITY CLASSIFICATION Unclassified 2b. GROUP

3. REPORT TITLE

Interim Technical Progress Report, Project Themis: A Center for Remote Sensing

4. DESCRIPTIVE NOTES (Type of report and inclusive dates)

First Semi Annual Technical Report, September 1967 to April, 1968

5. AUTHOR(S) (First name, middle initial, last name)

Compiled by R. D. Ellermeier

6. REPORT DATE April 25, 1968	7a. TOTAL NO. OF PAGES 196	7b. NO. OF REFS
8a. CONTRACT OR GRANT NO. DAAK02-68-C-0089 ARPA Order No. 1079 b. PROJECT NO. c. d.	9a. ORIGINATOR'S REPORT NUMBER(S) 133-2 9b. OTHER REPORT NO(S) (Any other numbers that may be assigned this report)	

10. DISTRIBUTION STATEMENT

No limitation

11. SUPPLEMENTARY NOTES Funded by DOD Project Themis under ARPA Order No. 1079	12. SPONSORING MILITARY ACTIVITY Monitoring U.S. Army Engineering Topographic Lab. Geographic Information Systems Branch Geographic System Division Ft. Belvoir, Virginia

13. ABSTRACT

This report summarizes the technical progress under the subject contract on a broad interdisciplinary effort for the improvement of user utility of remotely sensed data. This effort involves theoretical work, sensor development, processing and display, and data analysis for specific user application. A number of technical reports and memoranda describing work underway are attached.

DD FORM 1 NOV 65 1473

Unclassified

Security Classification